FATIGUE BEHAVIOR OF A FUNCTIONALLY-GRADED TITANIUM MATRIX COMPOSITE

THESIS

Scott R. Cunningham, Captain, USAF

AFIT/GAE/ENY/05-M06

DEPARTMENT OF THE AIR FORCE
AIR UNIVERSITY

AIR FORCE INSTITUTE OF TECHNOLOGY

Wright-Patterson Air Force Base, Ohio

The views expressed in this thesis are those of the author and do not reflect the official policy or position of the United States Air Force, Department of Defense, or the U.S. Government.

AFIT/GAE/ENY/05-M06

FATIGUE BEHAVIOR OF A FUNCTIONALLY-GRADED TITANIUM MATRIX COMPOSITE

THESIS

Presented to the Faculty

Department of Aeronautics and Astronautics

Graduate School of Engineering and Management

Air Force Institute of Technology

Air University

Air Education and Training Command

In Partial Fulfillment of the Requirements for the

Degree of Master of Science in Aeronautical Engineering

Scott R. Cunningham, BS

Captain, USAF

March 2005

AFIT/GAE/ENY/05-M06

FATIGUE BEHAVIOR OF A FUNCTIONALLY-GRADED TITANIUM MATRIX COMPOSITE

Scott R. Cunningham, BS

Captain, USAF

Approved:

_____/signed/_____ _____
Dr. Shankar Mall (Chairman) Date

_____/signed/_____ _____
Dr. Marina B. Ruggles-Wrenn (Member) Date

_____/signed/_____ _____
Dr. Robert A. Canfield (Member) Date

Abstract

Functionally-graded Titanium Matrix Composites (F/G TMCs) are an attempt to utilize the high-strength properties of a titanium matrix composite with a monolithic (unreinforced) alloy having the more practical machining qualities. Successful implementation of such a material would expand the use of composites in aerospace structures. This would allow the use of composite materials in components whose design requirements have challenged their use in the past and subsequently lead to enhanced performance in both military and commercial aircraft.

However, the basic properties of a functionally-graded titanium matrix composite need to be investigated. The deciding factor in the overall performance of such a material may be the characteristics of the composite/alloy transition region, or joint area, itself. Therefore, this work studied the mechanical characteristics of the joint region as a first step toward future evaluation of this material. The scope of this effort involved testing under monotonic tension and fatigue loading conditions. Mechanical properties (modulus of elasticity, failure strength) and cyclic behavior (fatigue and deformation/failure mechanisms) were evaluated for the joint area and then compared to those of the parent materials.

The results of this study found that the strength of the transition region was slightly higher than the unreinforced alloy. However, the presence of the fiber ends in the transition region proved to be the source of failure under fatigue loading conditions. These areas acted as seedbeds for early crack initiation, much like residual pores in the

unreinforced alloy. Failure in the transition region did not occur at the tip of the taper joint as anticipated. Instead, failure occurred at the transition to the next ply in the taper, corresponding to a transition from 25% composite to 50% composite. This indicates that fiber volume, in conjunction with the presence of fiber ends, plays a key role in the fatigue life of the entire material. These findings encourage and provide the basic scientific knowledge for further evaluation and development of functionally-graded titanium matrix composites.

Acknowledgments

The accomplishment of this research would not have been possible without the generous help and support of many individuals. I would like to thank Dr. Mall for his patience and guidance throughout this effort. His insight and experience in the area of fracture and fatigue was invaluable. Thanks also to Dr. Ruggles-Wrenn, who provided answers to many of my questions early on and helped me get started on my research. I would also like to thank my sponsor, Mark Derriso, for the financial support provided. My sincere appreciation goes to Jan LeValley, Condie Inman and the rest of the AFIT machine shop crew, for machining the specimens and the buckling guide. Thanks also to Jay Anderson and Barry Page for all their help with the MTS machines in the lab. The testing would not have gotten far without them. A "thank you" also goes to Randy Miller for taking the time to show me how to prepare specimens for the Scanning Electron Microscope (SEM) as well as how to use the SEM itself. I would also like to thank my family and friends for all their prayers and support throughout this whole endeavor. Finally, I would like to thank my loving wife for all of her love and support. Her companionship means the world to me.

Scott R. Cunningham

Table of Contents

Page

Page

Page

List of Figures

Page

Page

Page

Page

Page

Page

List of Tables

Page

FATIGUE BEHAVIOR OF A FUNCTIONALLY-GRADED TITANIUM MATRIX COMPOSITE

I. Introduction

Background

The use of metal matrix composites (MMCs) in aircraft structures has increased dramatically over the years. One class of MMCs uses a titanium alloy matrix reinforced with silicon carbide fibers. These titanium matrix composites (TMCs) have proven their superior strength and stiffness in many aerospace applications [13:4-11]. Due to their high strength and stiffness-to-weight ratios, they quickly began to replace aluminum and titanium alloys as the materials of choice for many aircraft components. With their impressive fatigue properties and crack growth resistance, they showed promise in the overall life of the structure. By decreasing the weight of the airframe, the use of composites revealed an increase in payload, speed, range, and endurance. Both military and commercial aerospace systems have benefited from the implementation of composite materials into their aircraft structures.

Problems arose as some areas were unsuitable for the use of composites. The fabrication of composite structures proved difficult for complex shapes, while many mechanical interfaces would show no benefit from the new material. By simply machining or drilling a hole into a composite material, the damage to the fibers negates some or all of the strength enhancing effect that was desired. These limitations require the use of monolithic materials in these areas, thereby hindering the advancement of composite materials in the aerospace industry.

Functionally-Graded Materials: A Possible Solution

"A functionally-graded material (FGM) is a material in which the composition and structure gradually change resulting in a corresponding change in the properties of the material." [16]. This concept can be applied to numerous materials with such incompatible functions as the refractoriness of ceramics and the toughness of metals. However, the design and processing of these FGMs are still relatively new and undeveloped, paving the way for the current research.

The current research studies a technique used to join a monolithic titanium alloy to a titanium matrix composite. This has the potential of removing the machinability limitations that has precluded the use of composites in many applications. However, a lack of material characterization exists for this F/G TMC, preventing its acceptance and use in the field. Although complete characterization exists for the two parent materials, the characteristics of the joint region are still in question. The objective of this study is to compare the properties of the composite/alloy transition region to those of the monolithic alloy and pure composite.

Research Focus and Methodology

This research investigates the mechanical behavior of a functionally-graded titanium matrix composite. The material is composed of a titanium matrix composite and a monolithic titanium alloy functionally-graded through the thickness (see Figure 1).

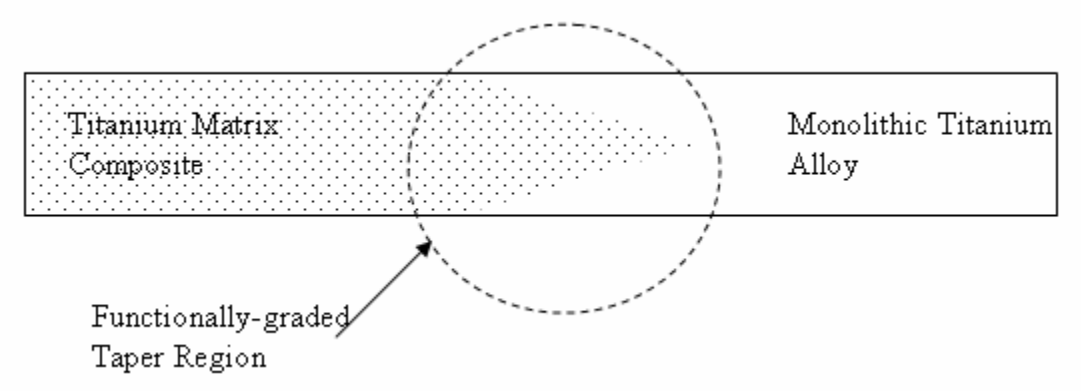

Figure 1: Functionally-graded, double scarf joint

Both tension-tension and tension-compression fatigue loading conditions were investigated. Monotonic tensile tests were also performed on a titanium alloy, a Ti-6-4V unidirectional composite material and a functionally-graded material. From these tests, the modulus and ultimate tensile strength of the functionally-graded material were compared with those of the two parent materials. Next, both tension-tension and tension-compression fatigue tests were conducted under room temperature conditions to obtain and compare fatigue life data for the three materials. Finally, post-failure analysis using fractography and microscopy was accomplished to determine damage mechanisms for the different loading conditions, and then compared for each material.

By understanding the mechanics of the joint (or taper) section, more steps can be taken to improve the design of the joint, the manufacturing process of the material, or both. This may lead toward the acceptance and implementation of such a material in aerospace vehicles.

Preview

The following chapters contain a description of the efforts mentioned above. First, significant contributions in titanium alloy production and MMC research are reviewed from previous studies as well as current work in the area of functionally-graded materials. Second, a complete description of the experimental set-up and testing procedures used in this study are provided. Third, a detailed discussion of the experimental results and analysis are presented. Included in this discussion are examples of the mechanical responses of the different materials, fatigue-life analyses, and microscopic analyses. Finally, a brief discussion of the conclusions and recommendations are given.

II. Literature Review

Chapter Overview

The purpose of this chapter is to provide a background summary of studies conducted on the parent materials as well as any studies done that may be pertinent to the present work of characterizing the joint region. These studies are broken up into sections pertaining to the three materials studied in this research. In addition, a summary of these past studies and how they apply to the current work is provided.

Titanium Alloys

Early efforts in studying titanium alloys stemmed from the desire to overcome the cost barrier associated with the design, fabrication and use of such a material [11]. Although titanium alloys offered increased performance with their high strength-to-weight ratios as well as excellent corrosion resistance and fracture behavior, their cost-effectiveness was still in question. Titanium formed by powder metallurgy (PM) demonstrated the widest range of process variations and potential applications in the aerospace industry to overcome the cost associated with machining and part production.

Peebles and Kelto [17], in the late seventies, studied several different processes used to produce titanium powder at that time and characterized each material produced as well as tested their mechanical properties. These early fabrication efforts proved undesirable as none were able to produce a clean titanium powder free of defects.

Vaughan and Blenkinsop [22] also studied the mechanical properties of several titanium powders obtained from different sources. They met with similar results and

found “metallurgical inhomogeneities” in all products, leading to early crack initiation in at least two of them. Again, all were found to be inferior when compared with conventional cast and wrought material of a similar section.

Eylon et al. [7] studied the premature fatigue failures associated with titanium formed by powder metallurgy. They divided the crack initiation sites into three categories: a) inclusions (both metallic and nonmetallic), b) residual pores and c) micro-structural features such as grain boundary alpha phase. Findings such as these ultimately lead to modifications of the powder making process and improved fatigue performance of PM products.

Titanium Matrix Composites (TMCs)

Jeng et al. [10] studied the tensile behavior of several TMCs, including an SCS-6 fiber reinforced Ti-6-4 matrix composite. They concluded that the fiber/matrix interface region is very sensitive to cracking, leading to the formation of notches on the fiber surface. Their work ultimately found that the strength of the fiber decreases as the thickness of this interface region (or “reaction zone”) increases.

Jeng et al. [9] conducted low-cycle fatigue tests of several TMCs, including an SCS-6 fiber reinforced Ti-6-4 matrix composite with 35% fiber volume. They classified the fatigue damage of these composites into three regimes: Regime 1, 2 and 3. Regime 1 failure is dominated by overload of the fibers and fiber breakage. Regime 2 is dominated by matrix/interface cracking and fiber breakage. Regime 3 is matrix cracking dominated.

Sanders, Mall and Pittman [19] examined the effects of frequency on the fatigue response of a unidirectional SCS-6/Ti-6-4 composite at elevated temperatures. In their

study, isothermal tests were performed at four different frequencies (0.01, 0.1, 1 and 10 Hz) and four different temperatures (23°C, 370°C, 427°C and 538°C). They concluded that there was no dependence on frequency below 400°C. However, above this temperature the fatigue life was more cycle-dependent at higher frequencies and more time-dependent at lower frequencies. These frequency effects were magnified with increasing temperature. This was due to the longer exposure to the high temperatures and more creep at the lower frequencies.

Functionally-Graded Materials (FGMs)

Ramamurty [18] investigated the fatigue response of a unidirectional SCS-6/Ti-6-4 composite that was clad on both sides with a layer of monolithic alloy. He concluded that although the cladding showed no effect on monotonic loading, the fatigue life of the cladded material was much shorter than the uncladded material. Matrix cracks would initiate in the cladded alloy and resulted in accelerated crack propagation through the composite core. He also related fatigue life to the thickness of the cladding. As the thickness of the cladding increases, the fatigue life of the material decreases.

Clyne and Watson [5] studied the effects of discontinuous fibers in TMCs. They determined that interfacial cavitation occurs at the fiber ends, which ultimately leads to failure as these cavities (or voids) link-up in the matrix adjacent to the fiber ends. This cavitation at the fiber ends leads to Mode I loading of the crack (opening), while reaction zone cracks parallel to the loading axis leads to Mode II loading of the crack (sliding, in-plane shear).

Miller [15] tested a Trimarc 1 fiber reinforced F/G TMC. Much like the current work, he studied the properties and mechanical behavior of the joint area. After studying the effects of 4:1 and 20:1 taper ratios, he found that the matrix material was the location of premature failure. He concluded that the cause of premature crack initiation in the alloy was due to contamination of the material during fabrication. These findings prompted a change in the fabrication and quality processes, which ultimately led to the current work.

Summary

The research conducted on the mechanical properties and behavior of titanium alloys and titanium matrix composites provides valuable insights to the properties and behavior of the joint region in the functionally-graded material. These insights will also provide upper and lower bounds for defining the characteristics of this new material. In addition, the past efforts relative to functionally-graded materials indicates that the fiber ends in the joint region may have a detrimental effect on the overall performance of F/G TMCs. It is therefore important to determine which deformation mechanism (damage or plasticity), or what combination of them, is dominant in order to fully characterize the F/G TMC material. Consequently, the current test method focuses on which of these failure/deformation mechanisms define the behavior of F/G TMCs and will be discussed in the next chapter.

III. Experimental Set-up and Testing Procedures

Chapter Overview

The purpose of this chapter is to give a detailed description of the materials tested, along with the test equipment and procedures that were used in this research. Each material's composition and specimen geometry and preparation are covered in this chapter. The test equipment, along with the buckling guide used, is also discussed. Finally, the experimental procedures used to perform the monotonic tensile tests, tension-tension and tension-compression fatigue tests are described with the post-failure analysis preparation and concluding remarks.

Material

The materials investigated in this research consisted of two parent materials and a functionally-graded material. The parent materials were a titanium alloy and a titanium matrix composite. The titanium alloy used was Ti-6Al-4V and is composed of 90% weight titanium, 6% weight aluminum, and 4% weight vanadium. Typically fabricated by forging and/or cold-rolling, the titanium used in this research was fabricated using powder metallurgy techniques.

The composite used was SCS-6/Ti-6Al-4V, a continuous fiber reinforced cross ply metal matrix composite (MMC) with an orientation of $[0]_8$, a unidirectional lay-up capable of high strength in the loading direction. The individual plies consisted of silicon carbide fibers, SCS-6, embedded in a titanium alloy matrix. The silicon carbide fibers compose $37 \pm 1\%$ of the volume of the laminate, or a volume fraction of 0.37. The SCS-

6 fiber (see Figure 2), produced by Textron (Textron Specialty Materials Inc., Lowell, MA), has a mean fiber diameter of 140 microns (µm). The inner core of the fiber is a 33 µm diameter pure carbon filament. Surrounding this core is a layer of bulk silicon carbide that is formed on the carbon core through a process of chemical vapor deposition. The final layer (~ 3 µm) is composed of alternating layers of silicon and carbon, the outermost of which is a carbon rich layer that enhances the surface strength of the fiber and improves the bonding with the surrounding matrix [20].

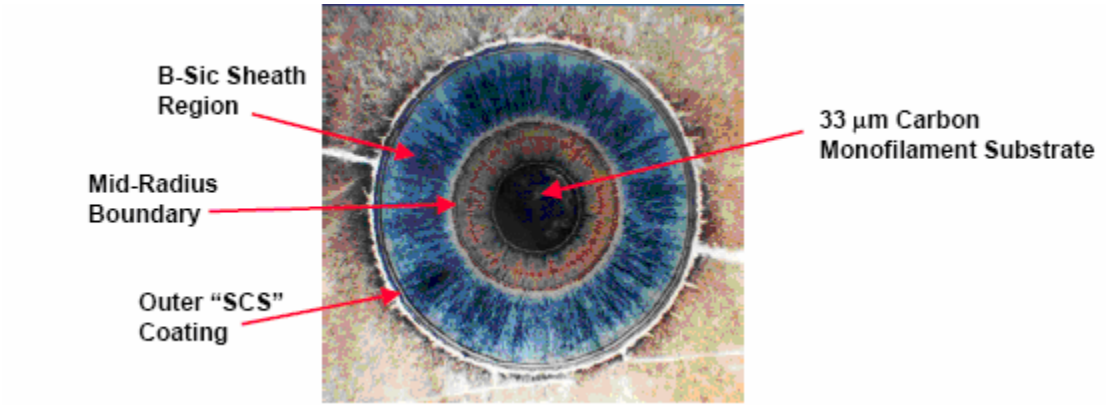

Figure 2: SCS-6 fiber (provided courtesy of Specialty Materials, Inc.)

The functionally-graded material was a combination of the two parent materials mentioned above. The plies were formed as described above, but this time the positioning of the fiber ends in each ply was carefully controlled to create the desired scarf joint transition region taper ratio of 20:1 (see Figure 3 and Figure 4).

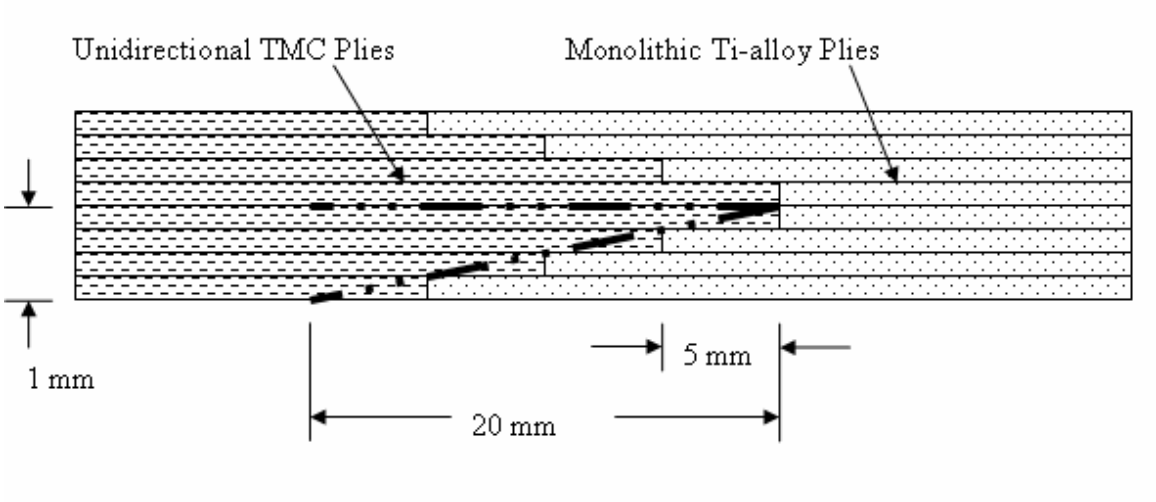

Figure 3: Functionally-graded 20:1 ply lay-up

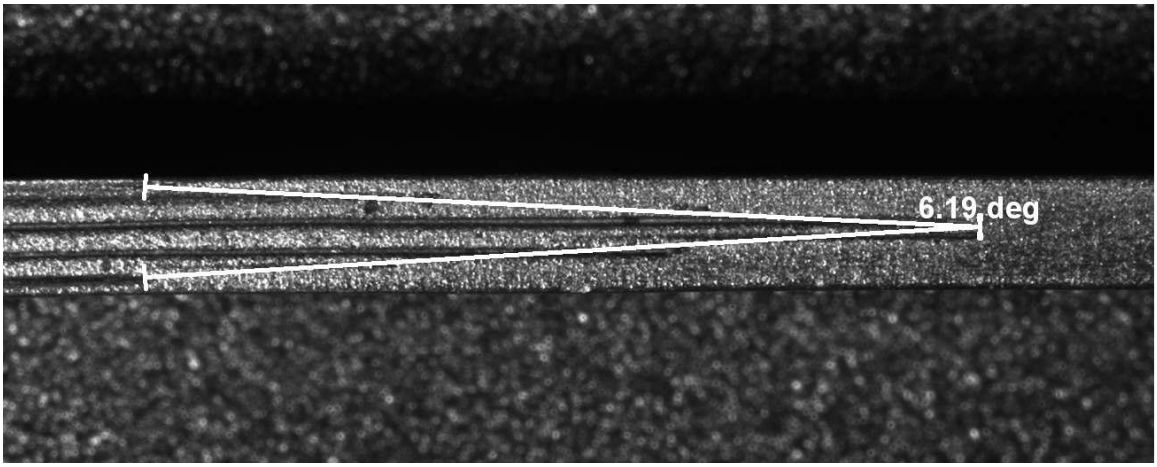

Figure 4: Specimen taper angle

Specimen Geometry

Three plates, one for each material, had been manufactured previously for study purposes. These plates had dimensions of 147 mm (in the fiber direction) by 220 mm and were each 2 mm thick. The F/G plate was tapered through the thickness, therefore a taper ratio of 20:1 made the length of the taper region 20 mm. This required the use of a 24.5 mm (1.0 inch) gage section. In addition, the use of a dogbone geometry for the test

specimen was needed to ensure failure in the gage section during fatigue loading. By reducing the gage section's cross-sectional area, the localized stress is increased. However, in order to minimize stress raisers on the specimen edge, the shoulder radius must be as large as possible. This design loop resulted in the chosen geometry (see Figure 5). All specimens were cut from the plates by technicians of the AFIT Model Shop using Electrical-Discharge Machining (EDM) techniques.

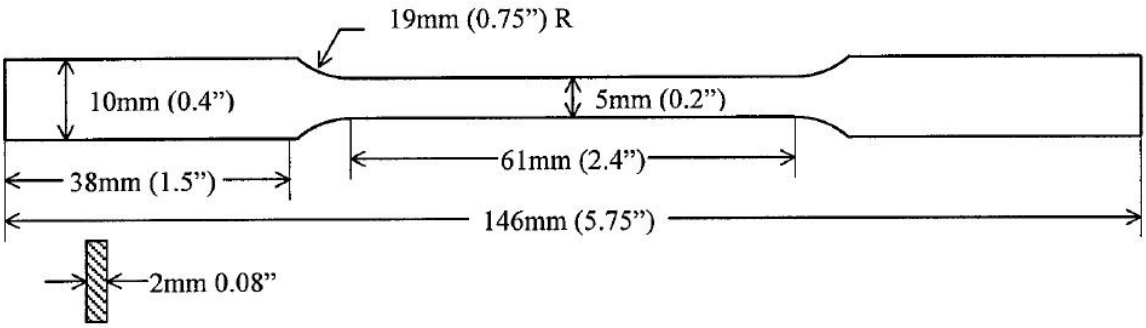

Figure 5: Dogbone specimen geometry

Tabbing Procedure

It was noted from earlier work that during fatigue testing, premature failure in the grip section might occur due to fretting fatigue [15]. This encouraged the use of tab fixtures in the grip area. Miller used brass shims and plumber's cloth to prevent localized stress raisers on the (alloy) grip surface while providing enough friction to prevent slip. In this study, simple tabs cut from a fiberglass sheet bonded to the grip surface using M-Bond 200 (strain gauge adhesive) prevented any specimen from failing in the grips.

Buckling Guide Description

The use of a buckling guide was needed as the long, slender specimens would buckle if unsupported in fully-reversed fatigue. Since all tests were conducted at room-temperature, a simple design was sufficient. Figure 6 shows the buckling guide used in this study. It was cut from 3 mm stainless steel with two grooves machined out for the placement of the extensometer. A thin strip of Teflon was placed on either side to minimize friction. Finally, the buckling guide was attached by finger-tightening four machine screws with nuts and washers.

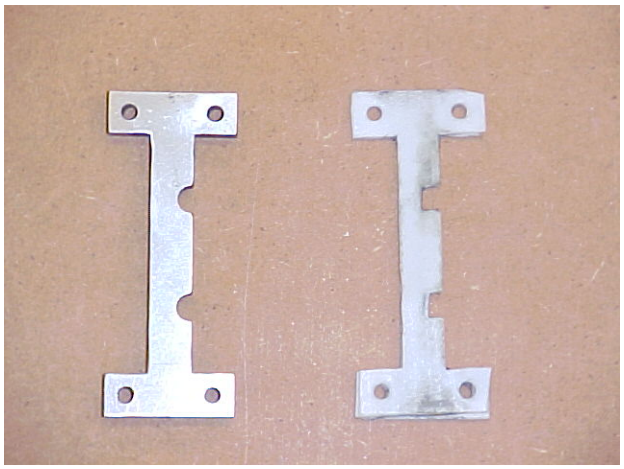

Figure 6: Buckling guide and teflon strip

Testing Setup

All tests were performed on a MTS 810 machine capable of handling 10 kN loads. Hydraulic friction grips were used to hold the specimen. Strain data was obtained with a MTS extensometer (model# 632.11B-20) and in some cases, a strain gage as well. The extensometer had a gage length of 25.4 mm (1.0 inch). The test software used was MTS Multipurpose Testware and allowed the user to input loads, loading rates, loading

frequencies, as well as data acquisition intervals. A standard desktop computer was used to run the software and store the data (see Figure 7).

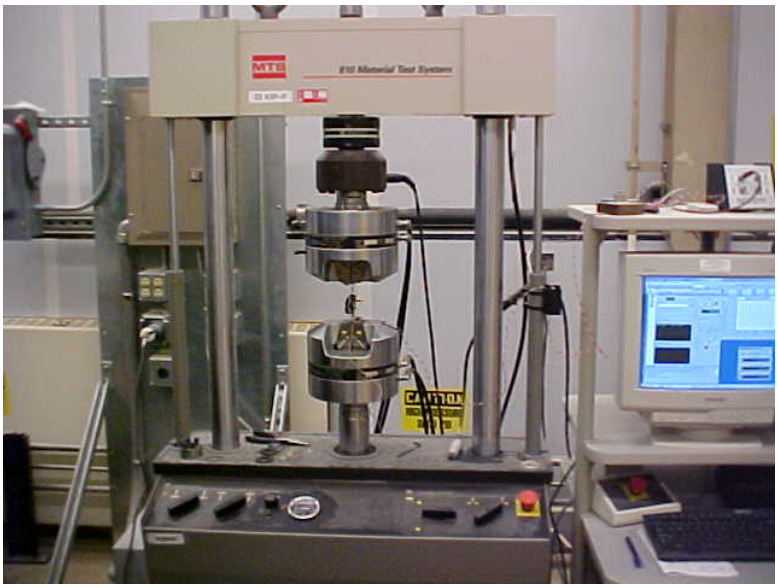

Figure 7: Test apparatus

Before anything was placed in the test fixture, the grips had to be aligned using a MTS alignment system. After this was accomplished, the specimen alignment fixtures had to be aligned (see Figure 8). This was done by placing the test stand in (manual) displacement control and moving the grips just enough to place a level against the specimen alignment fixtures. By ensuring that the specimen was centered in the grips as well as aligned, a true measure of axial loading was accomplished. With the test stand still in displacement control, the lower head was moved enough so that the specimen could be placed against both alignment fixtures and first gripped in the upper grip. At this point, the lower head position could be adjusted if needed. The test stand was then placed in load control and the lower grip quickly engaged, as the lower head tends to float while in load control.

Figure 8: Aligning the specimen alignment fixtures

With the test specimen in place, the load was verified to be zeroed and manual control switched off. From here, the next few steps were dependent on the type of test that was performed.

If the test to be performed was a tension-tension fatigue test, a specimen with a strain gage attached (see Figure 9) was chosen and no buckling guide was needed.

Figure 9: Strain gage placement

The strain gage signal was zeroed prior to testing. The extensometer was placed on the edge of the specimen where it was secured with orthodontic rubber bands. Once the extensometer was secured and zeroed, testing began (see Figure 10).

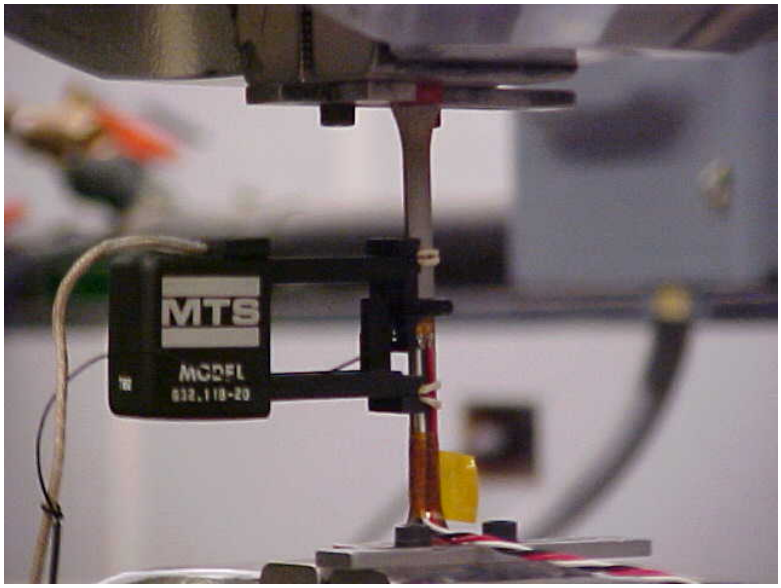

Figure 10: Tension-tension fatigue test setup

The setup for a monotonic (pure tensile) test was similar to the tension-tension fatigue test setup with the exception of the strain gage. For the initial measurements of modulus and ultimate strength, only the extensometer was used.

If the test to be performed was a tension-compression fatigue test, a specimen without a strain gage attached was chosen as the buckling guide would come in contact with the wires and/or the strain gage itself, thereby skewing the data. The buckling guide was secured around the specimen and the four nuts finger tightened just enough so that the guide could still move independently of the specimen. At this point, the extensometer could be placed on the specimen the same way as mentioned above. After the extensometer was secured and zeroed, testing began (see Figure 11).

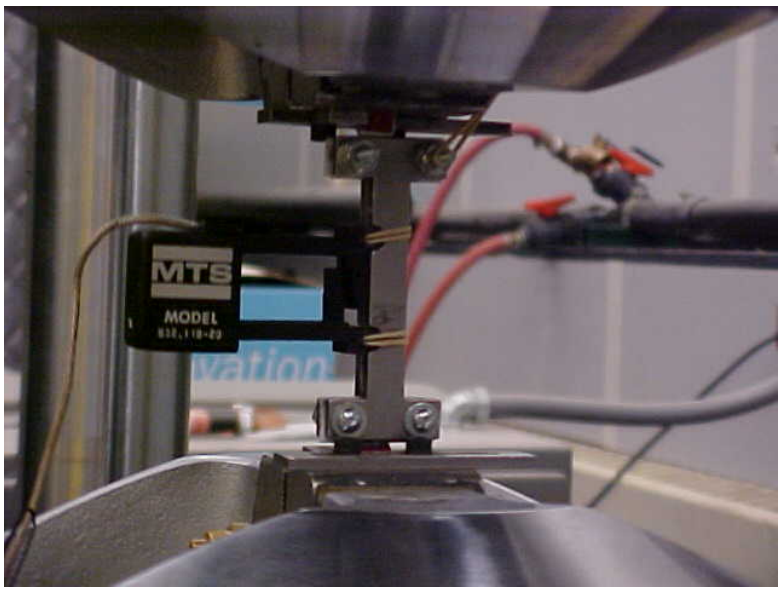

Figure 11: Tension-compression fatigue test setup

Testing Procedures

Monotonic Tests

Monotonic tests were performed on each material first to measure two parameters. The elastic modulus, which is taken from the slope of the linear portion of the stress-strain curve, and the overall (or ultimate) tensile strength of each material were needed.

These two parameters established a comparison of the material properties of the parent materials with the F/G material. The ultimate strength of the materials was also used as maximum stress-levels for the fatigue tests. All tests were conducted in room-temperature conditions, with the test profile being monotonic, or a simple "pull-to-failure" test. The loading rate was 4.45 kN/min (1000 lbf/min), while the data acquisition was 10 data points per second and recorded applied load and strain measurement.

Tension-tension Fatigue Tests

Tension-tension fatigue tests were then conducted on the three materials under room-temperature conditions at an R-ratio of 0.1. An R-ratio of 0.1 simply means that for each cycle, the ratio of the applied minimum stress to the applied maximum stress equaled 0.1. The maximum stress for each specimen ranged in value from 31 to 95 percent of their respective ultimate strength values. The loading profile was a sinusoidal wave form alternating between the maximum and minimum loads at a frequency of 10 Hz. Data acquisition occurred in a logarithmic pattern (cycles 1 through 10, 20, 30...90, 100, 200...900, 1000, etc.) and recorded applied load and strain measurements. At each data acquisition cycle, 500 data points were taken to accurately capture the peaks and valleys of each cycle. This means that, while running at a frequency of 10 Hz, data is recorded at each data acquisition cycle at a rate of 5000 data points per second or one data point every 0.002 seconds.

Tension-compression Fatigue Tests

Tension-compression fatigue tests were also conducted on the three materials under room-temperature conditions. This time, however, an R-ratio of -1.0 was used.

Also referred to as “fully-reversed”, this simply means that the maximum load (in tension) is equal in magnitude to the minimum load (in compression). The maximum stress for each specimen ranged in value from 25 to 70 percent of their respective ultimate strength values. The loading profile was again a sinusoidal wave form with a frequency of 10 Hz. Data acquisition occurred at the same rate as the tension-tension tests and recorded applied loads and strain measurements as well.

Post-failure Analysis

Post-failure analysis consisted of sectioning the specimens and evaluating the fracture surfaces with both optical and scanning electron microscopes (SEM). The location of these sections is shown in Figure 12.

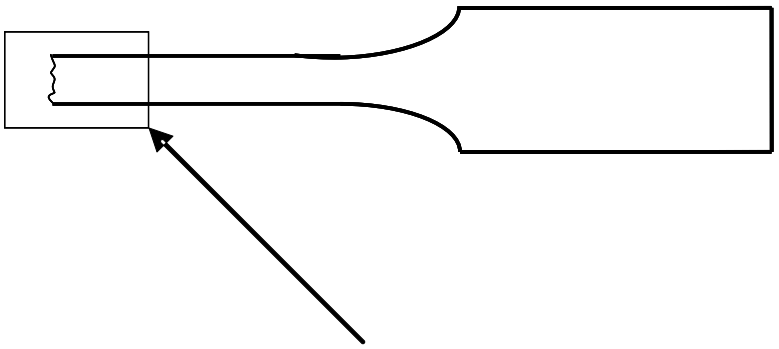

Figure 12: Location of section for microscopic analysis

IV. Analysis and Results

Chapter Overview

The results of the investigation of the tensile and fatigue behavior for the F/G material will be discussed in this chapter. This consists of both macro-mechanical and microscopic analyses. The macro-mechanical section will include observations of modulus, stress and strain histories throughout fatigue cycling. The microscopic section will include examinations of the fracture surfaces and details of the damage mechanisms and causes of specimen failure. The macro-mechanical and microscopic evaluations of the F/G material will be compared with the results of the two parent materials.

Fundamentals of Macro-mechanical Behavior

The macro-mechanical behavior of a composite includes the fatigue life, modulus degradation and strain response during cycling. The first, fatigue life, can be represented by a stress-life curve (also called a Wohler, or S-N, diagram). This curve plots either the maximum applied stress or the applied stress range versus the number of cycles to failure. Variables to consider when using the S-N curve are the matrix material, ply orientation, frequency, environment, interface properties, fiber volume fraction, type of loading and mean stress. Although three separate materials are investigated in the current work, only three factors vary. The type of loading investigated includes both tension-tension and tension-compression. The mean stress varies from a positive value in the tension-tension case (R=0.1) to zero in the tension-compression case (R=-1). Finally, the fiber volume

fraction varies from 35% in the pure composite specimens to zero in the pure alloy specimens with a gradually diminishing value in the taper region of the F/G TMC.

Many researchers have attempted to show the fatigue life diagram as three distinct regimes (Regime I, II and III) where each regime represents an area where certain failure mechanisms play dominant roles. Using Talreja's approach [21] for unidirectional composites, Region I failures correspond to overloading of the fibers resulting in fiber breakage and interfacial debonding. Damage in this region is characterized as catastrophic or non-progressive. Region II failures correspond to matrix, fiber and fiber/matrix interface cracking. Damage in this region is characterized as progressive. Region III corresponds to matrix cracking and the matrix fatigue limit. Damage in this region, if it occurs at all, is characterized as non-propagating or referred to as runout. A typical S-N diagram showing these regions is shown in Figure 13.

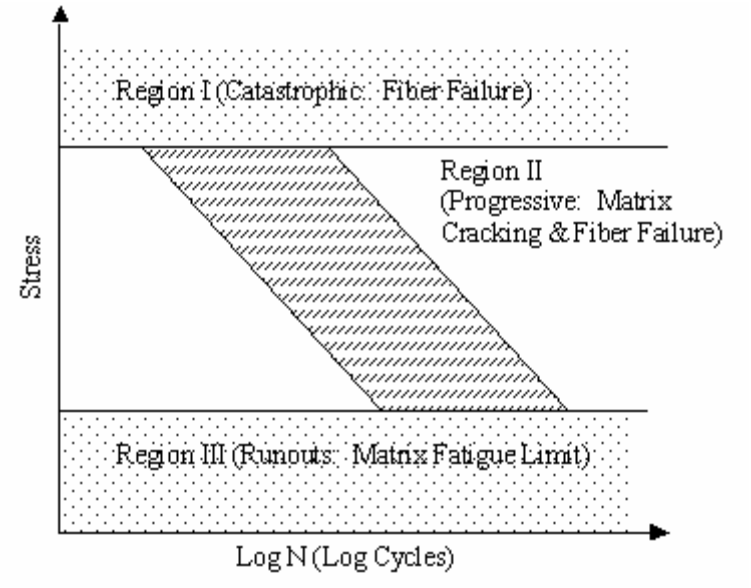

Figure 13: Typical S-N diagram

When plotting results from two different loading conditions (R = 0.1 and R = -1 in the present study), a shift in the tension-compression fatigue life curve down and to the left when compared with the tension-tension results can be observed. This is expected when fatigue life is plotted on a maximum stress basis. Note that for the tension-tension fatigue case (R = 0.1), the *stress range* is 90 percent of the maximum applied stress, while for the tension-compression fatigue case (R = -1), the *stress range* is twice the maximum applied stress. This would cause the tension-tension curve to shift down, while the tension-compression curve would shift up if plotted on a *stress range* basis. This phenomenon must be taken into consideration when comparing data generated at different loading conditions, or R-ratios.

In addition to fatigue life, the macroscopic evaluation can use the degradation of the modulus (E) or stiffness of the material to analyze the mechanical behavior of a failed specimen. The modulus is defined as the slope of the elastic portion of the stress-strain curve. This linear relation between stress and strain is known as Hooke's Law and is represented by the equation:

$$E = \sigma / \varepsilon \tag{1}$$

where:

E = Young's Modulus
σ = stress
ε = strain

If all testing is done in load-control, the maximum and minimum stresses on the specimen remain constant. Therefore, the only variable becomes strain and consequently, the modulus. When plotted, a single cycle takes on the characteristics of the linear

portion of the stress-strain curve. Each slope can then be referenced to the slope of the initial cycle to observe any changes in stiffness that may occur over the life of the specimen. If damage does occur, an increase in strain range will result. This increase in strain range will consequently show a decrease in modulus as the number of cycles increase. Although fatigue life and modulus degradation are strong indicators of damage, the exact nature of the damage can only be determined by microscopic analysis.

Fundamentals of Microscopic Behavior

While the macro-mechanical analysis looks at the trends in fatigue life testing, the microscopic analysis is a method to determine the cause of crack initiation as well as the type of crack progression throughout the specimen's life. Microscopic analysis in the current study is broken into two separate groups, damage and plasticity. Damage mechanisms include matrix cracks, fiber breaks, and fiber-matrix debonding. Plasticity includes slip band formation, crack nucleation and fatigue striations, which are similar to slip bands. The type of damage in each specimen is dependent not only on the material itself, but upon the applied stress level as well. An illustration of damage mechanisms in unidirectional composites is shown in Figure 14.

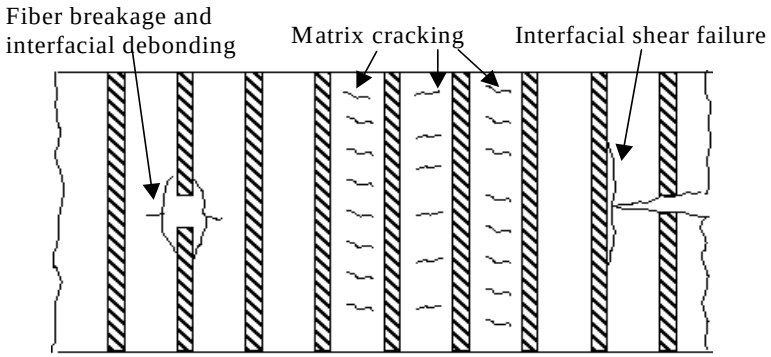

Figure 14: Fatigue damage mechanisms

Damage refers to the creation of new free surfaces from crack growth. When dealing with composites, these cracks may initiate in the matrix, the fibers, the fiber/matrix interfaces (reaction zones) or any combination of the three. Fiber cracking, and subsequently, fiber failure can have different interactions with the surrounding matrix, controlling the manner of crack propagation [4:300-301]. The crack can propagate through the matrix in a brittle manner. The surrounding matrix material can yield, blunting the crack and spreading the yield zone along the fiber. Finally, the fiber/matrix interface can fail and lead to debonding between the fiber and matrix. The latter prevents any load to be transferred to the matrix, greatly reducing the global strength. Extreme necking around debonded fibers shows catastrophic failure (or fiber overload) corresponding to Region I on the S-N diagram. Less necking indicates low interface strength caused by poor material processing.

The other damage mechanism, plasticity, includes the formation of slip bands and fatigue striations as well as microvoid coalescence. Slip is defined as the parallel movement of layers of material in a crystal past adjacent layers [4:122-127]. As a crack propagates along these slip planes, it may leave behind regions of depression and elevation called striations. These striations run perpendicular to the crack growth direction and the spacing between them is useful in measuring the amount of crack growth per fatigue cycle [1:543-545]. In addition to showing the direction of crack growth, they also indicate the location of the crack initiation site as well.

Microvoid coalescence is another indicator of plastic behavior. Also associated with slip, these voids are formed by the separation of the material internally [4:137-152].

Once they form, the connecting material continues to deform by slip. This expands the voids, which then connect to form the fracture surface. More ductile in nature, microvoid coalescence appears as cusps (or dimples) on the fracture surface.

The methods used in this study to observe these failure mechanisms include both optical and scanning electron microscopes (SEM). Through the examination of the sectioned specimens and fracture surfaces, the deformation mechanisms related to the fatigue behavior of F/G TMCs may be fully characterized. In the SEM pictures to follow, each outlined area is shown at a higher magnification in the following fractograph.

Monotonic Tensile Test Results

The first measurement taken from a monotonic tensile test is the modulus of the material. This modulus is a measure of how stiff the material is. For a given applied stress, the material will strain a proportionate amount. Initially, this relation is linear in the elastic region. As mentioned before, the modulus is defined as the slope of the linear portion of the stress-strain curve.

The other measurement taken is the ultimate strength of the material. Just as its name implies, it is the highest stress value reached before failure occurs. The results from the extensometer and load measurements for the three materials are shown in Figure 15 and summarized in Table 1.

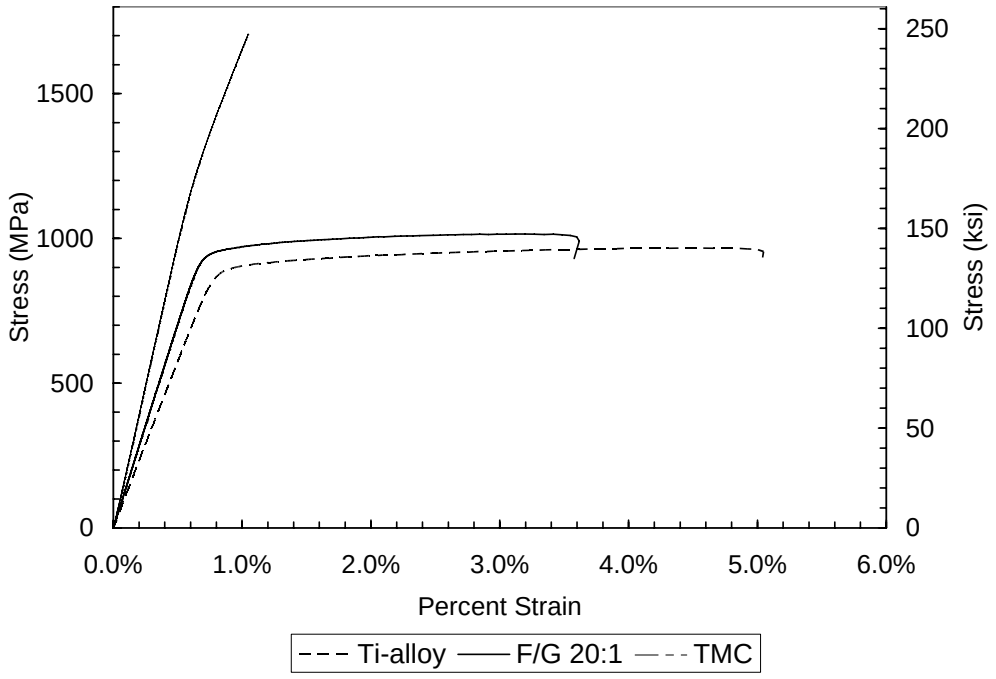

Figure 15: Tensile test results

Table 1: Tensile Test Results

Spec. #	Material	Modulus (E)* GPa (Msi)	Miller's data (E) GPa (Msi)	Ult. Strength MPa (ksi)	Miller's data (Ult.) MPa (ksi)
TMC-001	TMC	196 (28)	210 (30.5)	1273 (185)	1655 (240)
FG-001	F/G(20:1)	141 (20)	146 (21.2)	1014 (147)	945 (137)
Ti-001	Alloy	115 (17)	110 (16.0)	967 (140)	1000 (146)

***** *Values shown calculated from extensometer measurements*

Titanium Alloy (Ti-6Al-4V) Results

The values obtained for the modulus and ultimate strength of the titanium alloy came within five percent of the values found in Miller's research [15], showing good repeatability. Failure occurred outside the gage area (see Figure 16) and the results were lower than previous studies of Ti-6Al-4V material produced via powder metallurgy [22].

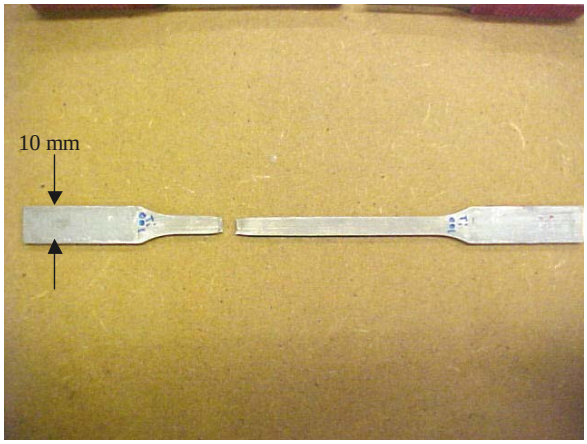

Figure 16: Specimen Ti-001, monotonic tensile test failure location

Titanium Matrix Composite (Ti-6Al-4V/SCS-6) Results

The value obtained for the modulus of the TMC was seven percent lower than that found in Miller's research [15], while the ultimate strength was 23 percent lower. This is due in part to the fact that Miller used a composite composed of Trimarc fibers rather than the Sigma (or SCS-6) fibers used in the present study. Because of this material mismatch, the results for the functionally-graded material may be affected. Failure occurred within the gage area as is shown in Figure 17.

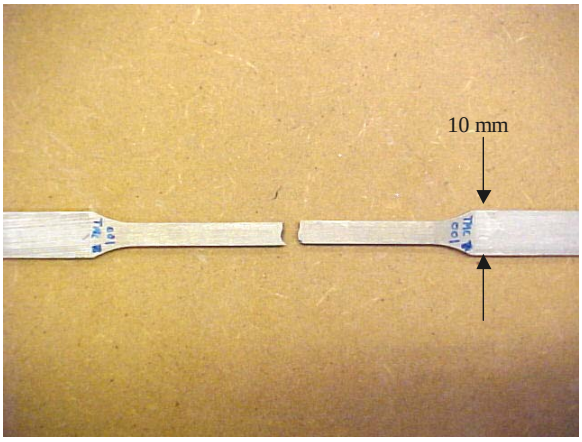

Figure 17: Specimen TMC-001, monotonic tensile test failure location

Functionally-Graded Material (20:1 taper ratio) Results

The value obtained for the modulus of the functionally-graded material was three percent lower than that found in Miller's research [15], while the ultimate strength was seven percent higher. Again, the fiber mismatch is duly noted. Failure occurred in the alloy region (see Figure 18), which deserves some explanation. The expected weakest section in the functionally-graded material is the joint. However, if the joint holds then the material can only be as strong as its weakest link. In the present case, the weakest link is the titanium alloy, which is why failure occurred here rather than at the taper. Nevertheless, the data shows an increase in both stiffness and ultimate strength when compared with the pure alloy, showing the addition of the strength enhancing effects of the TMC on a global scale.

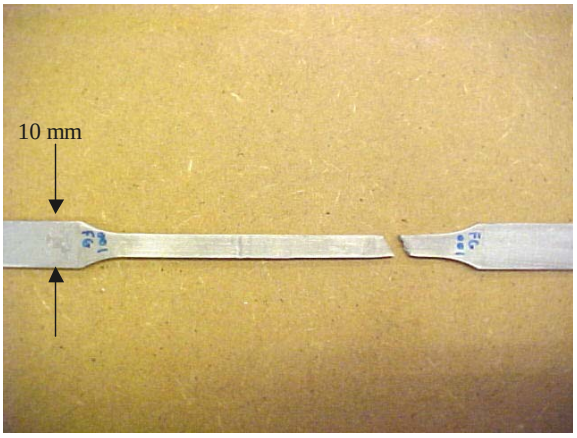

Figure 18: Specimen F/G-001, monotonic tensile test failure location

Tensile Test Comparison of Results

The results obtained from the composite and alloy materials provide the upper and lower bounds, respectively, for the functionally-graded material. Using the rule of

mixtures formula, the longitudinal modulus of a unidirectional composite lies between the moduli of the fiber and the matrix and is given by the equation:

$$E_L=E_fV_f+E_m(1-V_f) \quad (2)$$

where:

E_L = longitudinal modulus of composite
E_f = longitudinal modulus of fiber
E_m = longitudinal modulus of matrix
V_f = fiber volume fraction

Since the alloy used is the same as the matrix of the composite, we can rearrange the equation to be representative of the taper region in the functionally graded material:

$$E_t=E_cV_c+E_a(1-V_c) \quad (3)$$

Where:

E_t = longitudinal modulus of taper region
E_c = longitudinal modulus of pure composite
E_a = longitudinal modulus of pure alloy
V_c = composite volume fraction

When simply looking at the whole taper region, the volumes for the alloy and composite sections are both one-half of the total volume. This would estimate the modulus for the taper region to be exactly halfway between the moduli for the pure alloy and pure composite. In the present research, this value is calculated as 155 GPa, which is about nine percent higher than the measured value of 141 GPa. This is an acceptable difference from the theoretical value, which proved to be an accurate representation of the stiffness on a global scale. However, upon examining the ply lay-up of the taper region, a better approximation can be made. The taper section follows a “stair-step” pattern (see Figure

19) where each step encompasses a different region with differing volume fractions of composite.

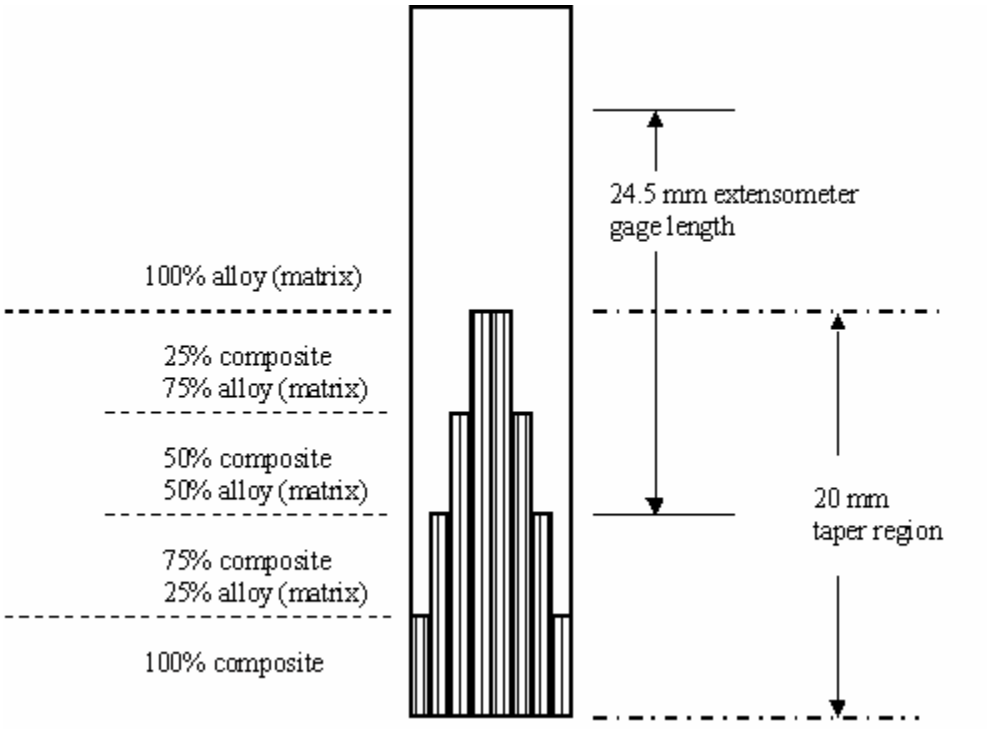

Figure 19: Taper section

Simply noticing that the tip of the taper region was approximately centered within the gage length can make a further improvement. Using the same analogy as above, this is equivalent to a composition of about 81.25% alloy and 18.75% composite within the gage section. This would calculate the stiffness at 130 GPa, bringing the measured value to within eight percent. By looking at the taper region's stiffness *locally*, it becomes apparent that the modulus changes with each "stair-step" and is a closer representation of the results found on a *global* scale.

Macro-Mechanical Analysis

Tension-tension Fatigue Results

As mentioned before, all tests were performed under room temperature condition. The stress, strain and fatigue life for the tension-tension tests are summarized in Table 2 and the fatigue life data is plotted on a maximum-stress basis in Figure 20.

Table 2: Tension-Tension Fatigue Test Results

Spec. #	Max Stress (MPa)	Stress Range (MPa)	Cycles to Failure
F/G-02	368.00	331.20	526182
F/G-01	495.00	445.50	58872
F/G-03	552.00	496.80	35242
F/G-10	800.00	720.00	7470
Ti-02	300.00	270.00	>1677668
Ti-04	400.00	360.00	116659
Ti-01	495.00	445.50	42278
Ti-03	600.00	540.00	22917
Ti-10	800.00	720.00	5917
TMC-02	662.00	595.80	3355745
TMC-11	750.00	675.00	299873
TMC-01	827.50	744.75	118853
TMC-03	993.00	893.70	36354
TMC-10	1200.00	1080.00	14646

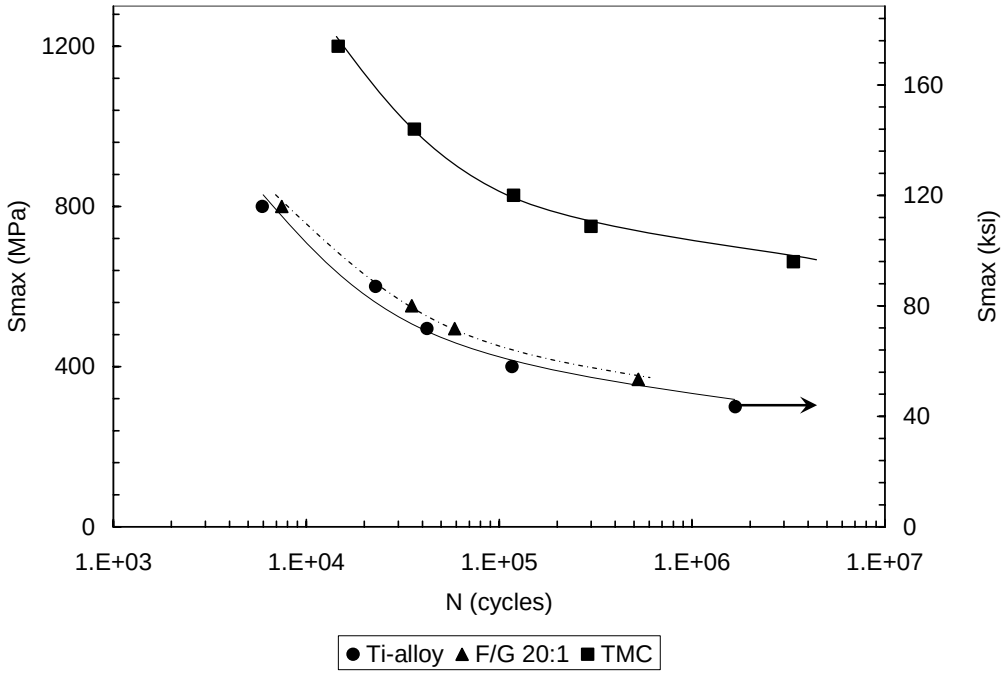

Figure 20: Tension-tension S-N curves

Tension-tension Macro-mechanical Evaluation of alloy (Ti-6Al-4V)

The fatigue life curve for the titanium alloy under tension-tension fatigue from the present work is shown in Figure 21 and is also compared with Miller's results [15]. These results form the lower bound for the functionally-graded material.

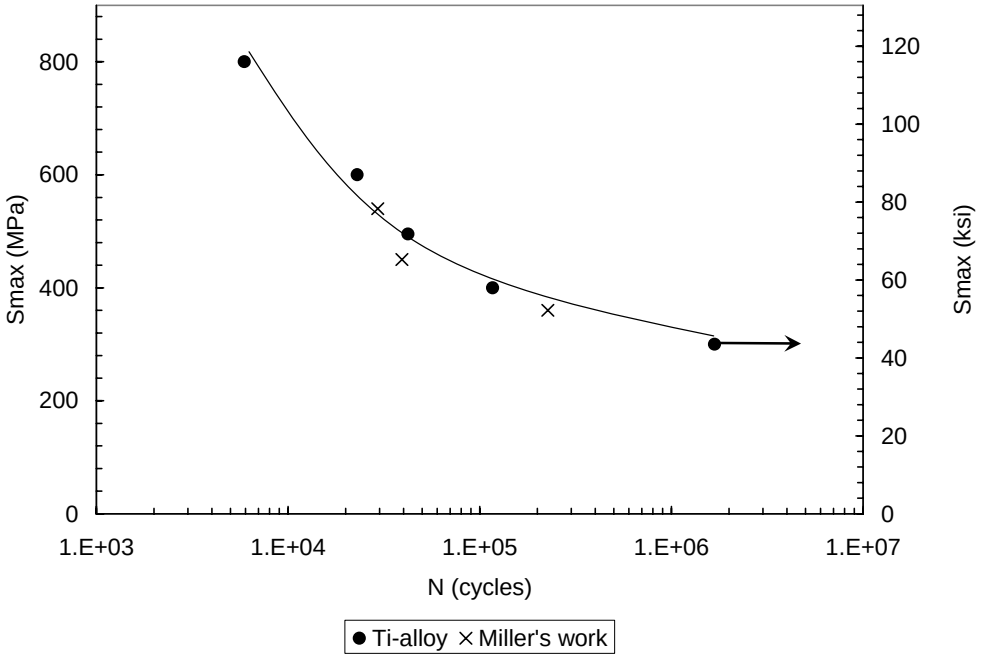

Figure 21: Titanium alloy comparison of tension-tension fatigue results

The alloy used in the present study showed similar results when compared with the alloy used in the work done by Miller [15]. The similarity of the materials as well as their form of processing is apparent from the figure.

Tension-tension Macro-mechanical Evaluation of TMC (Ti-6Al-4V/SCS-6)

The fatigue life curve for the composite under tension-tension fatigue produced similar results when compared with previous data [18]. A plot comparing Miller's results with the present work is shown in Figure 22.

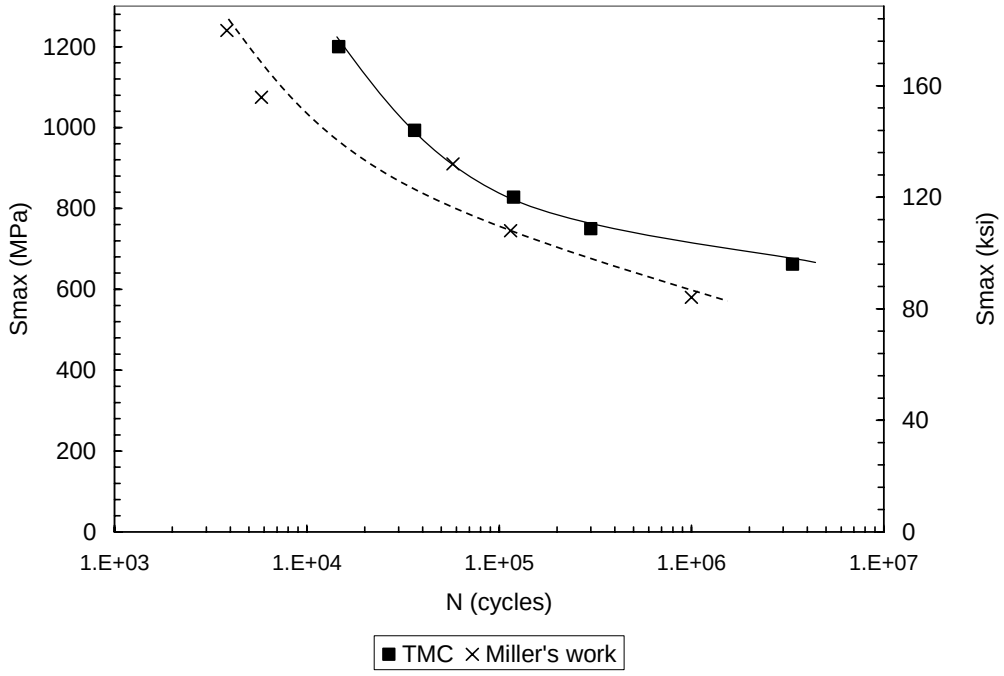

Figure 22: TMC comparison of tension-tension fatigue results

The material used in the present study seemed to display higher fatigue life characteristics when compared with Miller's data [15]. This is as expected in this case due to the different fibers used in the two studies. The SCS-6 fiber has a higher strength than the Trimarc 1 fiber explaining the apparent increase in fatigue life. This data forms the upper bound for the functionally-graded material.

Tension-tension Macro-mechanical Evaluation of F/G TMC (20:1 taper ratio)

The results for the functionally-graded material under tension-tension fatigue showed higher fatigue lives when compared with Miller's data [15]. It should be noted that Miller also performed tests on a F/G TMC with a taper ratio of 4:1, however the present work is focused on the 20:1 taper ratio. A plot comparing Miller's results with the present work is shown in Figure 23.

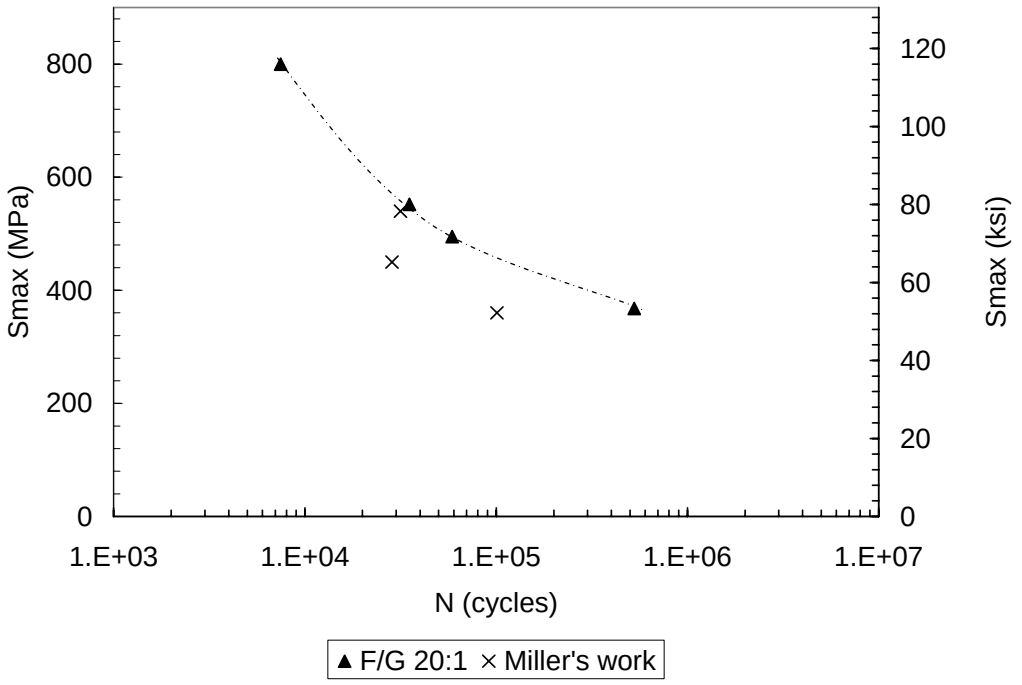

Figure 23: F/G TMC (20:1) comparison of tension-tension fatigue results

Again, the material used in the present study seemed to display higher fatigue life characteristics when compared with Miller's data [15]. Since the composite material in the present study demonstrated higher fatigue life curves than that used in Miller's work, it is no surprise that the F/G material shows a similar trend. Also, all of the 20:1 F/G specimens in the work done by Miller failed in the alloy region [15], thus making it difficult to analyze the characteristics of the joint region. In the present study, two out of the four F/G specimens failed in the taper region, while the other two failed in the alloy section. F/G-02 and F/G-03 both failed in the taper region near the tip. This will be investigated further in the microscopic analysis.

As mentioned earlier, indicators of damage include changes in stiffness and strain throughout the life of the specimen. This is shown below for the functionally-graded

material. Figure 24 and Figure 25 show plots of the normalized stiffness versus cycle number and normalized fatigue life, while Figure 26 and Figure 27 show plots of the percent strains versus cycle number and normalized fatigue life.

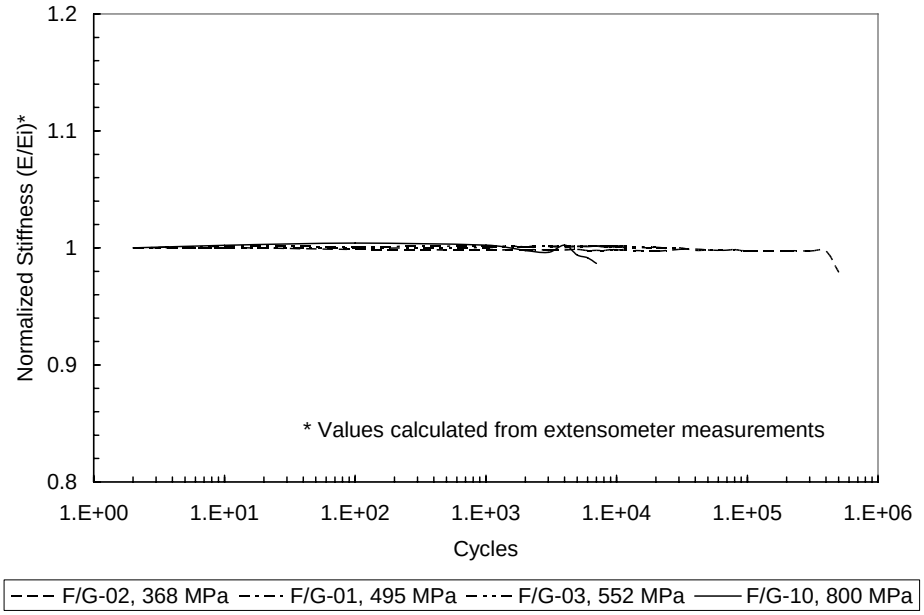

Figure 24: Tension-tension: normalized stiffness vs. fatigue cycles

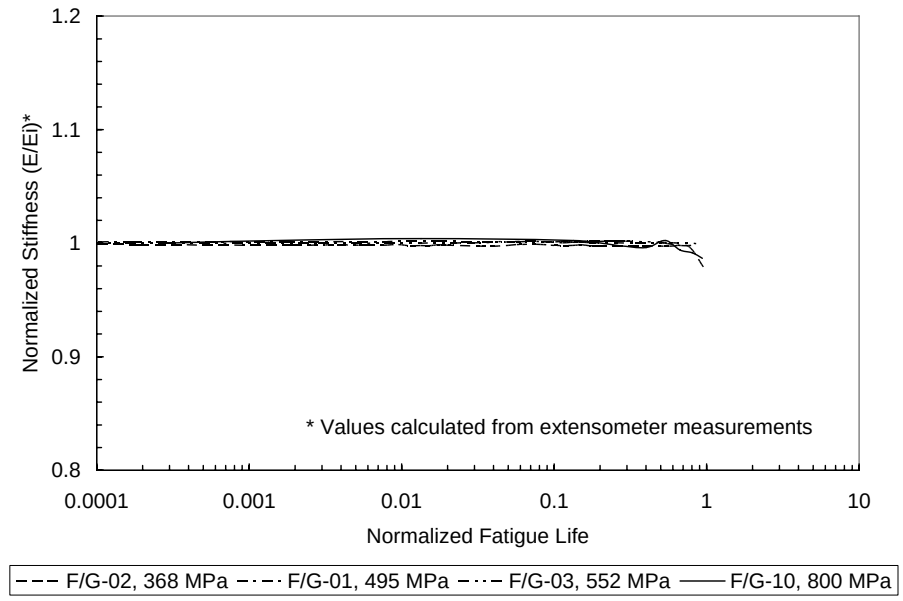

Figure 25: Tension-tension: normalized stiffness vs. normalized fatigue life

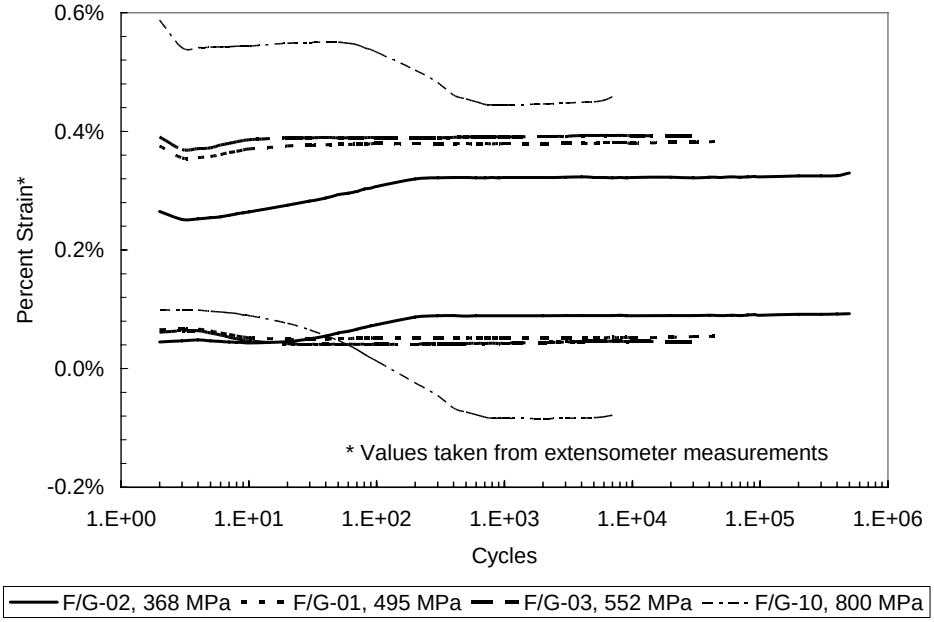

Figure 26: Tension-tension: max & min percent strain vs. fatigue cycles

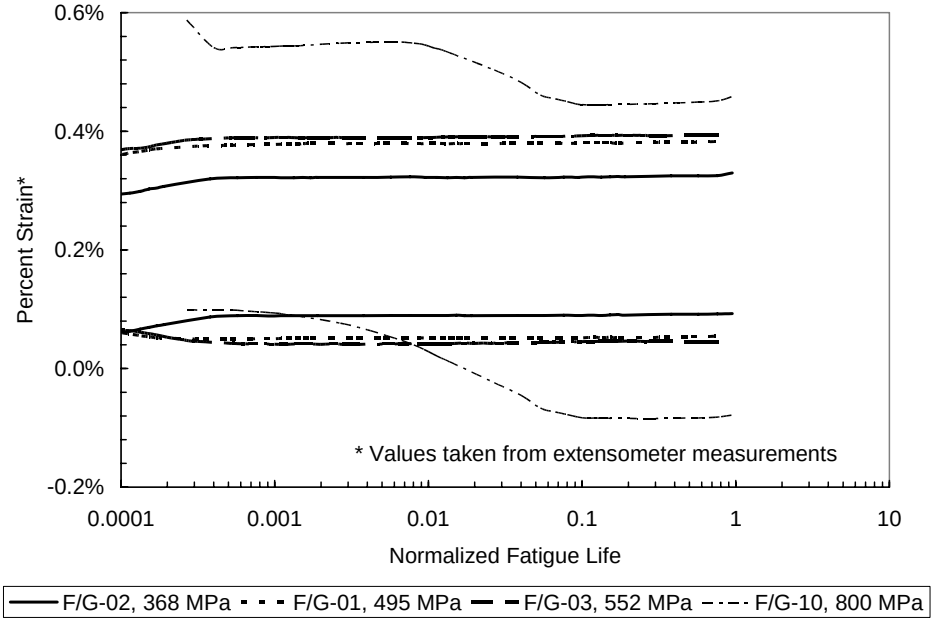

Figure 27: Tension-tension: max & min percent strain vs. normalized fatigue life

With the exception of specimen F/G-10, all specimens show relatively steady strain values over their respective lives. The apparent decrease in strain values for specimen F/G-10 can be explained by noting that this specimen represents the highest stress level tested in this group. At this high stress level, the extensometer has a greater tendency to slip, therefore skewing the results and showing a decrease in strain values. This is further explained by looking at the strain *range.* If damage were occurring within the specimen, the strain range, or the difference between the max and min values, would increase over time. (Not to mention that the individual max and min strain values would show an increase and decrease, respectively, over the life of the specimen.) This lack of strain range increase supports the previous plots of modulus vs. life, which indicate that plasticity, and not damage, is the governing failure mechanism. Similar plots using the

strain gage measurements can be found in the appendix as well as comparisons with the extensometer measurements.

Tension-tension Macro-mechanical Evaluation (Comparison of Results)

The fatigue life curve for the F/G material (reference Figure 20) shows a slight increase from the alloy. This increase in fatigue life, along with the increase in stiffness and ultimate strength shown from the tensile tests, shows that the alloy is benefiting from the composite section by way of the taper region. In addition, the plots of modulus and strain values vs. time both show no degradation in material characteristics over the life of the specimen. This indicates that plasticity, and not damage, is the major deformation mechanism. However, the micro-mechanical evaluation will provide more solid evidence to support this theory.

Tension-compression (Fully-Reversed) Fatigue Results

Again, all tests were performed under room temperature condition. The stress, strain and fatigue life for the tension-compression tests are summarized in Table 3 and the fatigue life data is plotted on a maximum-stress basis in Figure 28. Similar to the tension-tension case, the F/G material shows a slight increase in fatigue life when compared to the pure alloy. Although there is no data for which to compare the tension-compression results as was done for the tension-tension case, a brief discussion of the tension-compression results compared with those of the tension-tension case is provided below.

Table 3: Tension-compression fatigue test results

Spec. #	Max Stress (MPa)	Stress Range (MPa)	Cycles to Failure
F/G-08	250.00	500.00	153054
F/G-05	331.17	662.34	88922
F/G-04	414.00	828.00	44946
F/G-06	496.83	993.66	24101
F/G-09	650.00	1300.00	6442
Ti-08	250.00	500.00	209926
Ti-06	362.48	724.97	53341
Ti-05	453.10	906.21	39035
Ti-07	543.72	1087.45	14424
Ti-09	650.00	1300.00	6709
TMC-08	325.00	650.00	>5000000
TMC-05	595.79	1191.59	46934
TMC-04	744.76	1489.52	20955
TMC-06	893.72	1787.45	11117

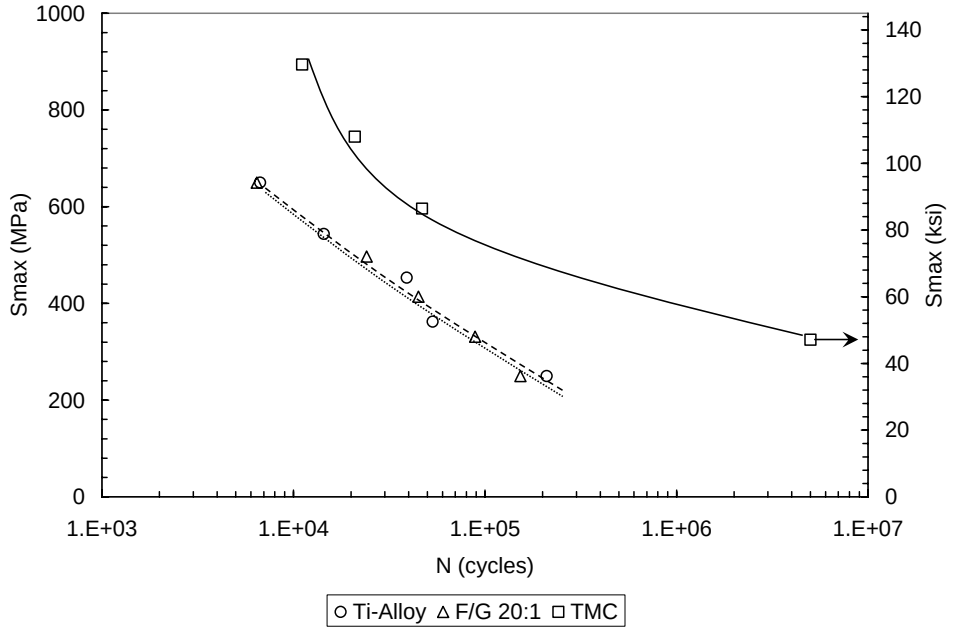

Figure 28: Tension-compression S-N curves

The fatigue life curve for the titanium alloy under tension-compression fatigue is shown in Figure 29. These results form the lower bound for the functionally-graded material under fully-reversed fatigue loading. As expected, when plotted on a maximum stress basis, the results show a shift in the fatigue life curve down and to the left when compared with the tension-tension results.

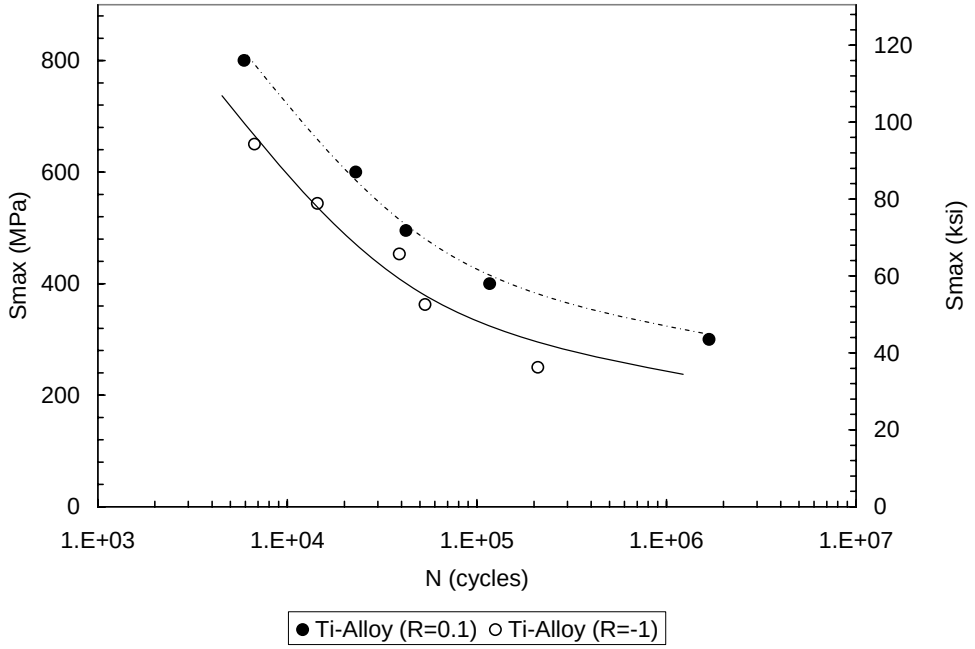

Figure 29: Titanium alloy TT and TC fatigue results (maximum stress comparison)

The effects of compression on the plastic zone surrounding a crack tip can explain this reduction in fatigue life under tension-compression loading. According to Broek [3:57-60], tension loading in metals forces the size of the plastic zone to increase as slip occurs. The crack tip is then blunted by work hardening and increasing stress. When the unloading portion of the cycle takes place, the elastic material around the plastic zone causes compressive forces resulting in reverse slip, thereby re-sharpening the crack tip.

If the cycle continuously applies a compressive force (as in the fully-reversed case here), this effect may be enhanced. Greater stress concentrations, resulting in increased sharpening of the crack tip, ultimately makes crack growth easier in tension-compression fatigue than in the pure tensile case.

However, when plotted on a stress range basis, a different phenomenon occurs (see Figure 30). The tension-compression fatigue lives are much longer than the tension-tension fatigue lives when plotted on a stress range basis. This would conclude that, while additional damage does occur during the compressive loading portion (representing half of the load range in the tension-compression case), it is not as detrimental to the fatigue life as a load range made up of tensile loads equal to twice the compressive range value.

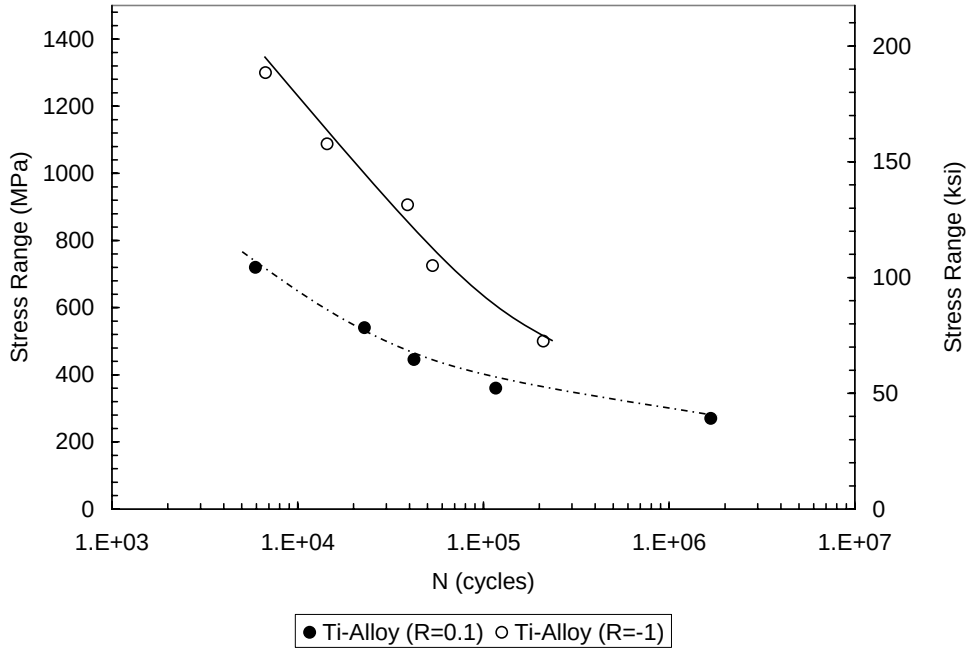

Figure 30: Titanium Alloy TT and TC fatigue results (stress range comparison)

Tension-compression Macro-mechanical Evaluation of TMC (Ti-6Al-4V/SCS-6)

The fatigue life curve for the composite under tension-compression fatigue is compared to the results from the tension-tension case on a maximum stress basis in Figure 31. This data forms the upper bound for the functionally-graded material under fully-reversed fatigue loading.

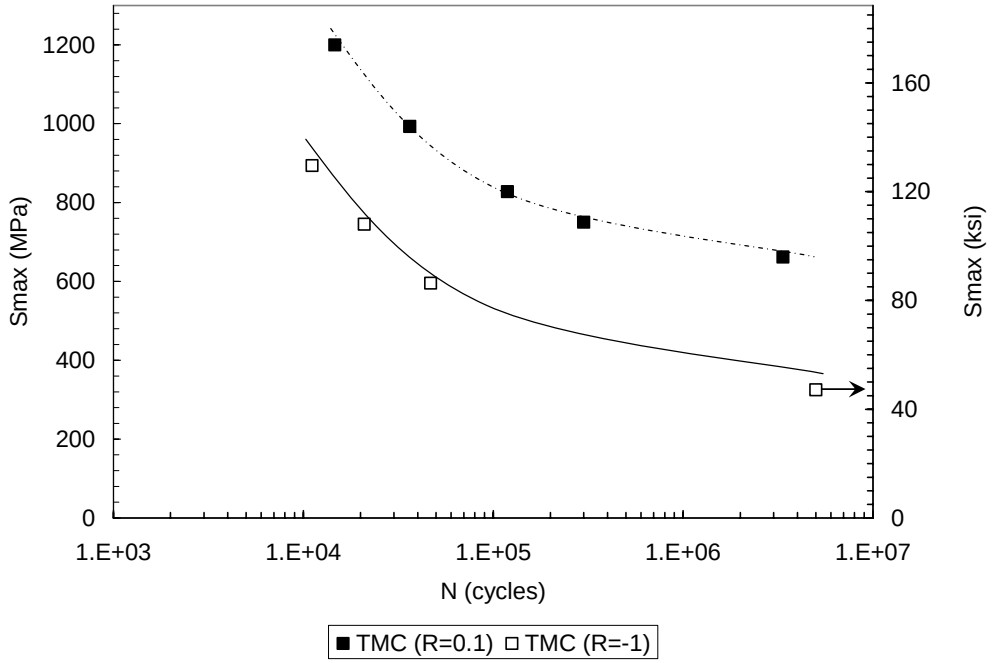

Figure 31: TMC TT and TC fatigue results (maximum stress comparison)

Again, when plotted on a maximum stress basis, the results show a shift in the fatigue life curve down and to the left when compared with the tension-tension results. This reduction in fatigue life under tension-compression loading can be explained by looking at the role of the fibers in the composite. Kraabel [12] noticed this same phenomenon when testing an SCS-6/Ti-15-3 unidirectional composite. He found that compression-induced effects such as fiber buckling and delamination reduced the

dominance of the fibers in determining fatigue life. He also stated, "The role of fibers in determining failure, the relatively slow speed of damage propagation, and the presence of fiber bridging under tension-compression suggest that fibers play an important role in hindering matrix crack propagation under tension-tension fatigue loading." This explains the results found in this study.

The fatigue lives for the tension-compression fatigue case are plotted on a stress range basis in Figure 32. As before, the tension-compression fatigue lives are much longer than the fatigue lives of the tension-tension case.

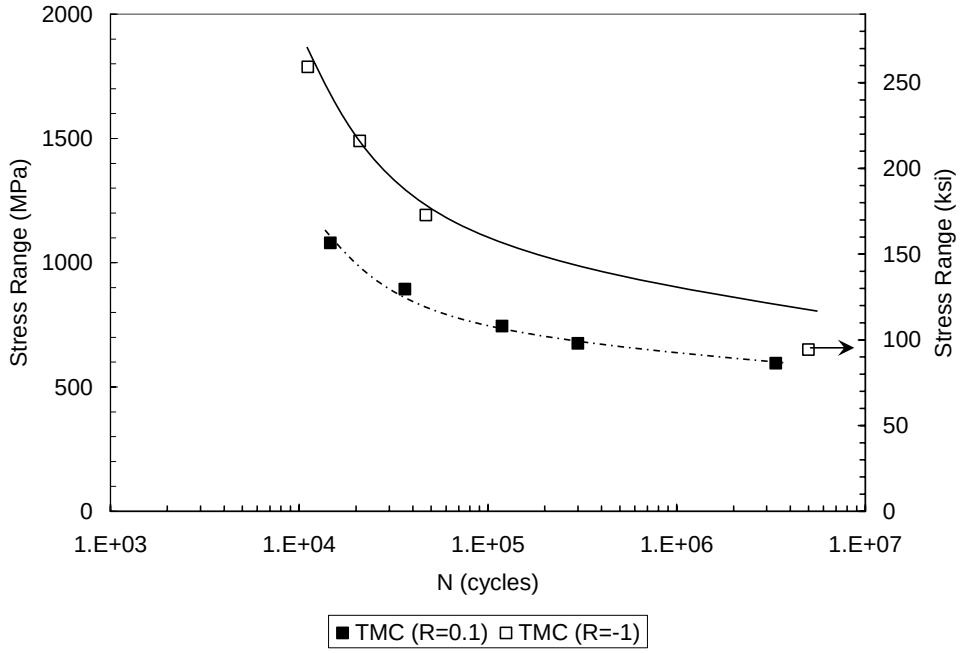

Figure 32: TMC TT and TC fatigue results (stress range comparison)

Another explanation can be found by looking at the mean stresses present in each case. Mean stress is defined as the average of the maximum and minimum stresses:

$$\sigma_m = (\sigma_{max} + \sigma_{min})/ 2 \quad (4)$$

This would result in a mean stress of zero for the fully reversed case and a positive, tensile mean stress for the tension-tension case. Thus, it is evident that the positive mean stresses present in tension-tension fatigue are detrimental to the fatigue life of the material.

Tension-compression Macro-mechanical Evaluation of F/G TMC (20:1 taper ratio)

The fatigue life curve for the functionally-graded material under tension-compression fatigue showed a slight increase when compared with the pure alloy. A plot comparing the tension-tension results with the tension-compression results on a maximum stress basis is shown in Figure 33.

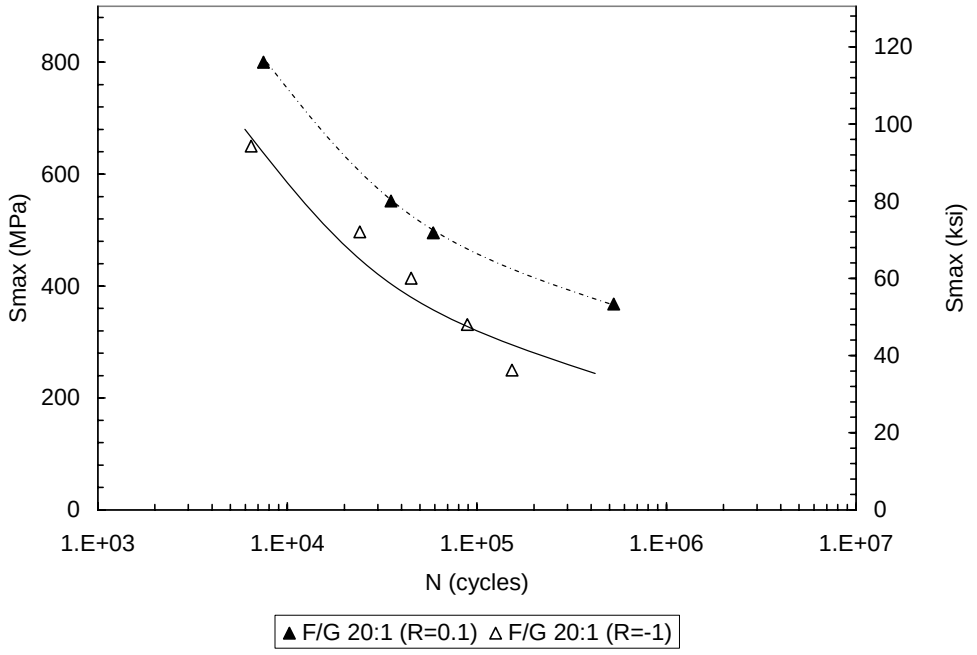

Figure 33: F/G TMC (20:1) TT and TC fatigue results (max. stress comparison)

Again, when plotted on a maximum stress basis, the results show a shift in the fatigue life curve down and to the left when compared with the tension-tension results.

This reduction in fatigue life under tension-compression loading can be attributed to additional damage resulting from the compressive portion of the loading cycle. According to Broek [3:57-60], compression loading in metals creates intrusions or extrusions that may grow into cracks. In tension-tension, the presence of residual compressive stresses during load release may still cause the formation of intrusions, however the mechanism for forming them is much weaker. These formations may have occurred at the fiber ends in the functionally-graded material causing matrix cracking to dominate the failure. Therefore, these same processes could very well have been occurring in this study.

The results are plotted on a stress range basis in Figure 34. Again, the fatigue lives for the tension-compression case are longer than the fatigue lives for the tension-tension case. These results support the observation that the tensile mean stresses present in tension-tension fatigue are detrimental to the fatigue life of the material, while the compressive loading portion is actually beneficial.

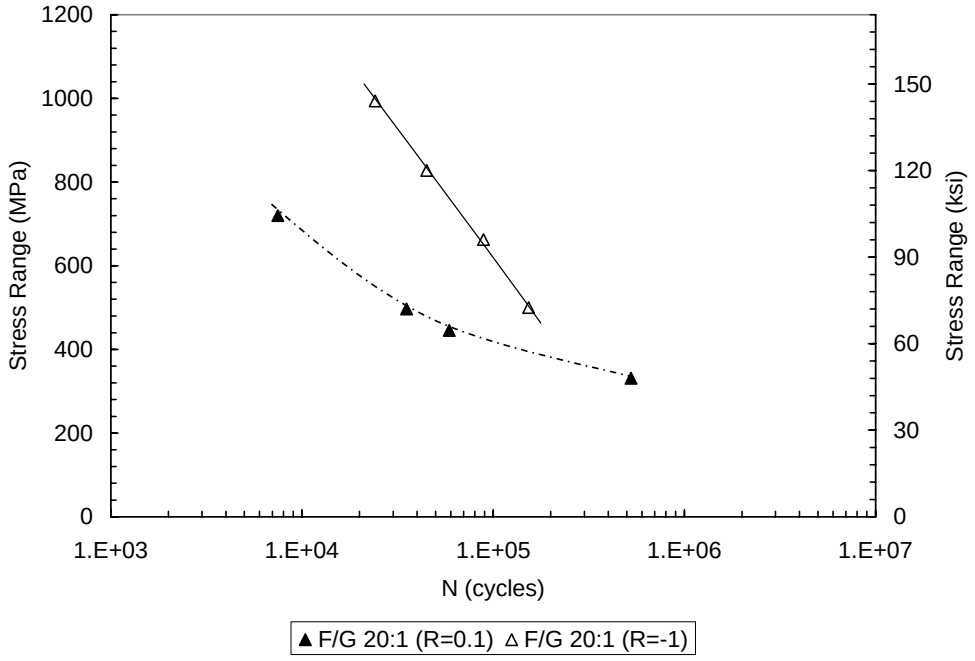

Figure 34: F/G TMC (20:1) TT and TC fatigue results (stress range comparison)

It should be noted at this point that three of the five F/G specimens failed in the taper region, while the other two failed in the alloy section. F/G-06, F/G-08 and F/G-09 all failed in the taper region at or near the tip. This will be investigated further in the microscopic analysis.

Again, normalized stiffness and percent strain histories are plotted below for the functionally-graded material. Figure 35 and Figure 36 show plots of the normalized stiffness versus cycle number and normalized fatigue life, while Figure 37 and Figure 38 show plots of the percent strains versus cycle number and normalized fatigue life.

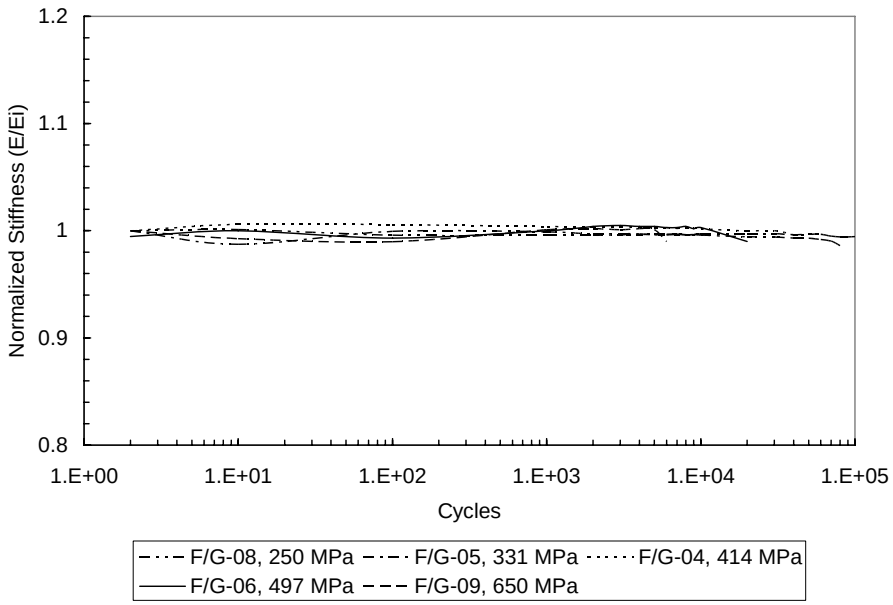

Figure 35: Tension-compression: normalized stiffness vs. fatigue cycles

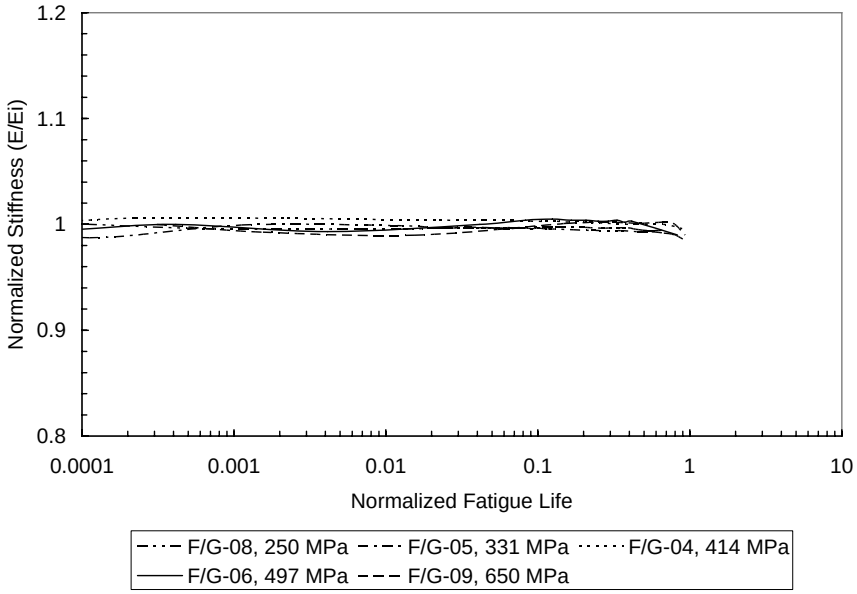

Figure 36: Tension-compression: normalized stiffness vs. normalized fatigue life

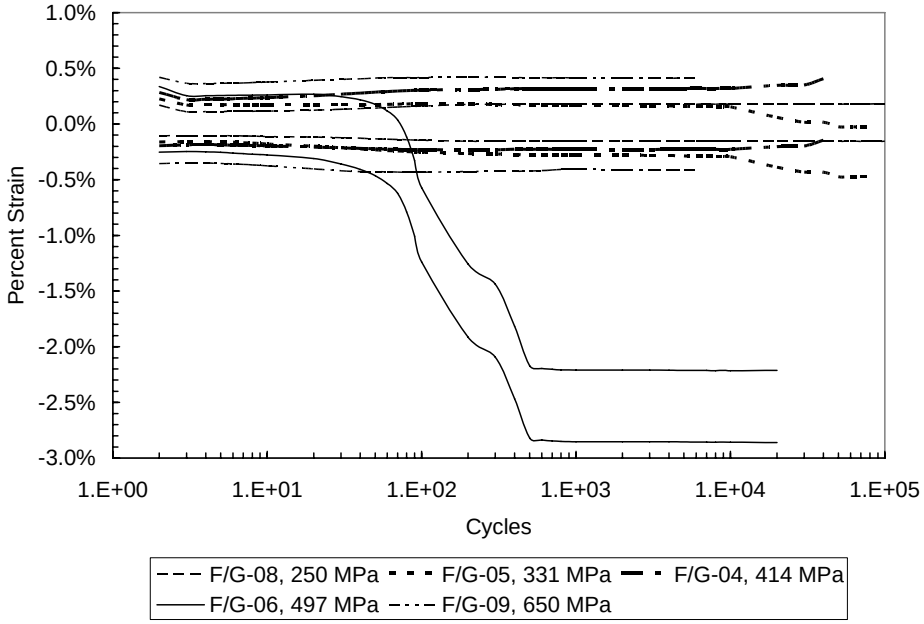

Figure 37: Tension-compression: percent strain vs. fatigue cycles

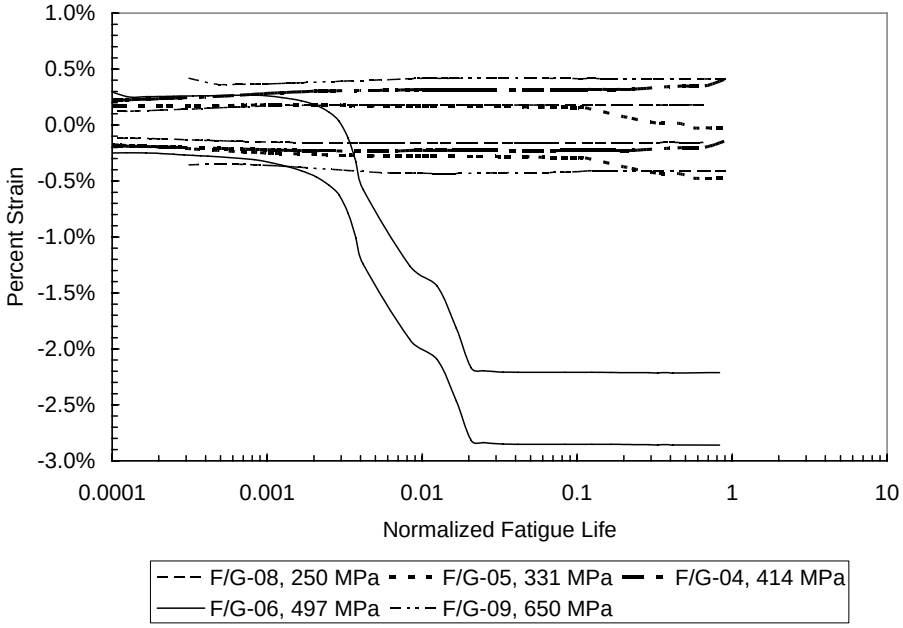

Figure 38: Tension-compression: percent strain vs. normalized fatigue life

With the exception of specimen F/G-06, all specimens show relatively steady strain values over their respective lives. The apparent decrease in strain values for specimen F/G-06 can again be explained by noting that this specimen represents one of the highest stress levels tested in this group. As was noticed in the tension-tension case, this is most likely due to the extensometer slipping during the test. Again, the strain range appears to remain constant and this is further supported by the previous plots of modulus vs. life which indicate that plasticity, and not damage, is the governing failure mechanism.

Tension-compression Macro-mechanical Evaluation (Comparison of Results)

The fatigue life curve for the F/G material in this case shows little increase when compared to that of the pure alloy (reference Figure 28). It is also noted that the *amount* of shift in the fatigue life curve is similar in the pure alloy and functionally graded materials, especially when compared to the greater amount of shift in the pure composite material. This, along with the plots of modulus and strain values vs. time showing no degradation in material characteristics over the life of the specimen, is another indicator that matrix plasticity, and not damage, is the major deformation mechanism. Again, the microscopic evaluation will provide more solid evidence to support this observation.

Microscopic Analysis

Monotonic Tensile Tests Microscopic Evaluation

The fracture surface for the alloy revealed mechanisms associated with plasticity (see Figure 39). Voids were clearly visible and the rough, dimpled surface indicates ductile failure. The slant fracture shows shear failure representative of a state of plane

stress [4:92-100]. Normally the stress distribution makes the center of the specimen susceptible to crack initiation. In this case however, the presence of pores in the material may have resulted in the failure shown (see Figure 40).

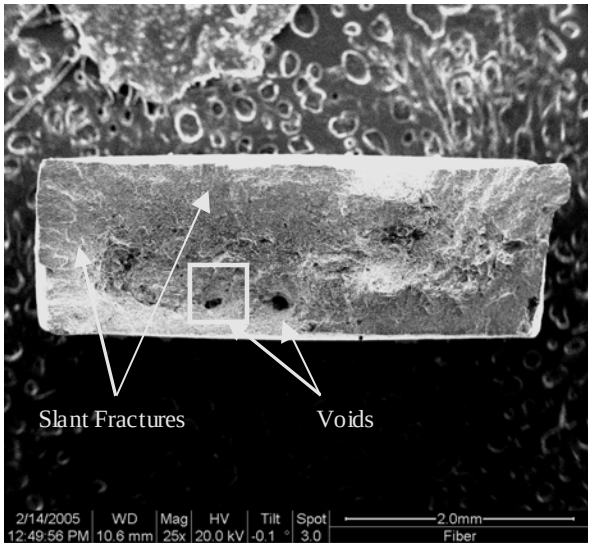

Figure 39: Specimen Ti-001, fracture surface from tensile test

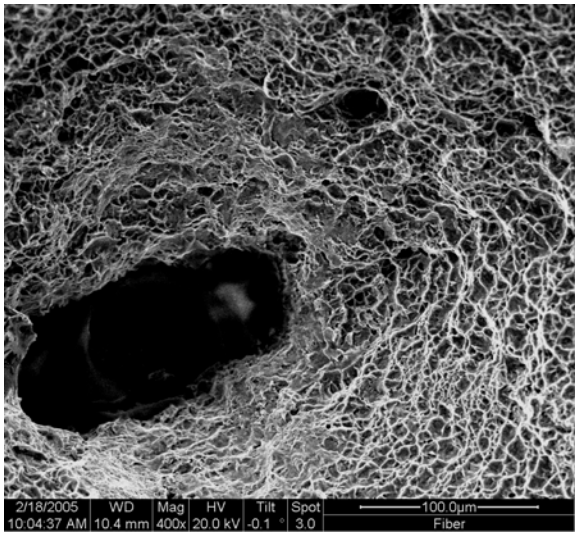

Figure 40: Specimen Ti-001, close-up showing pore and ductile void coalescence

The fracture surface for the composite showed evidence of fiber fracture and fiber pullout (see Figure 41). In order for failure to occur in a unidirectional composite where loading is in a direction parallel to the fibers, all fibers across the cross section must fracture [4:293-305]. The relative contributions of plasticity and damage can be seen in Figure 42. As discussed earlier, pores in the matrix material are prone to form voids representative of a plasticity failure mechanism. As the matrix fails, the load is then transferred to the fibers that ultimately fail either by fiber cracking, debonding or pullout, all of which are representative of damage.

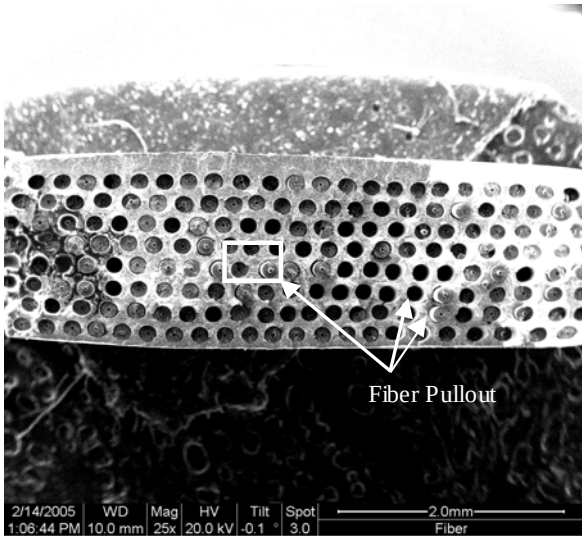

Figure 41: Specimen TMC-001, fracture surface from tensile test

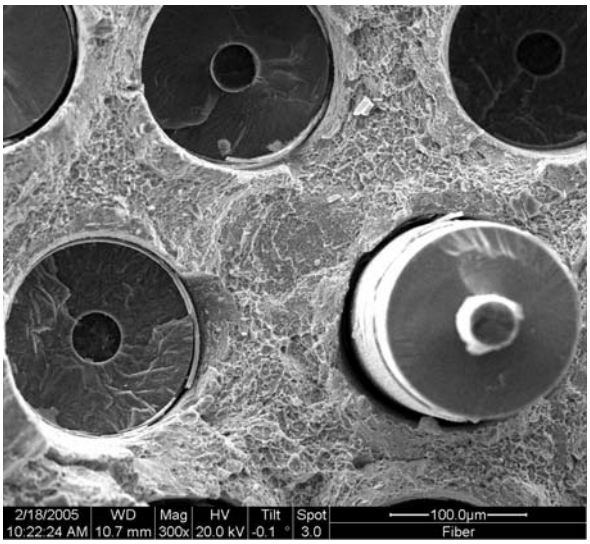

Figure 42: Specimen TMC-001, close-up showing fiber pullout & matrix ductility

The fracture surface of the functionally-graded material is shown in Figure 43. Since failure occurred in the alloy section, the mechanisms associated with the failure are similar to those discussed for the pure alloy specimen. This time the slant fracture can be seen on both sides of the specimen, indicating initial failure near the center. Again, the rough dimpled surface representative of ductile failure can be seen (see Figure 44).

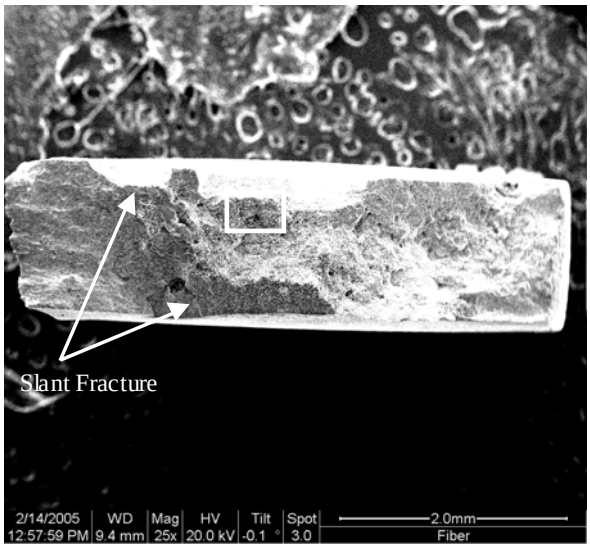

Figure 43: Specimen F/G-001, fracture surface from tensile test

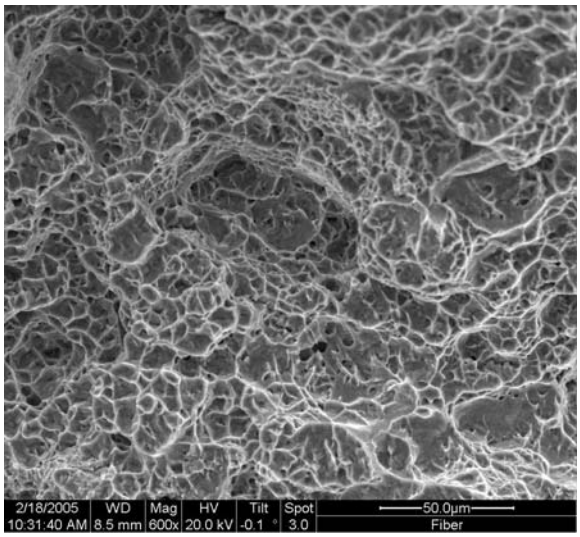

Figure 44: Specimen F/G-001, ductile void coalescence

Tension-tension Microscopic Evaluation of the alloy (Ti-6Al-4V)

Of the five pure alloy specimens tested, only one of them (Ti-03) failed in the gage section (see Figure 45). Specimen Ti-02 was stressed below the fatigue limit for the material and had no failure, while Ti-04, Ti-01 and Ti-10 all failed near the shoulder.

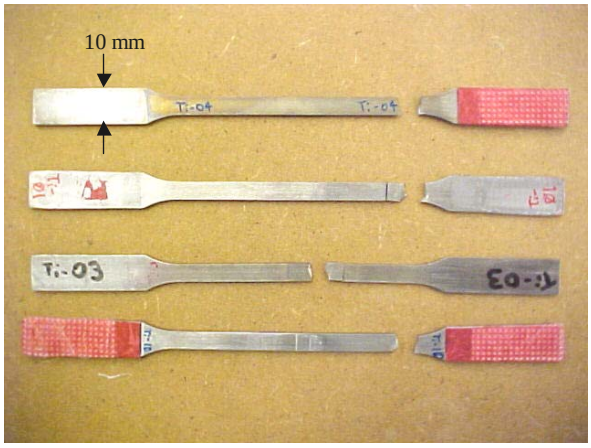

Figure 45: Ti-alloy tension-tension fatigue failure locations

(From Top: Specimens Ti-04, Ti-01, Ti-03 & Ti-10)

Regardless of this fact, the alloy specimens all had similar failure characteristics. From the overall view of the fracture surface, the transition from the fatigue crack propagation region and the final overload region could be distinguished and the point of crack initiation could be narrowed down to the flat, brittle crack face away from the more ductile, overload region (see Figure 46). Upon closer examination of this area, the crack initiation site seemed to be the edge of the specimen where stress raisers are present (see Figure 47).

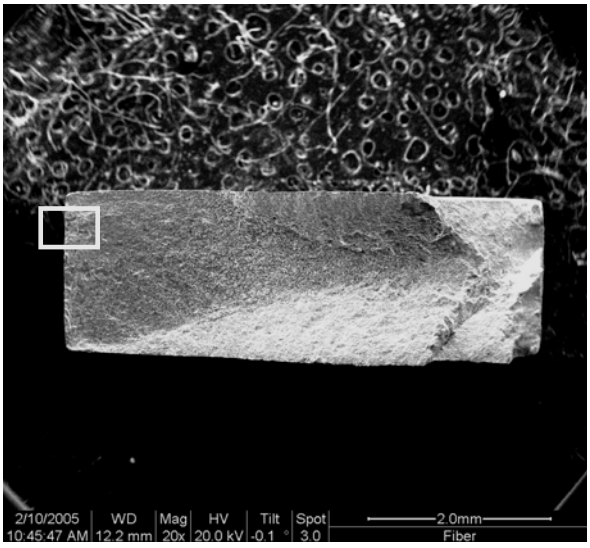

Figure 46: Specimen Ti-03, overall view of fracture surface

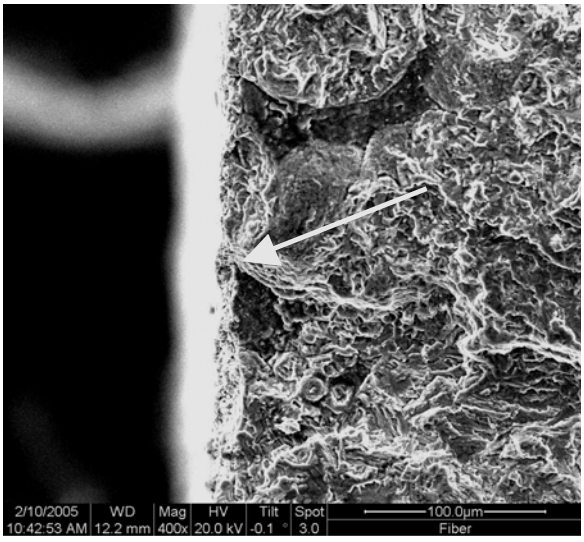

Figure 47: Specimen Ti-03, close-up of crack initiation site

In the pure alloy specimens, fatigue cracks would sometimes originate from stress raisers such as pores or "gaps" which formed during the manufacturing process. These results are common since "powder materials have a relatively fine-grain β-phase, which despite the presence of residual pores, makes for quite a high fatigue limit" [8]. These flaws were easily seen under the SEM at the crack initiation site (see Figure 48). Closer

examination of the crack center revealed the residual pores in the material (see Figure 49). As mentioned before, all of the alloy specimens that failed under tension-tension fatigue loading exhibited similar characteristics in the failure region. More examples of these types of failures can be found in the appendix.

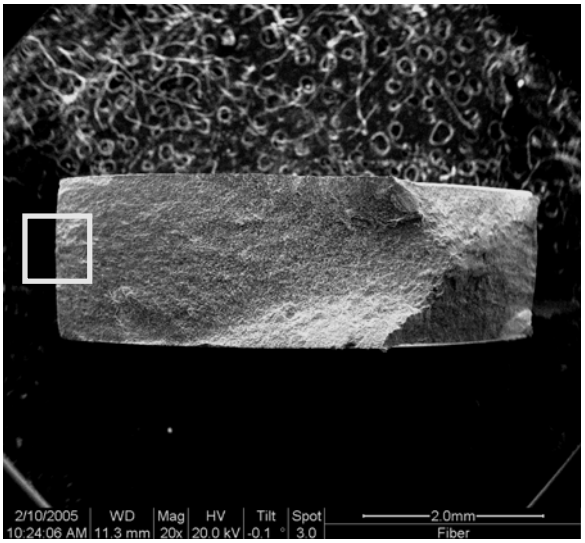

Figure 48: Specimen Ti-01, overall view of fracture surface

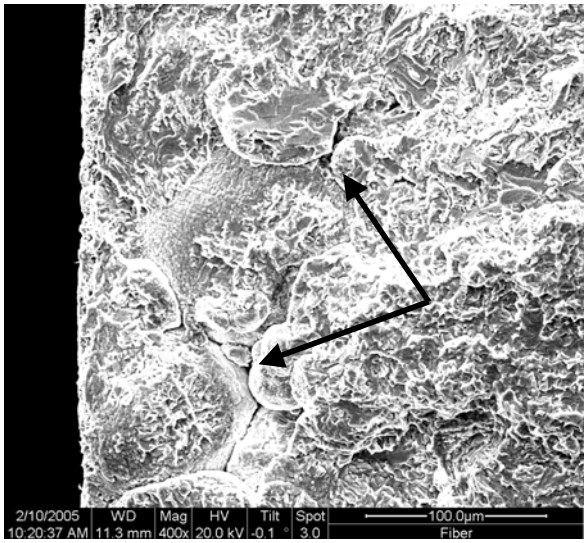

Figure 49: Specimen Ti-01, close-up view of residual pores

Tension-tension Microscopic Evaluation of the TMC (Ti-6Al-4V/SCS-6)

None of the five pure composite specimens tested failed in the gage section (see Figure 50). This could be attributed to the specimen geometry since unidirectional TMCs are sensitive to stress raisers in the shoulder region. However, the results obtained from the current work still reflect fatigue characteristics relative to unidirectional composites and are included as an additional reference for the F/G material studied.

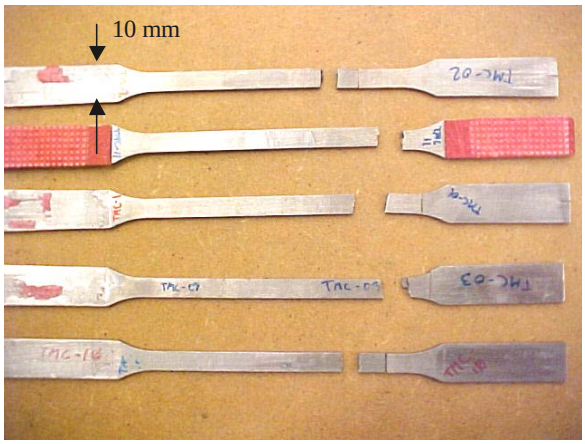

Figure 50: TMC Tension-tension fatigue failure locations

(From Top: Specimens TMC-02, TMC-11, TMC-01, TMC-03 & TMC-10)

Depending on the stress level, the TMC specimens would show characteristics relative to region I, II or III on the S-N curve (reference Figure 13). These characteristics of fiber failure and matrix cracking are discussed below in greater detail for regions I and II. Region III is representative of "runout" or the cases where failure did not occur and is excluded from the discussion.

Tension-tension Region I Failures: TMC-10

When looking at the fracture surface, fiber failure and pullout appear to dominate as damage mechanisms (see Figure 51). At this high stress level, the transition from Region II to Region I on the S-N curve becomes apparent. Upon closer examination of the fracture surface, evidence of ductile void coalescence and necking is observed (see Figure 52).

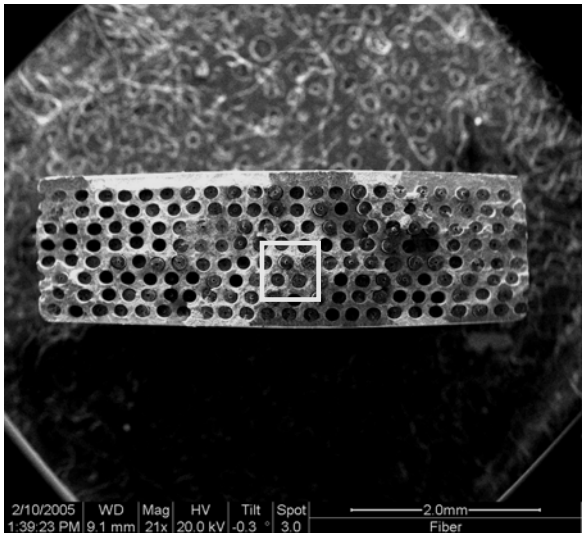

Figure 51: Specimen TMC-10, overall view of fracture surface

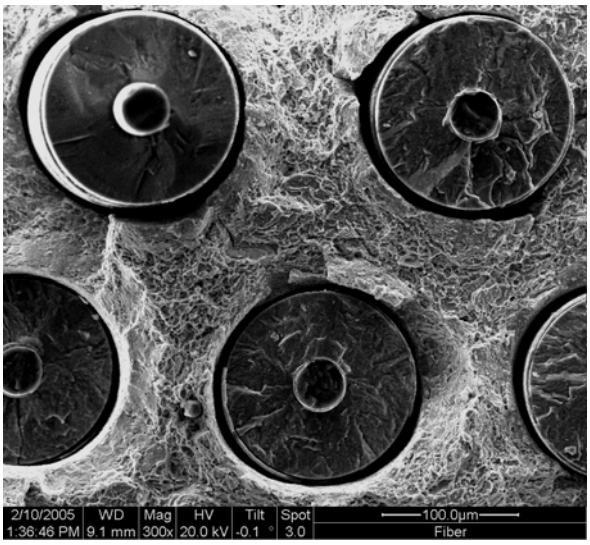

Figure 52: Specimen TMC-10, ductile void coalescence and necking

When looking at the fracture surface, the severe ductile failure of the matrix can be observed in the form of void coalescence. Matrix necking around the failed fibers is clearly seen, indicating catastrophic failure characterized by Region I of the fatigue life diagram. This supports the results found in the macro-mechanical analysis.

Tension-tension Region II Failures: TMC-03, TMC-01, TMC-11

When looking at the fracture surface, multiple crack planes can be seen (see Figure 53). Upon closer examination of the local fracture surface, the crack planes appear to be flat with little fiber pullout (see Figure 54).

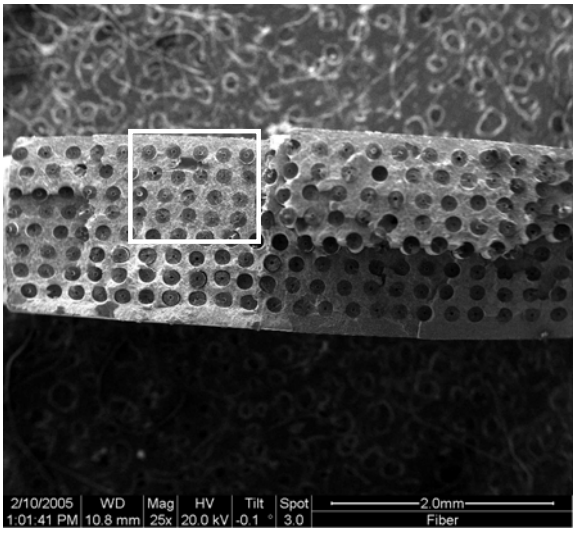

Figure 53: Specimen TMC-03, overall view of fracture surface

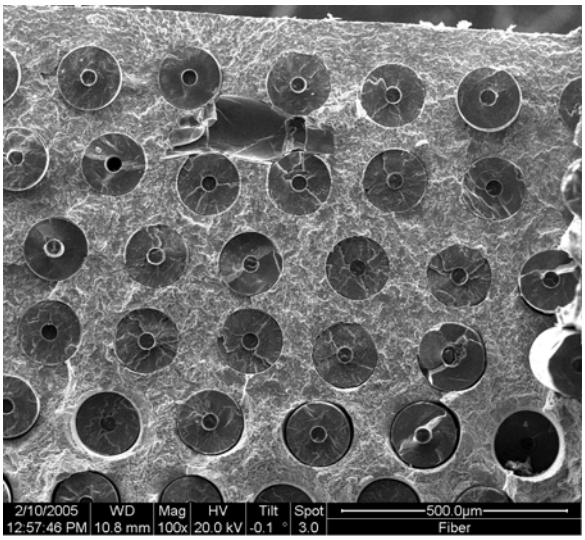

Figure 54: Specimen TMC-03, close-up view of fracture surface

Despite the presence of a fiber shard on the fracture surface, the flat appearance due to matrix cracking can be observed. On the individual crack fronts, the fracture surface shows characteristics of both fiber failure and matrix cracking. This is representative of Region II on the S-N diagram and supports the results found in the macro-mechanical analysis.

As the stress level lowers, less fiber failure and more matrix cracking can be seen (see Figure 55). Upon closer examination of the fracture surface, another fiber shard is observed (see Figure 56). The fiber shard can act as a crack initiator and is usually a sign of poor manufacturing processes. Nevertheless, the results found for this specimen place it also in Region II of the S-N curve.

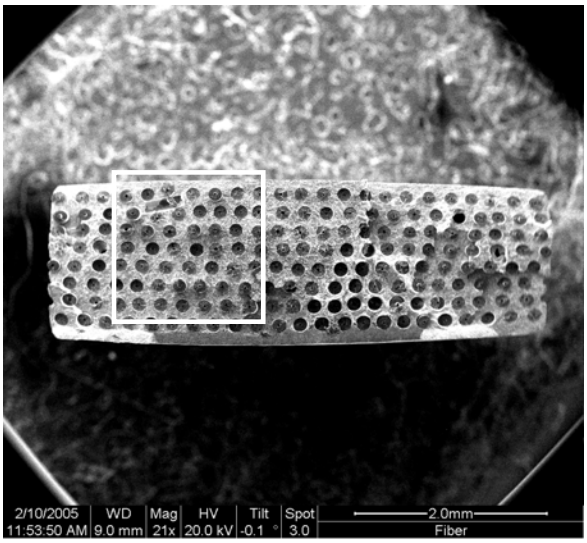

Figure 55: Specimen TMC-01, overall view of fracture surface

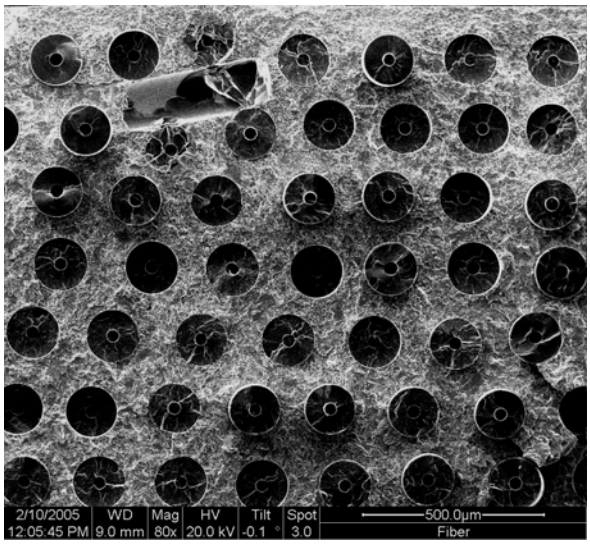

Figure 56: Specimen TMC-01, close-up view of fracture surface

Another case showing the effects of multiple crack fronts can be seen in Figure 57.

Again, matrix plasticity as well as some fiber failure can be seen (see Figure 58).

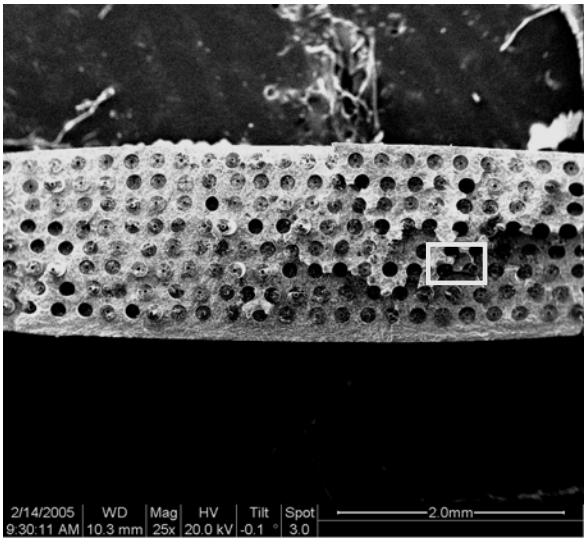

Figure 57: Specimen TMC-11, overall view of fracture surface

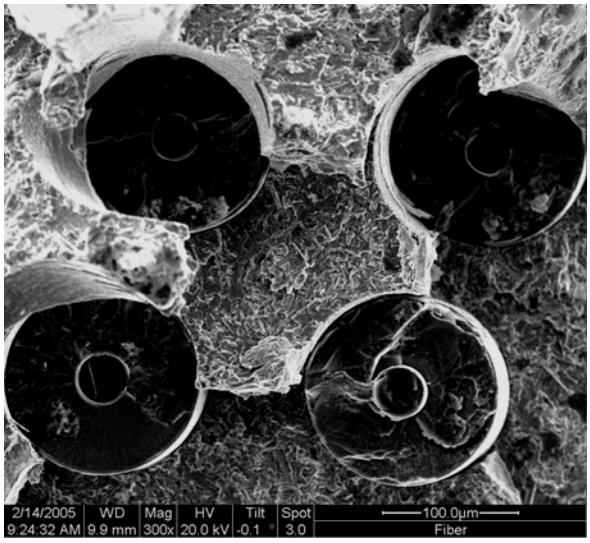

Figure 58: Specimen TMC-11, multiple crack fronts

Even though some fiber failure is observed, the individual crack fronts do not show evidence of ductile void coalescence. This is characteristic of the combined plasticity and damage mechanisms pertaining to Region II of the fatigue life diagram.

Tension-tension Microscopic Evaluation of the F/G TMC (20:1 taper ratio)

Of the four F/G specimens tested, two failed in the gage section (see Figure 59). F/G-02 and F/G-03 both had failures across the taper region, while F/G-01 and F/G-10 both failed in the pure alloy region.

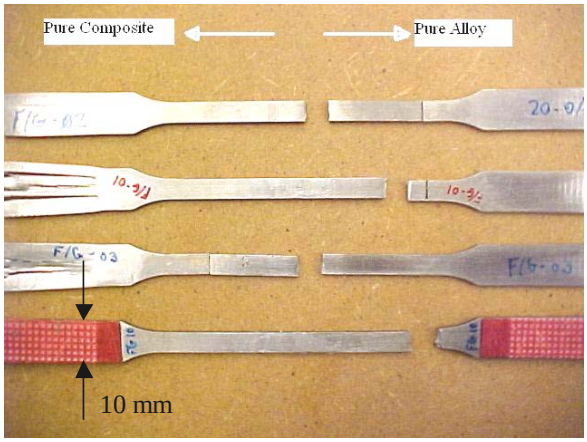

Figure 59: F/G Tension-tension fatigue failures
(From Top: Specimens F/G-02, F/G-01, F/G-03 & F/G-10)

While the two specimens that failed in the alloy region simply showed similar microscopic results as the pure alloy specimens mentioned above, the failures in the taper region showed more interesting results as they both failed in the same region of the taper (see Figure 60). A brief discussion of each failure is provided below.

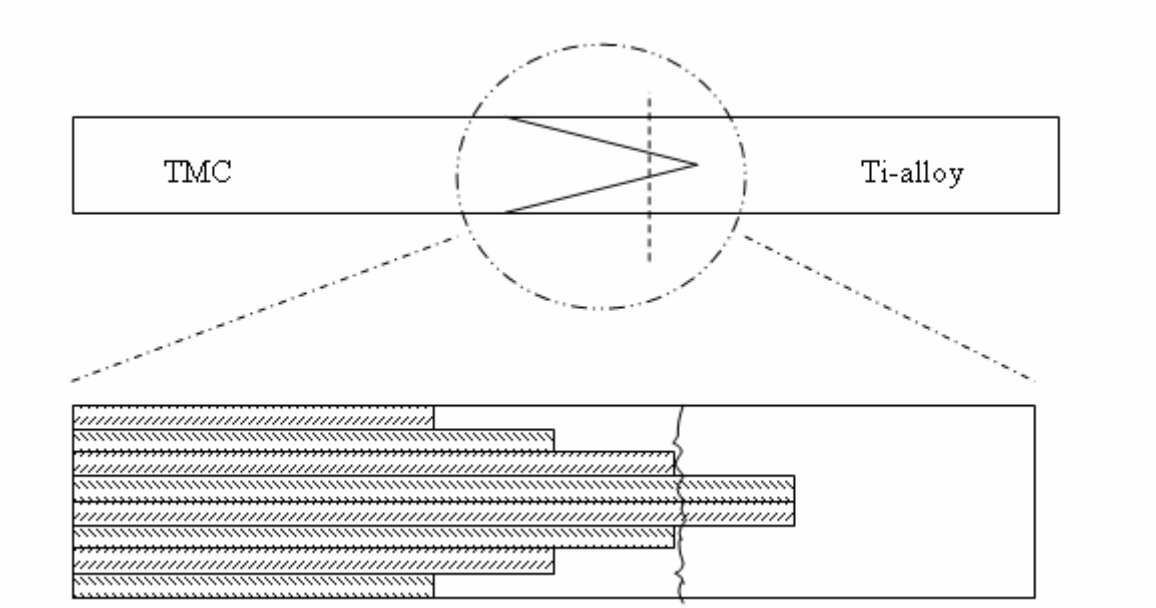

Figure 60: Schematic of failure locations in F/G taper region

Specimen F/G-10: 800 MPa. This highest stress level test failed after only 7,470 cycles and failed in the alloy section of the specimen. Examination of the sectioned specimen revealed similar findings as the pure alloy specimens. The final overload fracture associated with stage III crack propagation is clearly seen (see Figure 61). Following away from this area, the striations associated with stage II crack propagation lead to the point of crack initiation (see Figure 62). The matrix flaw at the crack initiation site is similar to those found in the pure alloy specimens. This is as expected since failure in the alloy region only serves to provide information about the alloy section itself.

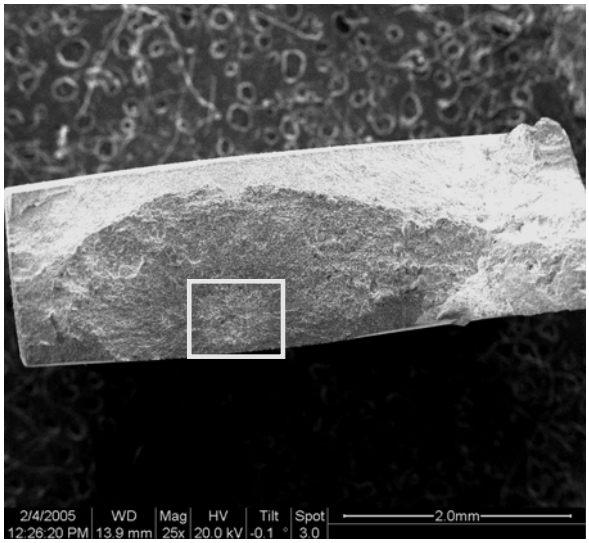

Figure 61: Specimen F/G-10, overall view of fracture surface

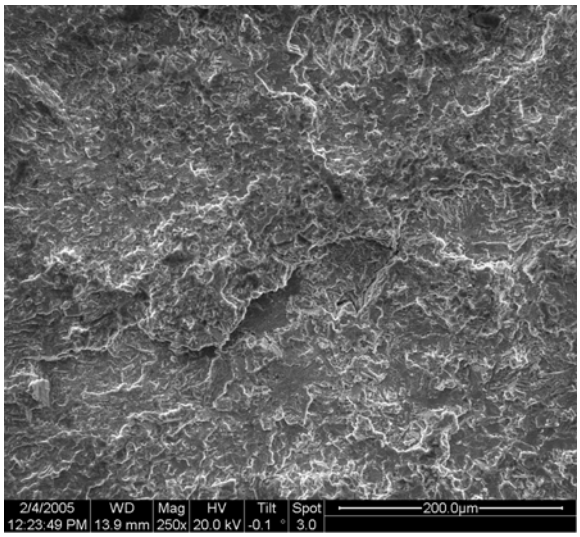

Figure 62: Specimen F/G-10, close-up view of matrix flaw

Specimen F/G-03: 552 MPa. This test failed after 35,242 cycles and failed in the taper region of the specimen. Under the microscope, the distance of the failure from the tip of the taper region was revealed to be ~ 4.22 mm (see Figure 63).

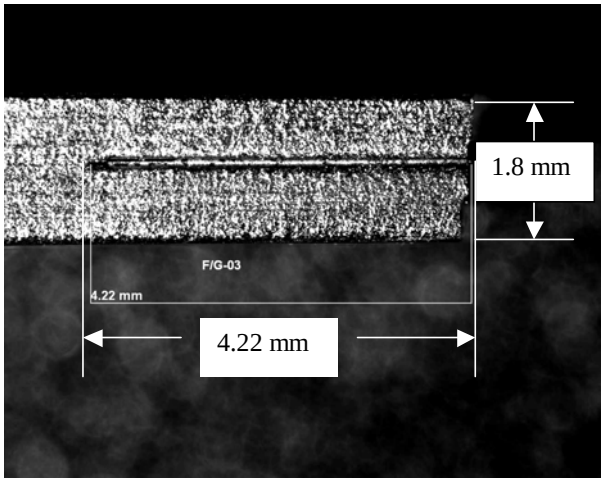

Figure 63: Specimen F/G-03, length of failure from tip of taper region

At first glance, failure seemed to occur in the first "stair-step" of the taper region (reference Figure 60). The SEM revealed that failure ultimately occurred at the transition

to the next step. The existence of four plies is readily seen (see Figure 64). Looking toward the pure composite end of the specimen, it is apparent that the areas of "missing fibers" along the upper and lower plies represent the higher "peaks" of the fracture surface. Upon closer examination, it was determined that the fiber ends were the points of crack initiation as deposits of the matrix material still existed on some of the fibers (see Figure 65). In this figure, the upper two fibers both show smooth textures characteristic of a fiber end, while the lower two fibers both show signs of fracture by their rough textures.

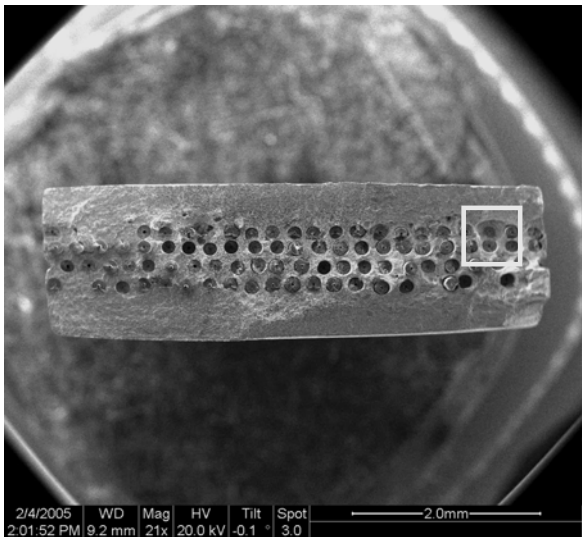

Figure 64: Specimen F/G-03, fracture surface (looking toward composite side)

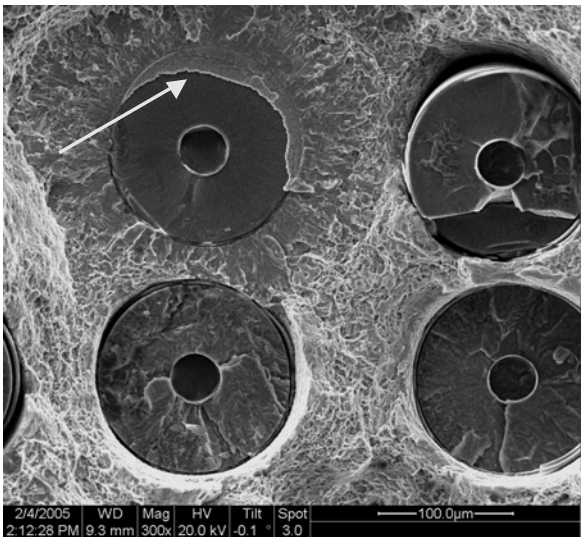

Figure 65: Specimen F/G-03, matrix material on smooth fiber end

Specimen F/G-01: 495 MPa. This specimen failed after 58,872 cycles and failure occurred in the alloy region. Examination of the sectioned specimen revealed residual pores as the cause of crack initiation (see Figure 66 and Figure 67). Just as in the pure alloy specimens, the residual pores become centers for crack initiation. Again, failures in the alloy region will exhibit characteristics similar to the pure alloy specimens.

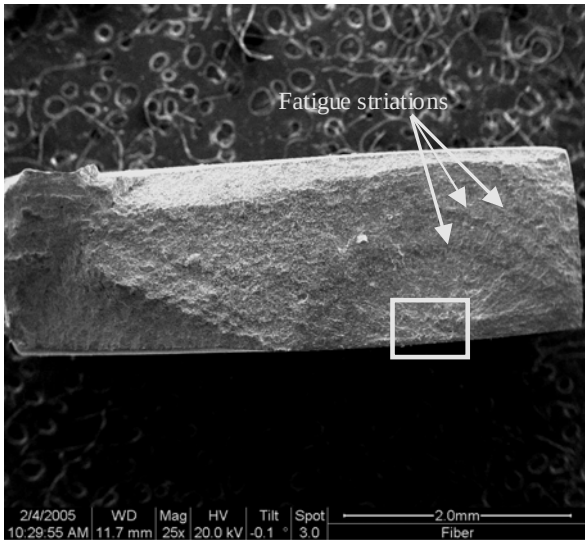

Figure 66: Specimen F/G-01, overall view of fracture surface

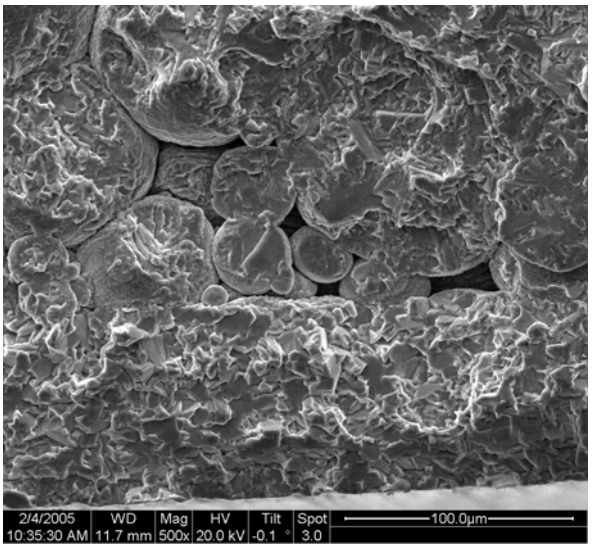

Figure 67: Specimen F/G-01, close-up view of residual pores

Specimen F/G-02: 368 MPa. This specimen failed after 526,182 cycles with failure occurring in the taper region. Under the microscope, the distance of the failure from the tip was revealed to be ~ 4.16 mm (see Figure 68).

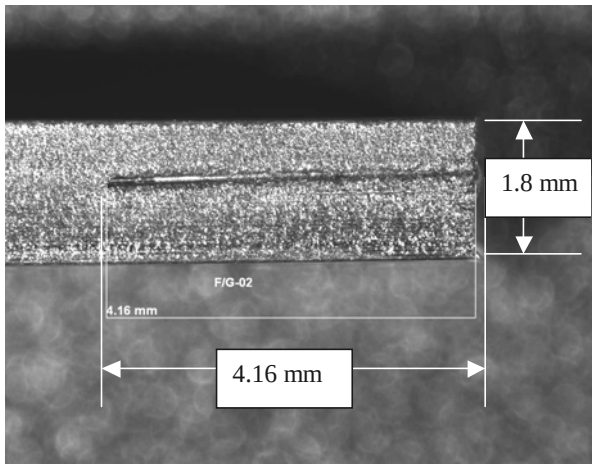

Figure 68: Specimen F/G-02, length of failure from tip of taper region

Just as in specimen F/G-03, the existence of four plies is readily seen (see Figure 69). Again, looking toward the pure composite end of the specimen, the transition from fiber ends to pure alloy are potential sites for crack initiation. Upon closer examination,

these areas showed deposits of the matrix material on some of the fibers (see Figure 70). The lower two fractured fibers can again be distinguished by their rough appearance, while over half of the upper fiber is covered by matrix material.

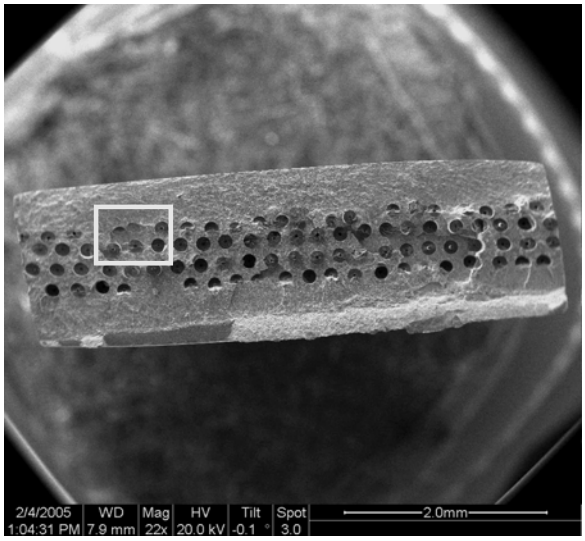

Figure 69: Specimen F/G-02, fracture surface (looking toward composite side)

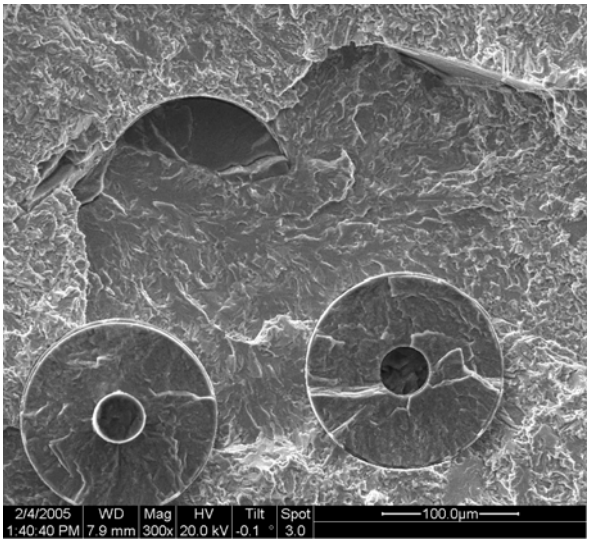

Figure 70: Specimen F/G-02, matrix material on fiber end

Tension-tension Microscopic Evaluation (Comparison of Results)

In all the specimens where failure occurred in the taper region, the fiber ends act in the same manner as the residual pores in the pure alloy. The mere existence of each fiber end within the material would be a potential site for crack initiation. This, in conjunction with the constantly diminishing volume fraction in the taper region, is reason for the lack of additional life in the FGM when compared to the pure alloy. However, the fact that both taper failures occurred in the same area of the taper region (regardless of stress level) raises additional questions about the characteristics of the joint section.

Tension-compression Microscopic Evaluation of the alloy (Ti-6Al-4V)

Of the five pure alloy specimens tested, only one of them (specimen Ti-07) failed in the gage section (see Figure 71). The rest of the specimens, Ti-08, Ti-06, Ti-05 and Ti-09, all failed near the shoulder.

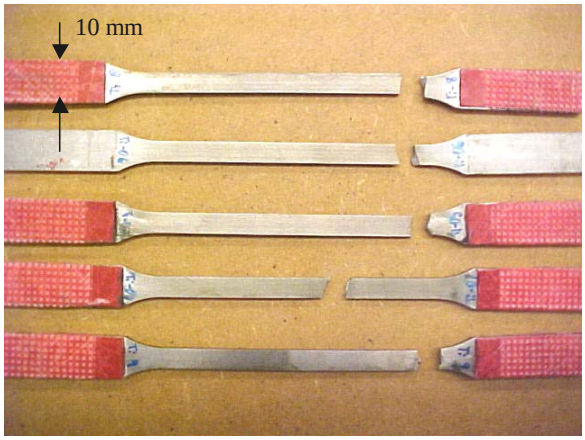

Figure 71: Ti-alloy Tension-compression fatigue failure locations (From Top: Specimens Ti-08, Ti-06, Ti-05, Ti-07 & Ti-09)

As before in the tension-tension case, the alloy specimens all had similar failure characteristics. The transition from the fatigue crack propagation region and the final overload region could again be distinguished from the overall view and the point of crack initiation could be found (see Figure 72). Just as in the tension-tension case, the crack initiation site seemed to be the edge of the specimen where stress raisers are present (see Figure 73).

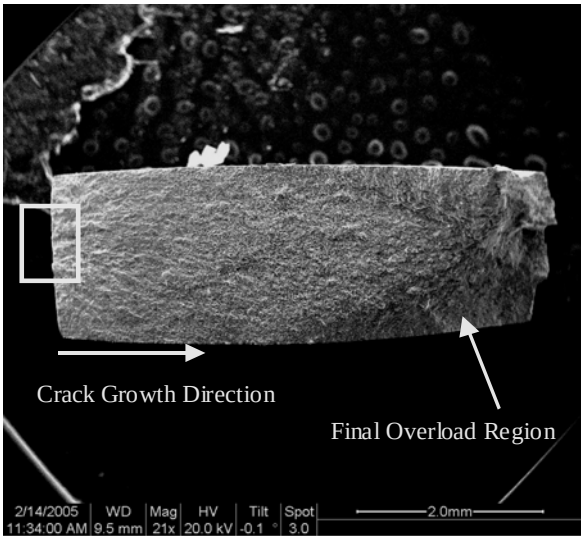

Figure 72: Specimen Ti-08, overall view of fracture surface

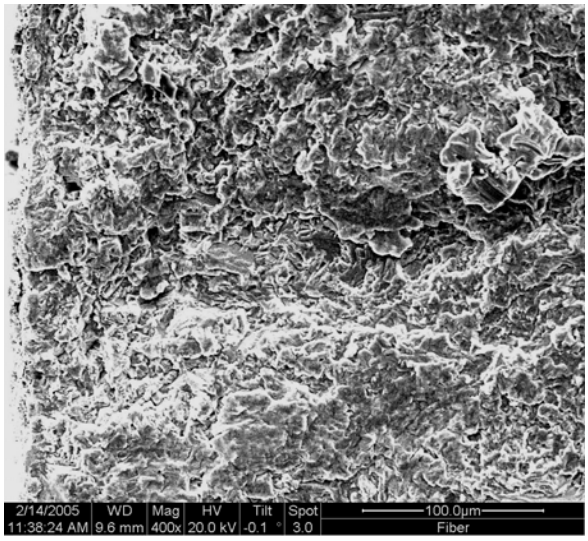

Figure 73: Specimen Ti-08, close-up of crack initiation site

These similar characteristics can be seen again in Figure 74 and Figure 75. Notice also the shortening of the fatigue crack propagation region and the respective lengthening of the final overload region when the stress level is increased. Even with this relatively small increase in stress level, the difference is clearly seen. Although residual pores can be observed as crack initiators, none of the specimens tested in tension-compression showed this phenomenon. Instead, all failures seemed to occur at stress raisers at the edge of the specimens. More examples of these types of failures can be viewed in the appendix.

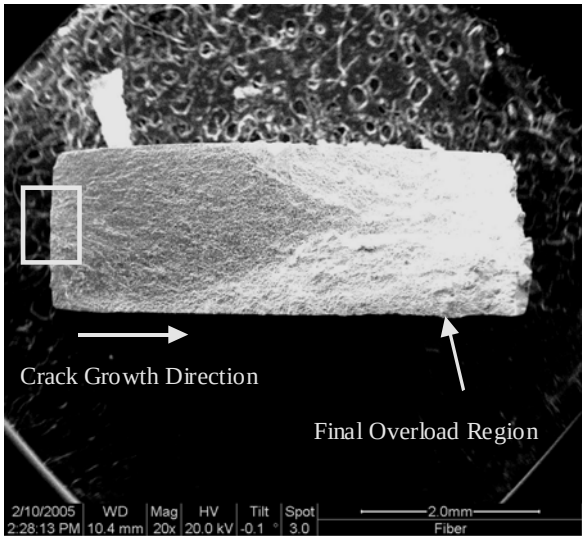

Figure 74: Specimen Ti-06, overall view of fracture surface

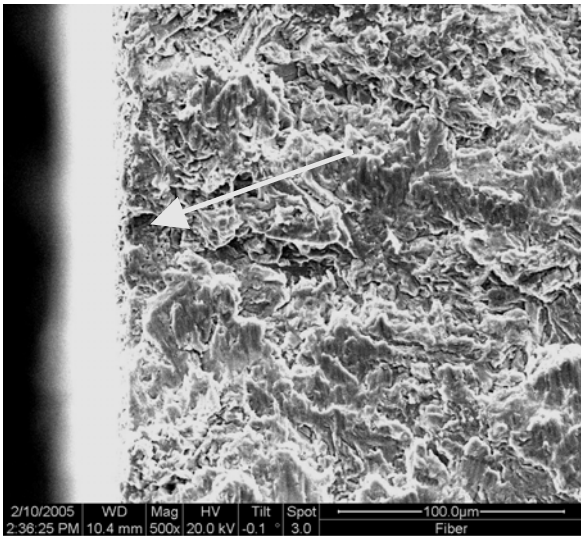

Figure 75: Specimen Ti-06, close-up view of crack initiation site

Tension-compression Microscopic Evaluation of the TMC (Ti-6Al-4V/SCS-6)

None of the four pure composite specimens tested failed in the gage section (see Figure 76). Specimen TMC-08 fell below the fatigue limit of the material and did not fail. The rest of the specimens all failed near the shoulder. Again, this can be contributed to the sensitivity of the composite to stress raisers in the shoulder region.

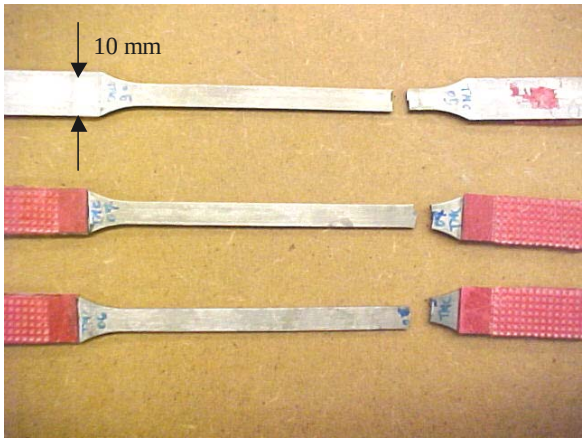

Figure 76: TMC Tension-compression fatigue failure locations (From Top: Specimens TMC-05, TMC-04 & TMC-06)

As before, the discussion for each failure is broken down by their respective dominant failure mechanisms. A section describing failure associated with Regions I and II on the S-N diagram is provided. Region III pertains to "runout" or no failure and is not included in the discussion.

Tension-compression Region I Failures: TMC-06

At this highest stress level, it is no surprise that fiber failure was the dominating mechanism (see Figure 77). Upon closer investigation of the fracture surface, evidence of ductile void coalescence and necking were observed (see Figure 77).

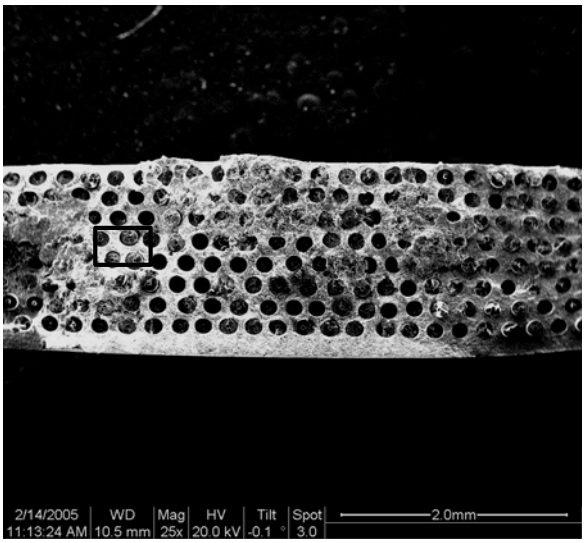

Figure 77: Specimen TMC-06, overall view of fracture surface

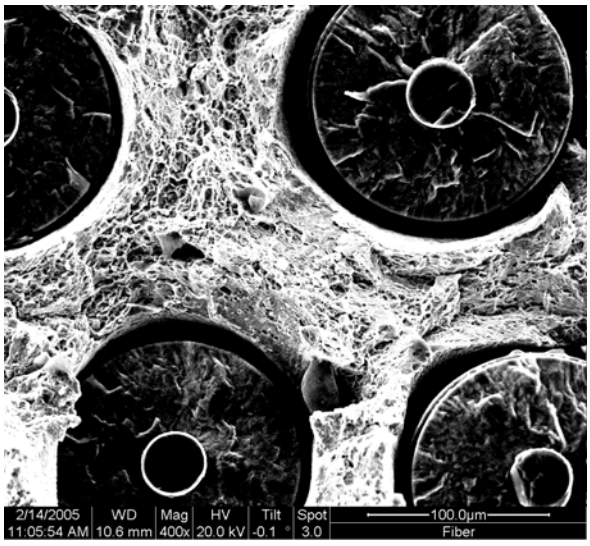

Figure 78: Specimen TMC-06, ductile void coalescence and necking

This specimen was clearly dominated by mechanisms associated with Region I failure. Matrix necking around the failed fibers is clearly seen indicating catastrophic failure characterizing Region I of the fatigue life diagram. The appearance of ductile void coalescence also supports the results found in the macro-mechanical analysis.

Tension-compression Region II Failures: TMC-04, TMC-05

When looking at the fracture surface, specimen TMC-04 seemed to be a Region I failure (see Figure 79). Catastrophic failure was dominant and ductile void coalescence surrounded the fiber failures (see Figure 81). However, closer examination revealed flat crack faces, indicating some plasticity was also involved (see Figure 84).

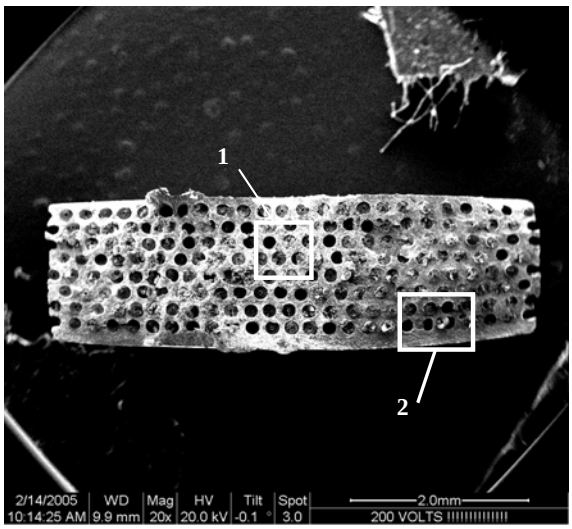

Figure 79: Specimen TMC-04, overall view of fracture surface

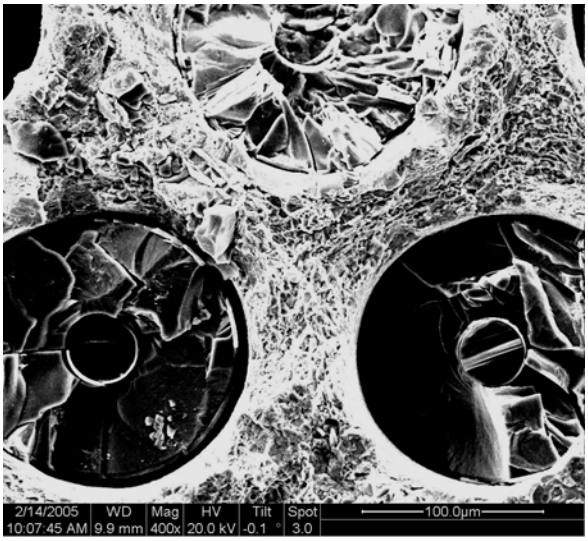

Figure 80: Specimen TMC-04, 1: catastrophic fiber failure

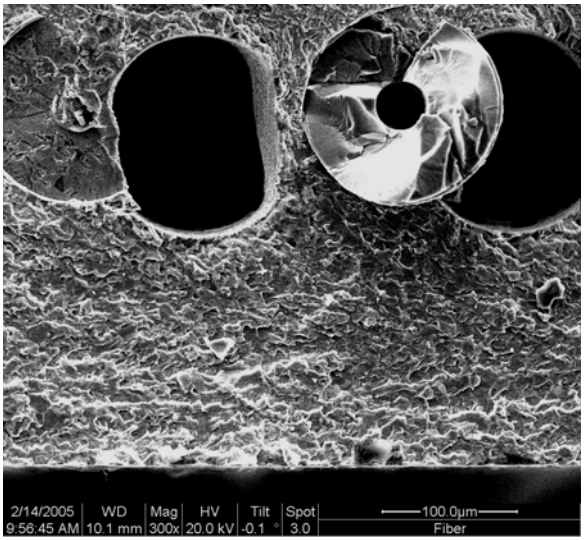

Figure 81: Specimen TMC-04, 2: fiber failure and compression damage

Evidence supporting damage associated with the compression portion of the cycle can be seen. Here, early fiber failure caused impressions in the surrounding matrix and in some cases left deposits of fractured fibers behind.

Another mixed-mode case can be seen in Figure 82. Again, characteristics of damage and plasticity could be seen (see Figure 83). On the left, a fiber fracture indicating catastrophic failure is seen. On the right, matrix cracking associated with plasticity can be observed. Notice also the fractured fiber deposit left behind from the compressive cycle.

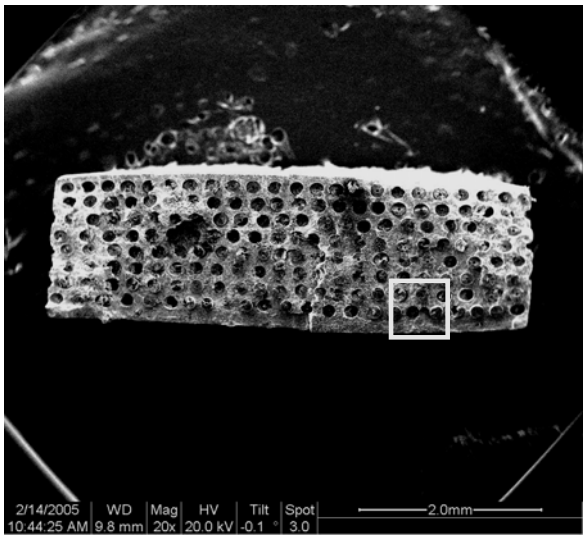

Figure 82: Specimen TMC-05, overall view of fracture surface

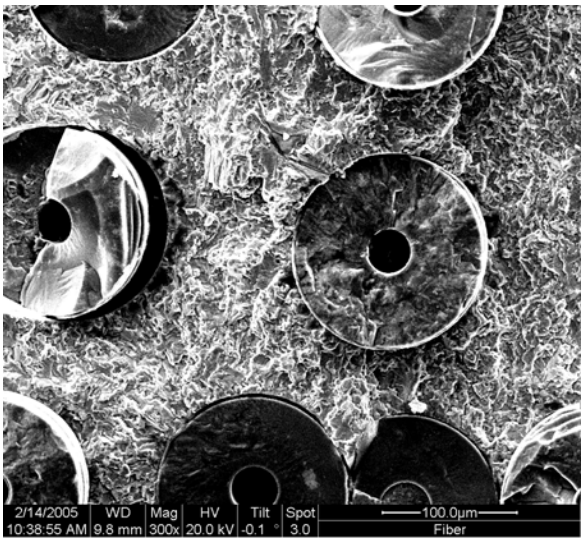

Figure 83: Specimen TMC-05, mixed mode failure

Tension-Compression Microscopic Evaluation of the F/G TMC (20:1 taper ratio)

Of the five F/G specimens tested, three failed in the gage section (see Figure 84). Specimens F/G-08, F/G-06 and F/G-09 all failed across the taper region, while specimens F/G-05 and F/G-04 both failed in the pure alloy region.

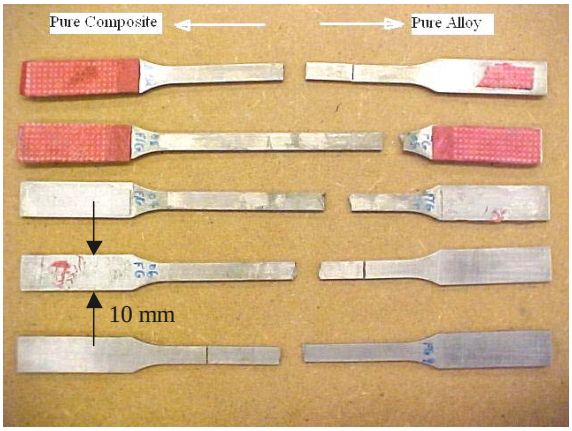

Figure 84: F/G TMC Tension-compression fatigue failure locations (From Top: Specimens F/G-08, F/G-05, F/G-04, F/G-06 & F/G-09)

Just as in the tension-tension case, the two specimens that failed in the alloy region showed similar results as the pure alloy specimens mentioned above. The failures in the taper region showed more interesting results, especially when compared with those of the tension-tension case. Specimens F/G-08 and F/G-09 both failed in the same region of the taper as those from the tension-tension case (reference Figure 60), while F/G-06 failed at the tip of the taper region. A brief discussion of each failure is provided below.

Specimen F/G-09: 650 MPa. This specimen failed after 6,442 cycles in the taper region. Under the microscope, the distance of the failure from the tip was revealed to be ~ 4.03 mm (see Figure 85).

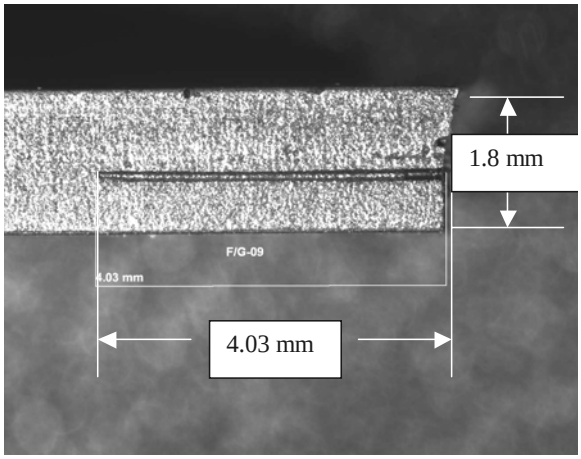

Figure 85: Specimen F/G-09, length of failure from tip of taper region

Just as in specimen F/G-03 and F/G-02, this failure originated at the transition to the second "stair step" (see Figure 86). Again, four plies are readily seen. Also note the stage II crack propagation through the center of the specimen and the final stage III overload failure along the edges. Upon closer inspection, the fiber ends were again found to be the points of crack initiation (see Figure 87). This picture, looking toward the pure composite end, shows a fractured fiber on the left, a smooth fiber end on the right and a crack originating from a fiber end below the matrix surface in the center.

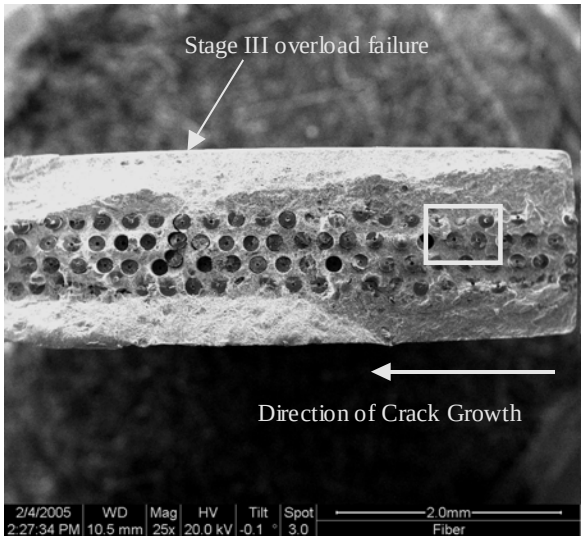

Figure 86: Specimen F/G-09, fracture surface (looking toward composite side)

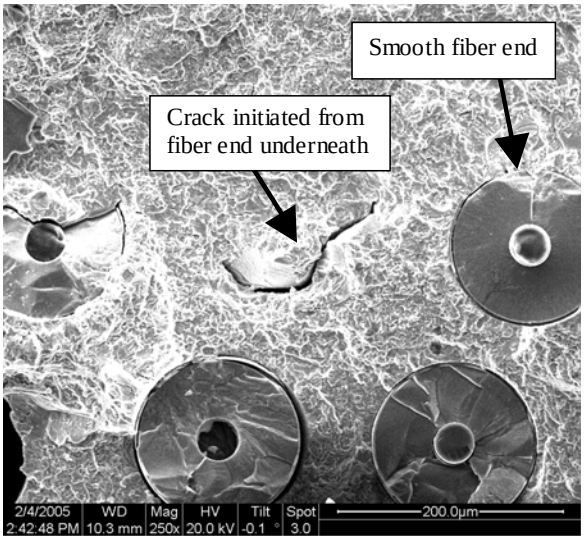

Figure 87: Specimen F/G-09, close-up showing crack originating from fiber end

Specimen F/G-06: 497 MPa. This specimen failed after 24,101 cycles and was the only specimen to fail at the tip of the taper in this study. Figure 88 and Figure 89 show how the crack started at the tip on one side of the specimen and propagated through the taper region on the other side of the specimen.

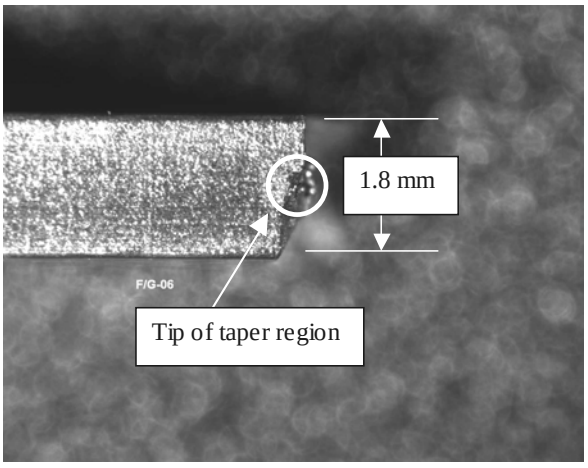

Figure 88: Specimen F/G-06, failure at tip of taper region

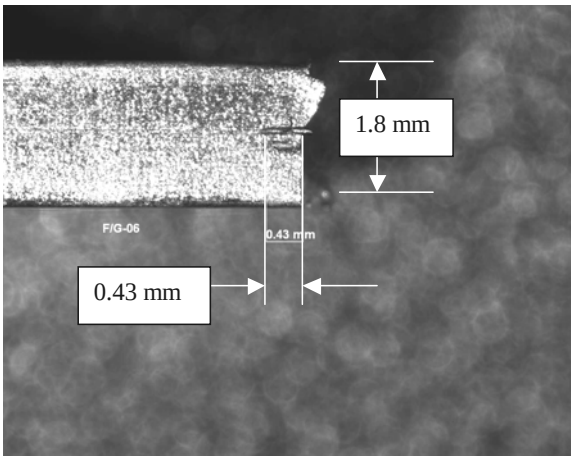

Figure 89: Specimen F/G-06, opposite side of failure section

Under the SEM, looking toward the pure alloy end of the specimen, two plies are readily seen (see Figure 90). Upon closer examination, an impression of a fiber end (rather than the fiber end itself) could be seen (see Figure 91).

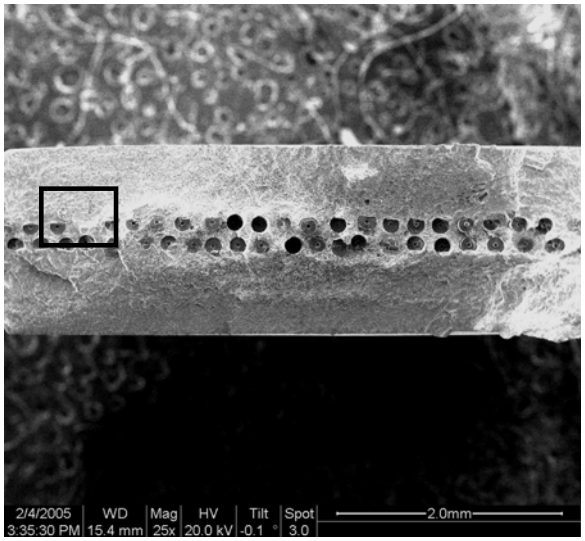

Figure 90: Specimen F/G-06, fracture surface (looking toward alloy side)

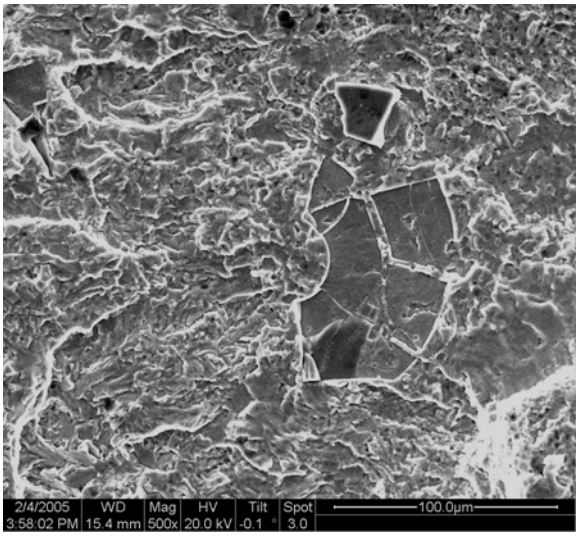

Figure 91: Specimen F/G-06, close-up of fiber imprint on matrix material

In this instance, the crack initiated at one or more of the fiber ends and quickly propagated through the matrix. By starting at the tip of the taper region, the crack can easily evade all of the fibers that would normally provide crack tip shielding and slow down the crack growth.

Specimen F/G-04: 414 MPa. This specimen failed after 44,946 cycles in the alloy region(see Figure 92). Similar to other functionally-graded specimens, this failure could be traced back to a flaw in the matrix (see Figure 93).

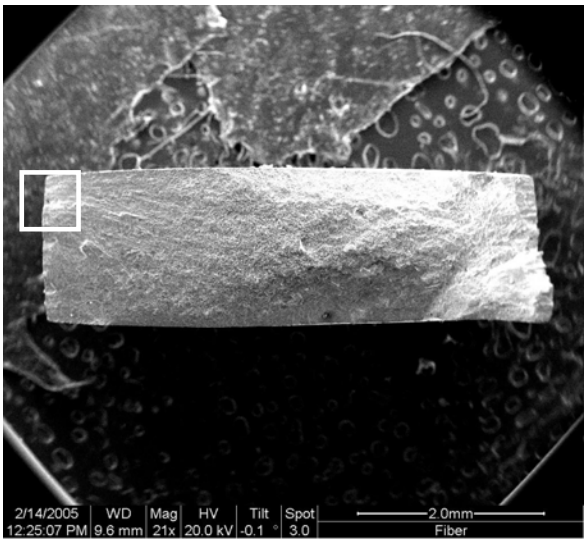

Figure 92: Specimen F/G-04, overall view of fracture surface

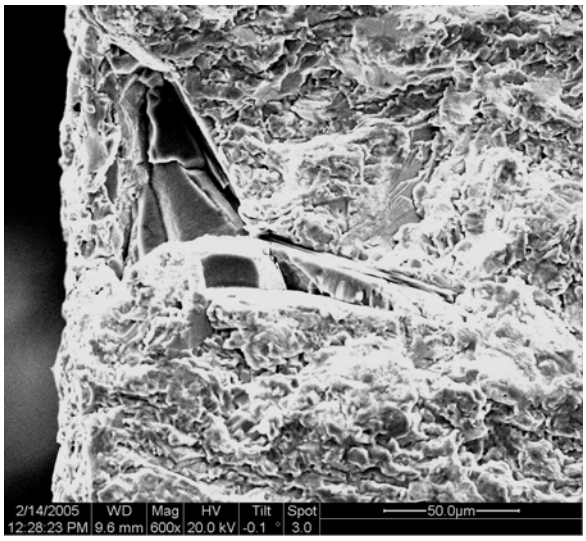

Figure 93: Specimen F/G-04, close-up showing matrix flaw

Again, these types of flaws are common in alloys manufactured by powder metallurgy and are expected to exist at least to some degree. However, it is interesting to note that none of the failures that occurred in the taper region showed these types of flaws or residual pores. Instead, cracks always initiated from the fiber ends.

Specimen F/G-05: 331 MPa. This specimen failed after 88,922 cycles in the alloy region (see Figure 94). However, this failure occurred at the specimen edge without any evidence of residual pores (see Figure 95).

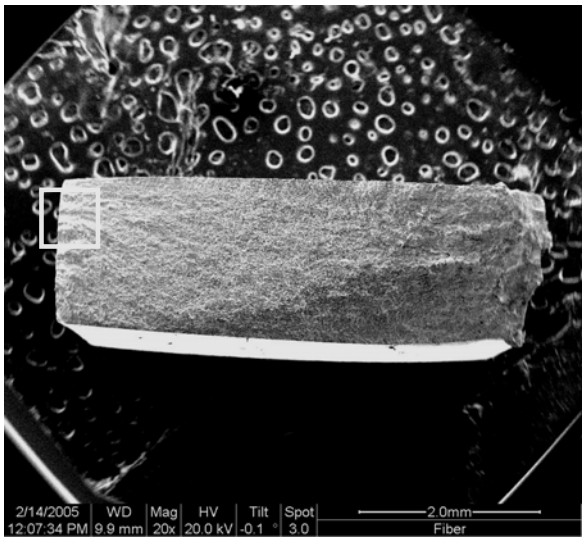

Figure 94: Specimen F/G-05, overall view of fracture surface

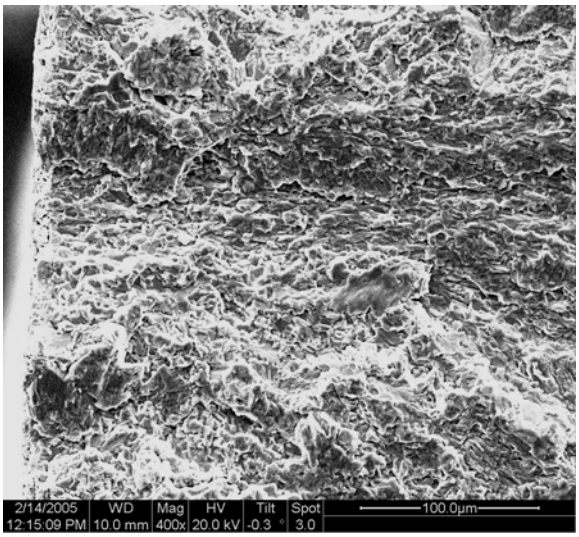

Figure 95: Specimen F/G-05, closeup of crack initiation site

Specimen F/G-08: 250 MPa. This specimen failed after 153,054 cycles in the taper region. Under the microscope, the distance of the failure from the tip was revealed to be ~ 4.28 mm (see Figure 96).

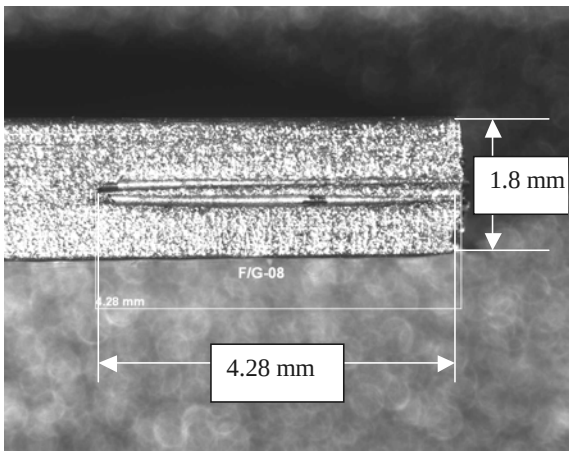

Figure 96: Specimen F/G-08, length of failure from tip of taper region

Similar to specimen F/G-09, four plies are readily seen (see Figure 97). Upon closer inspection, the fiber ends were again found to be the points of crack initiation (see

Figure 98). This figure, looking toward the pure alloy side of the specimen, shows a fiber imprint with a fractured piece of fiber on the left and more fractured pieces on the right.

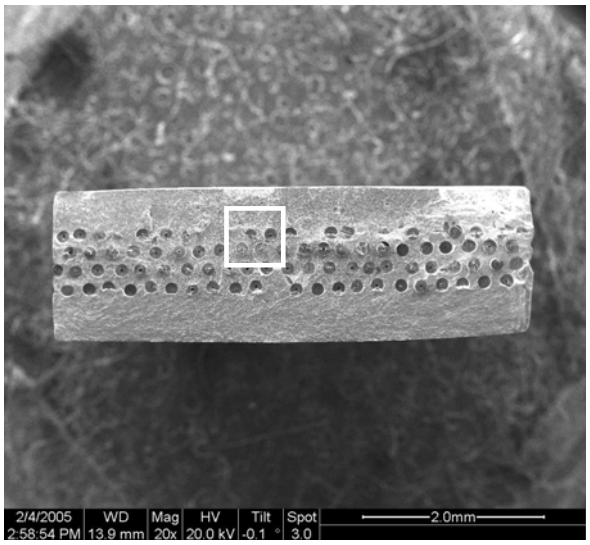

Figure 97: Specimen F/G-08, fracture surface (looking toward alloy side)

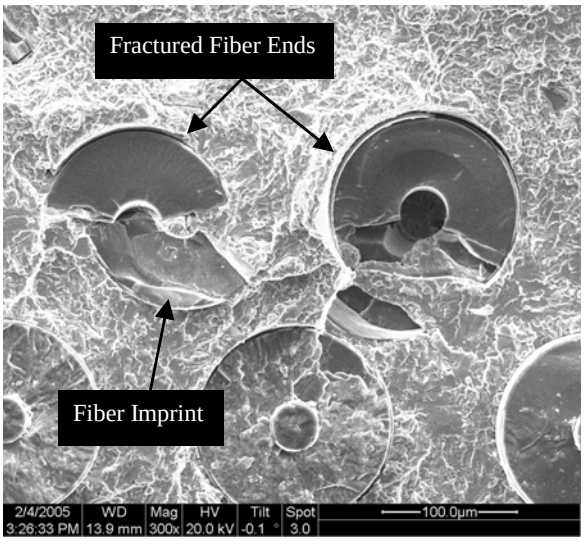

Figure 98: Specimen F/G-08, fractured fiber ends

Tension-Compression Microscopic Evaluation (Comparison of Results)

Just as in the tension-tension case, the failures in the taper region all showed similar flaws at the fiber ends. Again, regardless of stress level, failure in the taper region occurred mainly at the transition from the first to the second "stair step". Although one specimen (F/G-06) did fail at the tip of the taper region, this was an isolated incident and is not believed to be typical of failures in the taper region. In addition, its failure mechanisms were similar to the other four cases.

As mentioned earlier, each "stair step" represents an area where fiber ends are present, as well as a change in fiber volume fraction. The fact that each of these areas has roughly the same number of fiber ends draws the conclusion that something else must be forcing failure at the transition from the first to the second "stair step". The fact that the

first “stair-step” is the area with the lowest fiber volume fraction that still has the existence of these fiber ends suggests that this *area* may be the weakest in the material and not necessarily the tip of the taper region itself.

V. Conclusions and Recommendations

Overview

The purpose of this study was to characterize the monotonic tension and fatigue behaviors of a functionally-graded titanium matrix composite (F/G TMC) joint region. Damage mechanisms and fatigue life were investigated for the 20:1 taper ratio and compared with the results from the two parent materials. Tensile tests were done to evaluate the modulus and ultimate strength, while both tension-tension and tension-compression fatigue tests were performed for fatigue life analysis. The stress-strain data taken during fatigue cycling was used to evaluate the macro-mechanical behavior of the joint region, while microscopic evaluation was used to characterize the damage on a micro-mechanical level.

Conclusions of Research

Under tensile loading, the properties for the joint are slightly higher than the alloy. The joint region gains some strength from the composite with the modulus of elasticity following the rule of mixtures formula:

$$E_t=E_cV_c+E_a(1-V_c)$$

Therefore, by changing the taper angle of the joint region, one can control how quickly the modulus changes from the pure composite section to the pure alloy section.

The fatigue life curves for the two parent materials give the upper and lower bounds for the functionally-graded material. While the present study shows little to no increase in fatigue life of the functionally-graded material from the monolithic alloy, the

weakest part of the functionally-graded material is the fiber ends in the joint region and not the monolithic alloy section. As mentioned in chapter four, these fiber ends act in the same manner as residual pores in the pure alloy region. Also, the fracture sensitive reaction zone at these fiber ends proved to be more detrimental than the reaction zones around the fibers by changing the mode of loading from mode II (sliding along the fibers) to mode I (crack opening at fiber end).

Boyum [90] noticed a similar phenomenon when she studied the effects of a cross-ply metal matrix composite under fatigue loading. The reaction zones of the 90º fibers are susceptible to debonding, allowing cracks to propagate more rapidly. By rotating the reaction zone and allowing mode I to dominate, as in the fiber ends in the present study, early failure in the taper region can be expected. However, the point of failure in the taper region did not appear to be random. Neither did the point of failure in the taper region constantly occur at the tip, the predicted weakest point of the taper. The fact that four out of five specimens failed in the same area of the joint region leads to the conclusion that the transition from 50% composite to 25% composite is of some importance. Using the analogy of chapter four, this is equivalent to a transition from a volume fraction of 0.185 to a volume fraction of 0.0925 when the volume fraction of the pure composite is 0.37.

Coghlan, S.C. [90] studied the effects of fiber volume fraction on the fatigue life of a unidirectional SCS-6/Ti-6-4 composite. He found that as the fiber volume decreased, fatigue cracks propagated faster due to less crack tip shielding from fibers. This enforces the idea that the *effective* fiber volume fraction, controlled by the taper

angle, is an additional factor in determining the characteristics of the joint region. However, regardless of the taper angle, the area with the lowest volume fraction (the area that includes the tip, not the tip itself) is assumed to be the weakest area in the presence of the fiber ends. Therefore, until a better process is developed to strengthen the bond between the fiber ends and the matrix, a different type of joint altogether must be used in the joint region in order to possibly slow down the crack progression.

Recommendations for Future Research

It is assumed that failure will always occur, if not in the alloy section, within the first step of the taper region. The tip of the taper at the fiber ends or the fiber ends at the base of the first step were found to be major contributors to failure. However, it is not certain if changing the taper ratio or changing the shape of the taper region altogether would change or negate this effect. Brooks and Choudhurry [4:295] stated, "In the case of long-fiber (continuous fiber) composites stressed in a direction parallel to the fiber axis, all fibers across the cross section must fracture in order to cause failure of the composite. Conversely, in the case of short-fiber (discontinuous fiber) composites, the fracture path may evade all the fibers, traversing exclusively through the matrix." This enforces the case against too shallow of a taper angle, which would allow an easy path for the crack to travel.

Miller [15] tested both a 20:1 taper ratio and a 4:1 taper ratio with little success in achieving failure within the taper region. However, the current material performs much better for evaluating the strength of the joint. Therefore, different taper ratios to increase

or decrease the rate of changing the effective fiber volume fraction within this taper region would yield valuable insights to the joint area properties.

This study has provided a solid foundation for future research. Would different taper ratios show similar results to the present work? Would different joints, other than the double-scarf joint used in the present research, perform better? Additional research should be conducted to answer these questions.

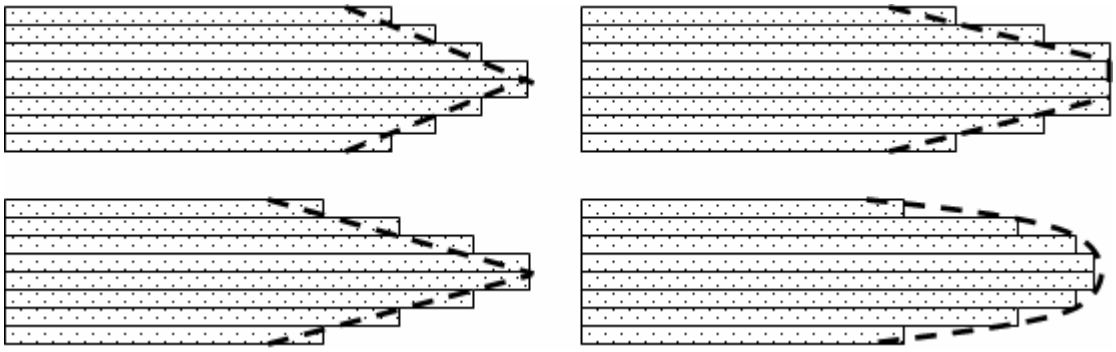

Figure 99: Sample ply lay-ups for taper region

Appendix A: TT fatigue (strain gage data): stiffness & strain histories

The following plots are given for use as a comparison between the strain gage measurements and the extensometer measurements taken in the tension-tension fatigue tests. During testing, the strain gage adhesive would fatigue and the signal would be lost. However, the data that was taken can be compared with the extensometer data to check accuracy and repeatability.

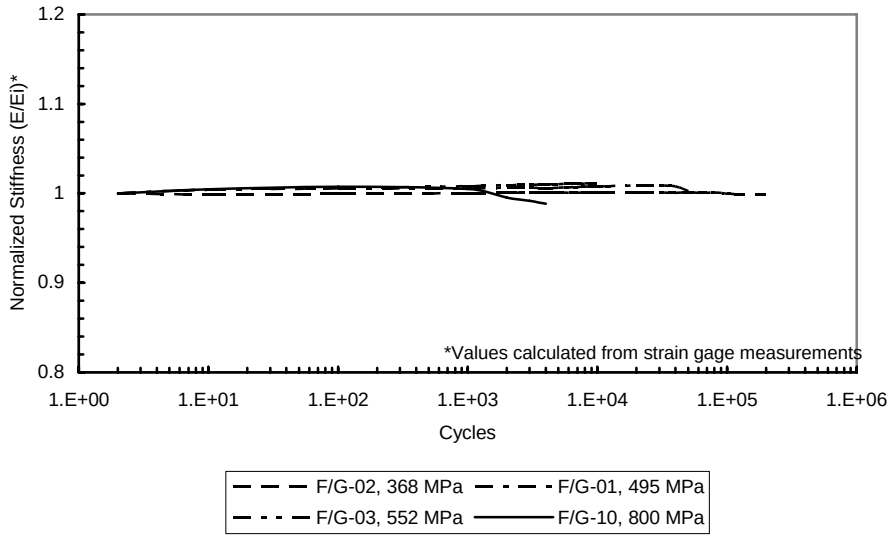

Figure 100: TT fatigue (strain gage data): normalized stiffness vs. fatigue life

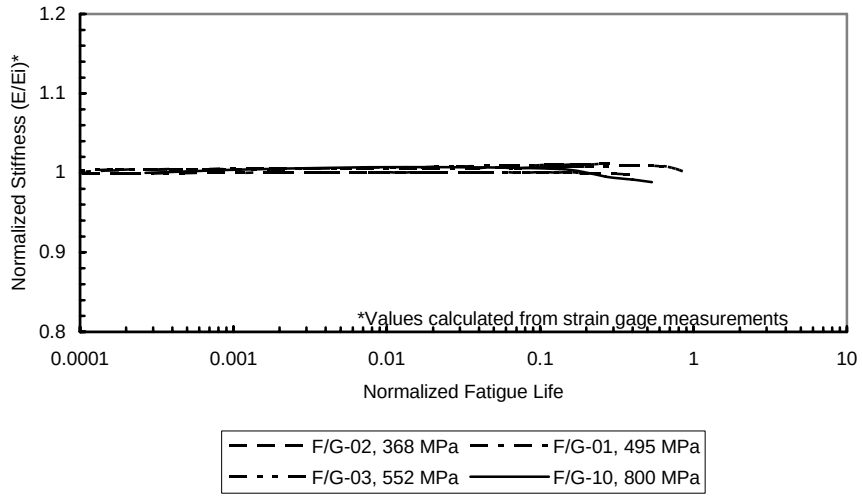

Figure 101: TT fatigue (strain gage data): normalized stiffness vs. fatigue life

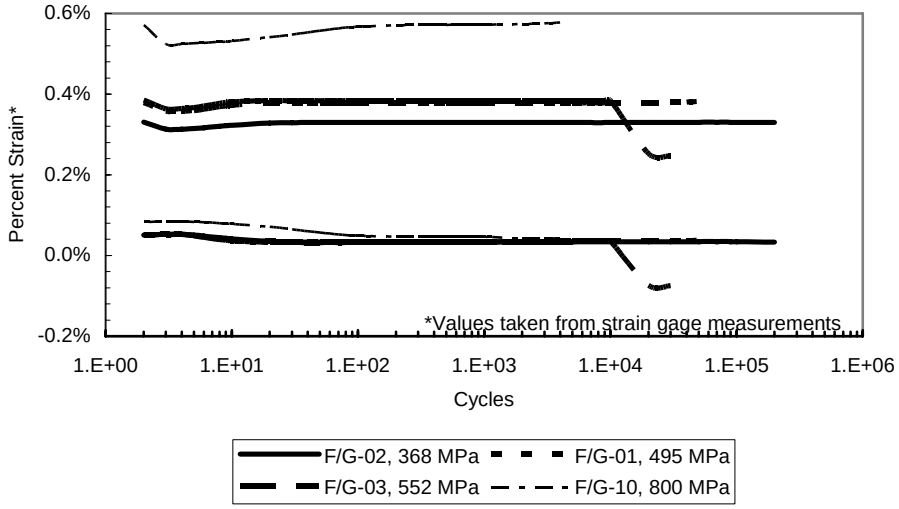

Figure 102: TT fatigue (strain gage data): max. & min. % strains vs. fatigue cycles

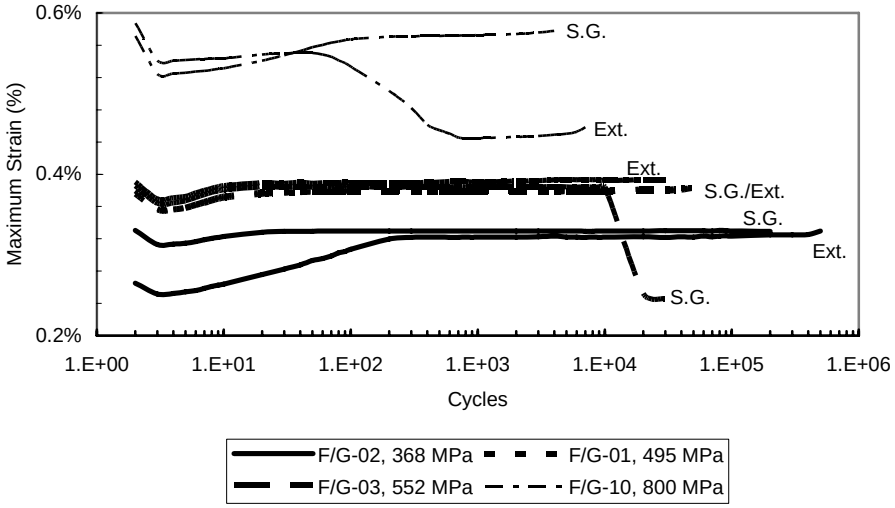

Figure 103: TT fatigue: comparison of strain gage & ext., max. % strain data

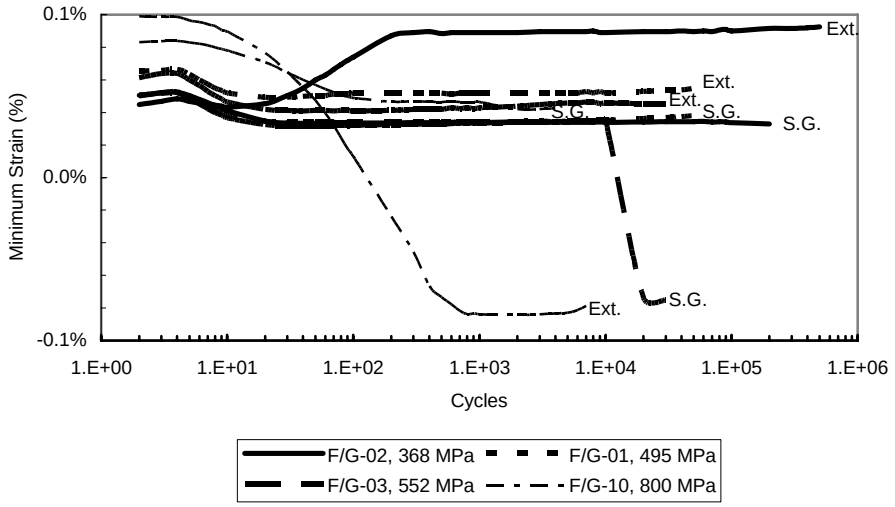

Figure 104: TT fatigue: comparison of strain gage & ext., min. % strain data

Appendix B: Titanium alloy fractographs

The following fractographs are additional SEM photos of the titanium alloy failures. Similar in characteristics to the alloy failures mentioned in chapter four, the following figures are presented for reference.

Tension-tension Fatigue Failures:

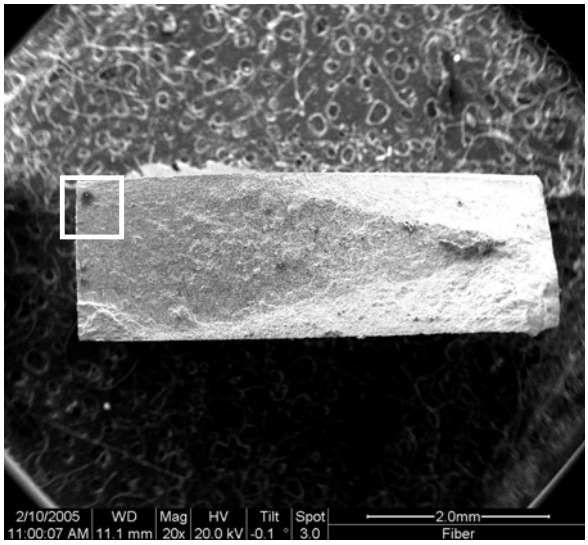

Figure 105: Specimen Ti-04, overall view of fracture surface

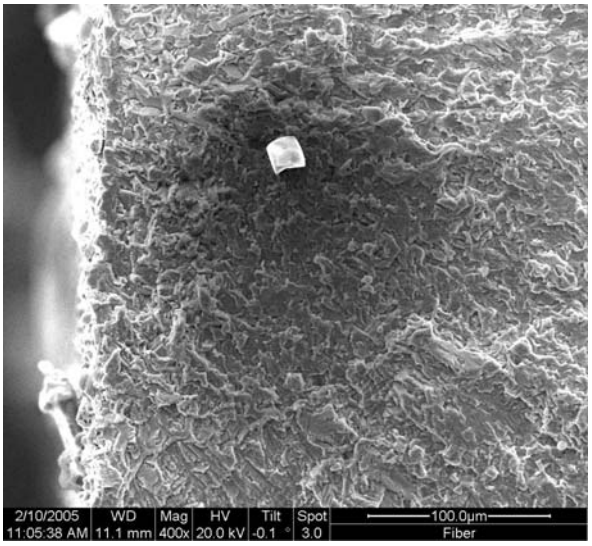

Figure 106: Specimen Ti-04, close-up view of void

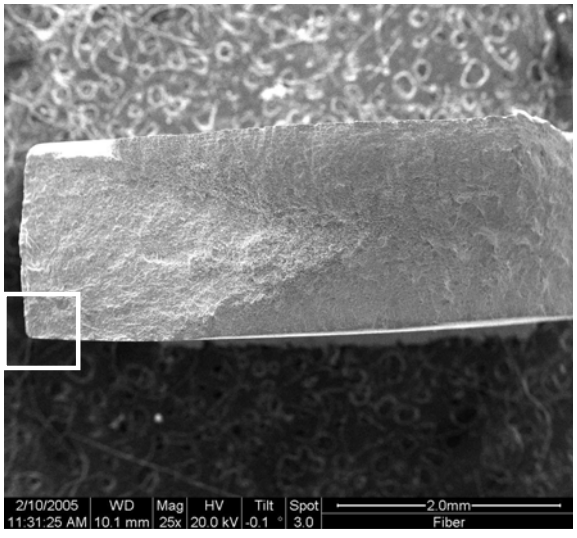

Figure 107: Specimen Ti-10, overall view of fracture surface

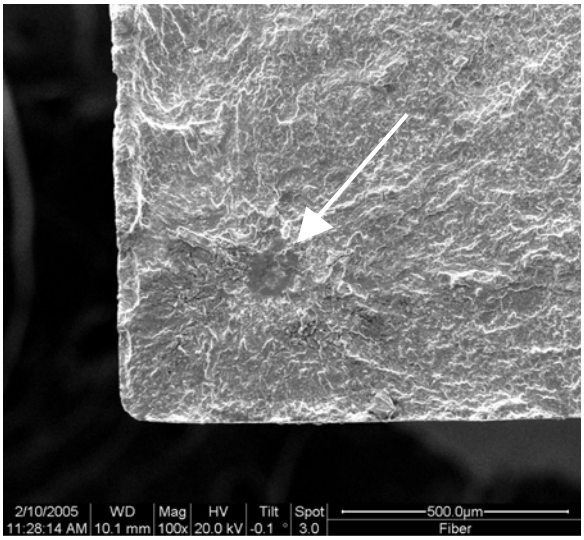

Figure 108: Specimen Ti-10, close-up of crack initiation site

Tension-compression Fatigue Failures:

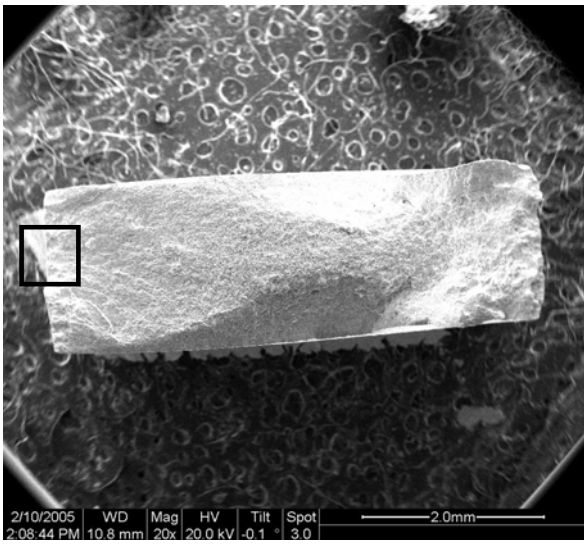

Figure 109: Specimen Ti-05, overall view of fracture surface

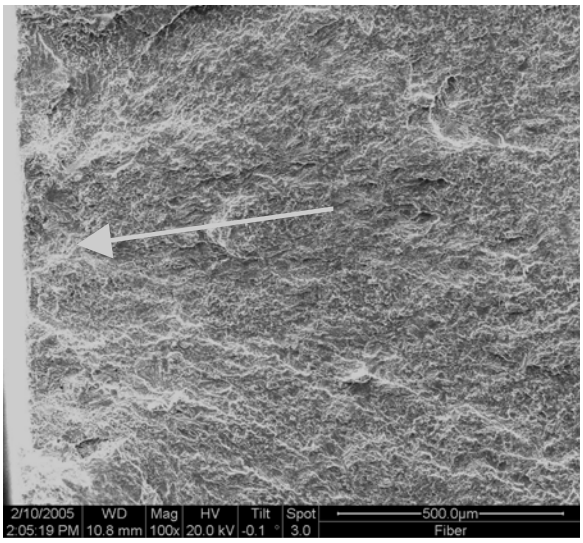

Figure 110: Specimen Ti-05, close-up view of crack initiation site

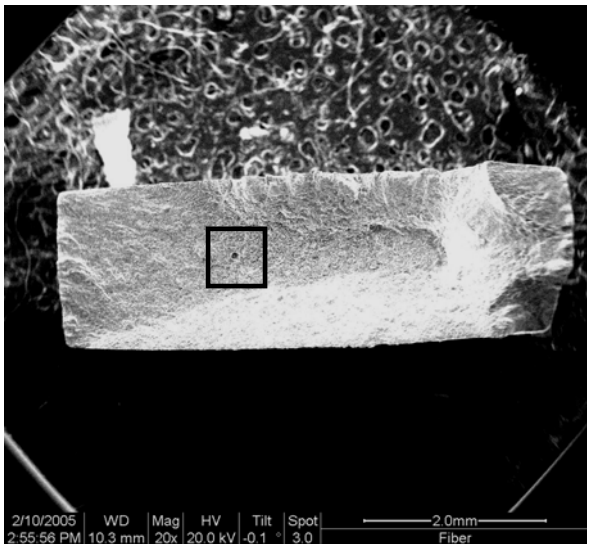

Figure 111: Specimen Ti-07, overall view of fracture surface

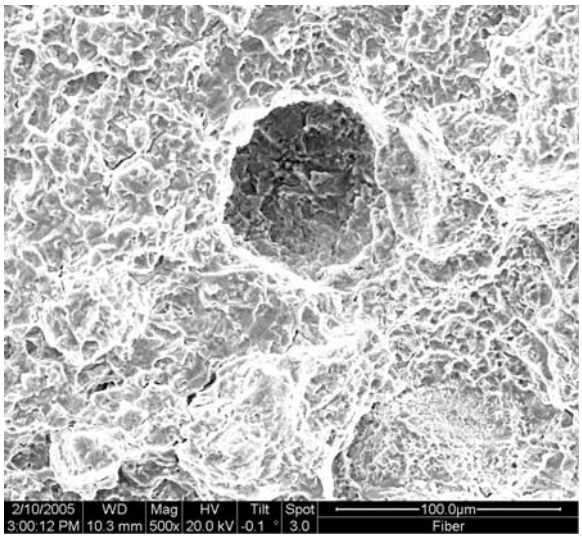

Figure 112: Specimen Ti-07, close-up of void in crack path

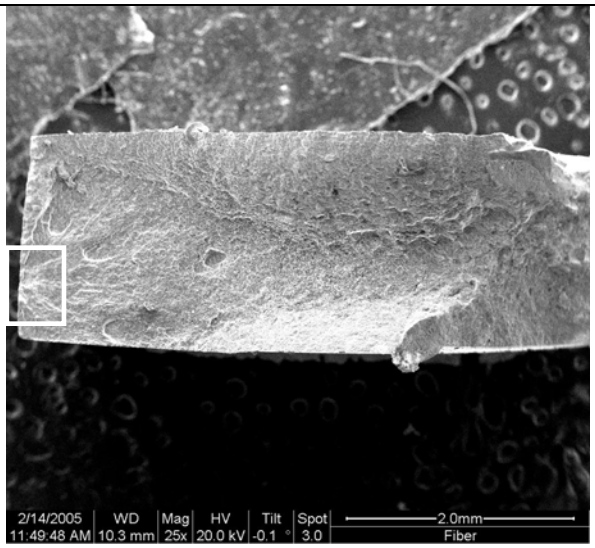

Figure 113: Specimen Ti-09, overall view of fracture surface

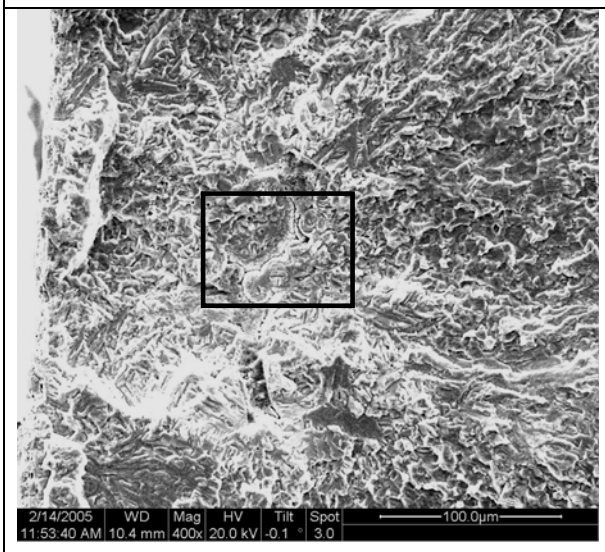

Figure 114: Specimen Ti-09, close-up of crack initiation site

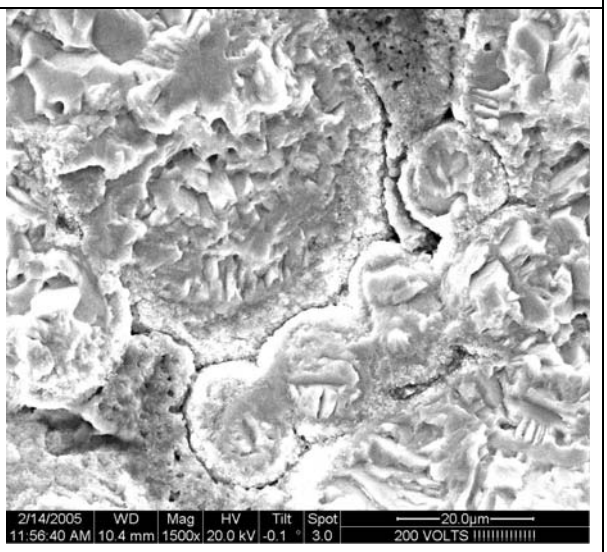

Figure 115: Specimen Ti-09, slip plane

Bibliography

1. Anderson, T.L., Fracture Mechanics: Fundamentals and Applications. 2nd ed. Florida: CRC Press LLC, 1995.

2. Boyum, E.A., "Investigation of Tension-compression Fatigue Behavior of a Cross-ply Metal Matrix Composite at Room and Elevated Temperatures," AFIT Thesis AFIT/GAE/ENY/93D-6, (Dec 93).

3. Broek, D., Elementary Engineering Fracture Mechanics. 4th ed. Boston: Kluwer Academic Publishers, 1991.

4. Brooks, C.R., Choudhury, A., Failure Analysis of Engineering Materials. New York: McGraw-Hill Companies, Inc., 2002.

5. Clyne, T.W. and Watson, M.C., "Interfacial Mechanics in Fiber-Reinforced Metals," *Composites Science and Technology*, Vol. 42, 1991, pp. 25-55.

6. Coghlan, S.C., "Fiber Volume Fraction Effects on Fatigue Response of a SCS-6/Ti-15-3 Metal Matrix Composite at Elevated Temperature," AFIT Thesis AFIT/GAE/ENY/97S-01, (Sept 97).

7. Eylon, D., Mahajan, Y., Ontko, N.R. and Froes, F.H. "Fatigue Crack Initiation of Titanium Alloy Powder Compacts," *Powder Metallurgy of Titanium Alloys*, ed. by Froes, F.H. and Smugeresky, J.E., pub. by the Metallurgical Society of AIME, 1980, pp. 93-102.

8. Ivasishin, O.M., Bondareva, K.A., Bondarchuk, V.I., Gerasimchuk, O.N., Savvakin, D.G. and Gryaznov, B.A. "Fatigue resistance of powder metallurgy Ti-6Al-4V alloy," *Problemy Prochnosti*, n 3, 2004, pp. 5-13.

9. Jeng, S.M., Alassoeur, P. and Yang, J.M., "Fracture Mechanisms of Fiber-reinforced Titanium Alloy Matrix Composites Part IV: Low Cycle Fatigue," *Materials Science and Engineering*, Vol A148, 1991, pp. 67-77.

10. Jeng, S.M., Yang, J.M. and Yang, C.J., "Fracture Mechanisms of Fiber-reinforced Titanium Alloy Matrix Composites Part II: Tensile Behavior," *Materials Science and Engineering*, Vol A138, 1991, pp. 169-180.

11. Kelto, C.A., Kosmal, B.A., Eylon, D. and Froes F.H. "Titanium Powder Metallurgy – A Perspective," *Powder Metallurgy of Titanium Alloys*, ed. by

Froes, F.H. and Smugeresky, J.E., pub. by the Metallurgical Society of AIME, 1980, pp. 1-19.

12. Kraabel, D.L., "Investigation of Tension-compression Fatigue Behavior of a Unidirectional Metal Matrix Composite at Elevated Temperature," AFIT Thesis AFIT/GAE/ENY/94D-16, (Dec 94).

13. Mall, S. and Nicholas, T., editors, Titanium Matrix Composites: Mechanical Behavior. Pennsylvania: Technomic Publishing Company, Inc., 1998.

14. Majumdar, B.S., Matikas, T.E. and Miracle, D.B. "Experiments and Analysis of Fiber Fragmentation in Single and Multiple-fiber SiC/Ti-6Al-4V Metal Matrix Composites," *Composites Part B: Engineering*, v29, issue2, 1998, pp. 131-145.

15. Miller, G.B., "Mechanics of a Functionally-graded Titanium Matrix Composite," AFIT Thesis AFIT/GAE/ENY/00M-01, (Mar 00).

16. Miyamoto, Y., Niino, M. and Koizumi, M. "FGM Research Programs in Japan—from Structural to Functional Uses," Functionally Graded Materials 1996, ed. by Shiota, I. and Miyamotot, Y., pub. by Elsevier Science B.V., 1997, pp. 1-8.

17. Peebles, R.E. and Kelto, C.A. "Investigation of Methods for the Production of High Quality, Low Cost Titanium Alloy Powders," *Powder Metallurgy of Titanium Alloys*, ed. By Froes, F.H. and Smugeresky, J.E., pub. by the Metallurgical Society of AIME, 1980, pp. 47-58.

18. Ramamurty, U., "Fatigue in Selectively Fiber-Reinforced Titanium Matrix Composites," Metallurgical and Materials Transactions, Vol. 30A, August 1999, pp. 2237-2248.

19. Sanders, B.P, Mall, S. and Pittman, R.B. "Effects of Frequency and Temperature on the Fatigue Behavior of a Unidirectional Titanium-matrix Composite," *Composites Science and Technology*, v59, n4, 1999, pp. 583-591.

20. Specialty Materials, Inc. http://www.specmaterials.com/silicarbsite.htm/ Accessed 24 Jan 2005.

21. Talreja, R., Fatigue of Composite Materials. Lancaster: Technomic Publishing Company, 1987.

22. Vaughan, R.F. and Blenkinsop, P.A. “A Metallurgical Assessment of Ti-6Al-4V Powder,” *Powder Metallurgy of Titanium Alloys*, ed. By Froes, F.H. and Smugeresky, J.E., pub. By the Metallurgical Society of AIME, 1980, pp. 83-92.

Vita

Captain Scott R. Cunningham was born in Bradenton, Florida. He graduated from Hopewell-Loudon High School in Bascom, Ohio in 1993. He entered the University of Toledo, Toledo, Ohio later that year. In December of 1998, he graduated with a Bachelor of Science in Mechanical Engineering. After working in the civilian sector for a while, he entered the Air Force Officer Training School in October of 1999. Upon receiving his commission as a Second Lieutenant in January, 2000, he began his first assignment as a structural engineer in the Air Vehicles Directorate at Wright-Patterson AFB, Ohio. During his time there, he was involved in crack-growth/life prediction models, materials testing and finite element modeling (FEM). Following his assignment at Wright-Patterson, he entered the Air Force Institute of Technology Graduate School of Engineering in August of 2003. After graduation, he will be assigned to the Space and Missiles Center at Los Angeles AFB, California.

REPORT DOCUMENTATION PAGE

Form Approved
OMB No. 074-0188

1. REPORT DATE *(DD-MM-YYYY)*	2. REPORT TYPE	3. DATES COVERED *(From – To)*
21-03-2005	Master's Thesis	August 2003 – March 2005

4. TITLE AND SUBTITLE

Fatigue Behavior of a Functionally-graded Titanium Matrix Composite

5a. CONTRACT NUMBER

5b. GRANT NUMBER

5c. PROGRAM ELEMENT NUMBER

6. AUTHOR(S)

Cunningham, Scott R., Captain, USAF

5d. PROJECT NUMBER

5e. TASK NUMBER

5f. WORK UNIT NUMBER

7. PERFORMING ORGANIZATION NAMES(S) AND ADDRESS(S)

Air Force Institute of Technology
Graduate School of Engineering and Management (AFIT/EN)
2950 Hobson Way, Building 640
WPAFB OH 45433-8865

8. PERFORMING ORGANIZATION REPORT NUMBER

AFIT/GAE/ENY/05-M06

9. SPONSORING/MONITORING AGENCY NAME(S) AND ADDRESS(ES)

Mr. Mark M. Derriso, AFRL/VASA
2790 D Street
WPAFB, OH 45433

10. SPONSOR/MONITOR'S ACRONYM(S)

11. SPONSOR/MONITOR'S REPORT NUMBER(S)

12. DISTRIBUTION/AVAILABILITY STATEMENT

APPROVED FOR PUBLIC RELEASE; DISTRIBUTION UNLIMITED.

13. SUPPLEMENTARY NOTES

14. ABSTRACT

Functionally-graded Titanium Matrix Composites are an attempt to utilize the high-strength properties of a titanium matrix composite with a monolithic alloy having the more practical machining qualities.

This work studied the mechanical characteristics of the joint region as a first step toward future evaluation of this material. The scope of this effort involved testing under monotonic tension and fatigue loading conditions. Mechanical properties and cyclic behavior were evaluated for the joint area and then compared to those of the parent materials.

The results of this study found that the strength of the transition region was slightly higher than the unreinforced alloy. However, the presence of fiber ends in the transition region proved to be the source of failure under fatigue loading conditions. Failure in the transition region did not occur at the tip of the taper joint as anticipated. Instead, failure occurred at the transition to the next ply in the taper. This indicates that fiber volume, in conjunction with the presence of fiber ends, plays a key role in the fatigue life of the entire material. These findings encourage and provide the basic scientific knowledge for further evaluation and development of functionally-graded titanium matrix composites.

15. SUBJECT TERMS

Titanium alloy, Titanium Matrix Composites, tension-tension fatigue, tension-compression fatigue, functionally-graded joint, integrally fabricated joint

16. SECURITY CLASSIFICATION OF:			17. LIMITATION OF ABSTRACT	18. NUMBER OF PAGES	19a. NAME OF RESPONSIBLE PERSON
a. REPORT	b. ABSTRACT	c. THIS PAGE			Dr. Shankar Mall
U	U	U	UU	111	19b. TELEPHONE NUMBER *(Include area code)* (937) 255-3636, ext 4587 (Shankar.Mall@afit.edu)